Examination of binding elements and conditions of *Cryptosporidium parvum* oocysts to assess its detection potential in water

by

Irene Rodriguez Ruiz-Andino

A thesis

presented to the University of Waterloo

in fulfilment of the

thesis requirement for the degree of

Master of Applied Science

in

Chemical Engineering (Water)

Waterloo, Ontario, Canada, 2022

Author's Declaration

I hereby declare that I am the sole author of this thesis. This is a true copy of the thesis, including any required final revisions, as accepted by my examiners.

I understand that my thesis may be made electronically available to the public.

Abstract

Cryptosporidium parvum is an intestinal parasite that can be spread through environmental and recreational waters, most often in the form of oocysts. As an oocyst, this parasite is resistant to chlorine disinfection, and it is the known cause of the diarrheal disease Cryptosporidiosis. In this thesis, binding elements like antibodies and aptamers are studied and compared with the purpose of assessing their binding under different conditions and therefore their potential as biorecognition elements to detect *C. parvum* in water. Several methods have been used to fulfill this purpose. Flow cytometry and imaging flow cytometry was used to compare and assess the binding of commercial fluorescently labelled antibodies, and aptamers reported in literature, under different conditions such as pH, inactivation procedures or heat-inactivation contact time. Horseradish peroxidase (HRP)-labelled antibodies was used to assess the colorimetric potential for *Cryptosporidium* detection both as a part of an in-filter detecting scheme and to assess the binding differences between live and inactivated *Cryptosporidium*. It was found that antibodies had better binding affinity than aptamers for *Cryptosporidium* that was inactivated under different methods such as desiccation, heat-treatment, freeze-treatment, and formalin-treatment. Furthermore, aptamers show an increase of non-specific binding under low pH conditions.

An in-filter detection method involving the preincubation of HRP-labelled antibodies with the target and passing this solution through a syringe filter followed by the addition of 3,3',5,5'-Tetramethylbenzidine (TMB), which could allow visual observation of a color change, was also explored. This biosensor was developed as part of a detection scheme to avoid any detection sensitivity loss due to poor recovery from filters and was meant to help make detection simpler for the public. The limit of detection of this approach was found out to be 10^5 oocysts/mL . While this limit of detection is rather high, improvements could be made by changing the labelling of the antibodies or by changing the type of antibodies.

Acknowledgements

First, I would like to thank my supervisors Dr. William Anderson and Dr. Marc Aucoin for giving me the opportunity to work on this project and their invaluable guidance and support. I would also like to thank Dr. Shazia Tanvir for her guidance and teachings in this field during this project and Dr. Amandeep Kaur for teaching me my way around the lab and how to operate the equipment I needed to fulfill this thesis as well as supplying the *E. coli* cultures needed to fulfill this thesis.

Secondly, I would also sincerely like to thank Dr. Brian Ingalls for showing me how to use and letting me use the Imaging Flow Cytometer in his lab. I would also like to thank Madhuja Chakraborty for her help with the flow cytometer in the Aucoin lab.

Finally, I would like to thank Exact Blue Technologies and NSERC for funding this work. And to appreciate the financial support given to complete this research by the International Master's Award of Excellence (IMAE) and the RBC Water Scholars Graduate Entrance Scholarship.

Table of Contents

List of Figures

List of Tables

List of Abbreviations

ALP: Alkaline phosphatase

CPV: *Cryptosporidium parvum* virus

DAP: 2,3-diaminophenazine

DAPI: 4',6-Diamidino-2-Phenylindole, Dihydrochloride

DI: Deionized water

DIC: Differential interference contrast

EIS: Electrochemical impedance spectroscopy

DPBS: Dulbecco's Phosphate Buffer Saline

ELISA: Enzyme-linked Immunosorbent assays

6-FAM: 6-carboxyfluorescein

FITC: Fluorescein isothiocyanate

FSC-vs-SSC: Front versus side scatter

HRP: Horseradish-Peroxidase

IMS: Immunomagnetic separation

IDT: Integrated DNA Technologies

LOD: Limit of detection

ODP: o-phenylenediamine

p-NPP: p-nitrophenol phosphate

p-NP: p-nitrophenol

PBS: Phosphate buffer saline

QCM-D: Quartz crystal microbalance with dissipation monitoring

SAM: self-assembled monolayer

S/N: Signal to noise

SPR: Surface plasmon resonance

SELEX: Systematic evolution of ligands by the exponential enrichment

TMB: 3,3',5,5'-Tetramethylbenzidine

WTP: Water treatment plant

(S/N) : Signal to noise ratio

1. Introduction

1.1. Research motivation

Cryptosporidium is an obligate gastro-intestinal protozoan parasite that can be spread through water or food. *Cryptosporidium* has been the causative agent of 50% of the diarrheal disease outbreaks (herein referred to simply as outbreaks) linked to recreational waters in the US and it has been reported to be the second leading cause of death in children due to a diarrheal disease worldwide (Gibson & Striepen, 2018). In the US, for the period between 2009 to 2017, 444 outbreaks linked to *Cryptosporidium* have been reported (Gharpure et al., 2019). In Canada, since the disease became reportable in the year 2000, cases have been somewhat constant ranging from 588 to 875 a year (Health Canada, 2019).

The gold standard for *Cryptosporidium* detection in environmental and recreational waters is EPA Method 1623. This method involves several steps and the need for highly qualified personnel to correctly identify this pathogen via microscopy. It also occasionally involves shipping large volumes of water to laboratory facilities, if the filtration step cannot be carried out on-site. Detecting *Cryptosporidium* in water is time-consuming and expensive.

Moreover, the United States Environmental Protection Agency (US EPA) has a Maximum Contaminant Level Goal of zero for *Cryptosporidium* and requires that drinking water be either disinfected and filtered or, if exempt from filtration, systems must include *Cryptosporidium* in their control provisions (US EPA, 2015).

For the period from 2015 to 2019, 208 outbreaks associated with recreational waters were reported in the United States of America. A total of 76 these outbreaks were caused by *Cryptosporidium*, followed by *Legionella*, which caused 65 of these outbreaks. *Cryptosporidium* outbreaks resulted in 2492 cases (Hlavsa et al., 2021).

Cryptosporidium's high resistance to chlorination methods and the nature of recreational water settings (close contact with possible infected individuals, small volume of water and therefore less dilution, etc.) make recreational waters such as pool or spas an important source of transmission. Having access to on-site detection

methods, available to use by the general public could make *Cryptosporidium* early detection an important asset to avoid outbreaks.

To overcome some of the drawbacks of EPA 1623, several novel detection methods, from immunological techniques such as Enzyme-linked Immunosorbent assays (ELISA), immunomagnetic separation (IMS) or flow cytometry using fluorescently labelled antibodies to molecular methods such as PCR, have been developed. Moreover, several biosensors for the detection of *Cryptosporidium* have also been developed. Biosensors are usually made up of a recognition element, a transducer and a detector. Several recognition elements have been used for the detection of *Cryptosporidium* from antibodies to aptamers, nucleic acids or even whole cells (Hassan, Örmeci et al., 2021; Luka, George et al., 2022).

Methods that target the oocysts surface and that involve aptamers or antibodies have the potential to become an easy to use, rapid biosensors since they involve a smaller number of steps and do not require excystation or lysing the cells. In this work, the binding properties of various agents such as aptamers and antibodies in different conditions are explored with the goal of creating an easy to use, rapid biosensor for *Cryptosporidium* oocysts.

Although there are already numerous articles published that use antibodies and aptamers as binding mechanisms for the development of biosensors towards *Cryptosporidium* oocysts, these biosensors are not yet easy enough to use by the general public and some of them either fail to address the filtration of large quantities of water, needed to obtain *Cryptosporidium* in significant enough numbers for its detection or the need to elute the oocysts from the filters.

Antibodies have been extensively used as capture probes in biosensors and they are still considered a gold standard. However, antibodies present certain disadvantages such as high costs, low long-term stability, and an increased complexity for conjugation with labels. Aptamers have emerged as an alternative to antibodies that can overcome some of these disadvantages (Arshavsky-Graham et al., 2022). However, while aptamers show binding affinity similar to that of antibodies for protein detection, this technology is not as well-established for other uses (Schüling et al., 2018). Moreover, unlike

antibodies, aptamers are highly dependent on solution conditions (McKeague & DeRosa, 2012)

In this work the binding strength of antibodies and aptamers are first explored to determine their suitability for the creation of a biosensor. Antibodies were then chosen for the creation of a proof-of-concept sensing mechanism that could overcome some of the disadvantages that are in the field, such as recovery efficiencies from filtration and ease of use by the general public.

1.2. Research objectives

The overall objective of this thesis was to develop ways to detect *Cryptosporidium parvum* in low concentrations in water in an easy, fast and cheap way that could be translated into a biosensor for use by the general public. The specific steps taken to reach this goal were:

- Screening of a range of aptamers identified in literature with selectivity for *C. parvum* with the goal of finding an aptamer that could bind to inactivated *Cryptosporidium*.
- Comparing binding affinities of antibodies and aptamers for oocysts, inactivated by different methods, using fluorescently labelled capture molecules and flow cytometry.
- Studying of the effect of different conditions such as pH and inactivation contact time on aptamer binding affinity
- Determining the binding performance and limit of detection (LOD) achievable with Horseradish-Peroxidase (HRP)-labelled antibodies via naked-eye colorimetric detection.
- Optimizing sensing parameters and membrane conditions to develop a sensing platform that uses HRP-labelled antibodies to detect *Cryptosporidium* oocysts within a filter.

1.3. Thesis outline

This thesis is comprised of seven sections: an overview of the thesis contents, relevant literature review, four sections that include results from experiments, followed by a section that includes final conclusions and possible next steps.

Chapter one includes an overview of the thesis contents and the research objectives and questions that will be addressed through the body of the thesis. It also provides context as to why this research is pursued and the motivation behind it.

Chapter two includes a relevant literature review that summarizes recent work on biosensors that use capture probes like aptamers and antibodies, with the goal of finding troubleshooting points and areas of improvement. It also explores literature relevant to procedures used in the experimental sections of this thesis, as well as a general overview of *Cryptosporidium*, antibodies and aptamers.

Chapter three explores the binding properties of antibodies and aptamers to *Cryptosporidium* inactivated by different procedures. This was meant as a way of assessing the influence of inactivation procedures on cell surface changes and binding properties, as well as its influence on the LOD. The goal of working with inactivated *Cryptosporidium* was to work with this pathogen in a lower risk setting.

Chapter four screens different aptamers sequences found in the literature that are specific against *Cryptosporidium* with the aim of testing the hypothesis that a different sequence could possibly bind to a structure that is conserved during *Cryptosporidium* inactivation. The main goal was to find a sequence that could bind to inactivated *Cryptosporidium*.

Chapter five explores the binding capabilities of *Cryptosporidium* aptamers under different pH and heat-inactivation contact time conditions, with the goal of determining if there are specific conditions that could improve aptamer binding in a sensitive and specific way.

Chapter six involves the development of a proof-of-concept in-filter biosensor to detect *Cryptosporidium* oocysts. This Chapter explores different membrane operation conditions and characteristics and its influence on *Cryptosporidium* detection, such as effect of membrane preconditioning, pore size and antibody-oocyst contact time.

Finally, Chapter seven summarizes the findings of this thesis and its conclusions and provides next steps and possible future directions in this field.

2. Literature review

In this Chapter, literature that is relevant to identifying gaps and troubleshooting points in the biosensing of *C. parvum* are examined. Furthermore, literature that is necessary to understand some of the components and procedures of *C. parvum* sensing is analyzed.

2.1. Introduction

Cryptosporidium is a protozoan parasite that can be spread through water or food. The most prevalent species that infect humans are *C. parvum* and *C. hominis*. This parasite is resistant to chlorine disinfection and while for immunocompetent adults the post-infection sequalae is similar to that of bacterial gastroenteritis, those who are immunocompromised, such as HIV patients, immunodeficient or hematopoietic stem-cell transplant patients, are susceptible of severe or fatal Cryptosporidiosis (Chalmers et al., 2019).

One of the biggest challenges addressing *Cryptosporidium* detection is the low infectious doses needed to cause disease. While the infectious dose of *C. parvum* depends on multiple parameters, such as the definition of infectious dose or type of isolate, a study carried out by Messner et al. (2001) on healthy volunteers found that the *C. parvum* infectious dose (defined as the presence of oocysts in stool and/or the development of diarrheal illness by volunteers) was dependent on the *C. parvum* type of isolate and ranges between 12.1 to 2066 oocysts, the TAMU isolate being the most infectious. Another study carried out by DuPont et al. (1995) using healthy volunteers, with similar definitions of infection but using the IOWA isolate, found an infectious dose of 132 oocysts.

A key characteristic of *Cryptosporidium* lies in its complex life cycle and different morphologies in each step of the cycle. *Cryptosporidium* is found as sporulated oocysts in nature. Each oocyst encapsulates four sporozoites which are the infectious phase of the life cycle. The ability to encapsulate the infectious phase in oocysts makes *Cryptosporidium* highly resistant to natural decay in the environment as well as some water treatment processes like traditional chlorination, being able to survive for months in soil and up to a year in water (EPA, 2001).

Oocysts are highly resistant to environmental and chemical influences due to the layered nature of its wall. The outer layer consists of a glycocalyx matrix, followed by a lipid bilayer that provides high resistance to liquid intrusion. The inner protein-rich layer, consisting mostly of two proteins, *Cryptosporidium* Oocyst Wall Protein 1 being the most prevalent and *Cryptosporidium* Oocyst Wall Protein 8 to a lesser extent, provides certain rigidity and mechanical resistance to the oocyst (Lendner & Daugschies, 2014). An illustration of these components is presented in Figure 1. This resistivity to environmental stress and chemical influences as well as some water treatment methods makes early detection of *Cryptosporidium* crucial to avoid outbreaks.

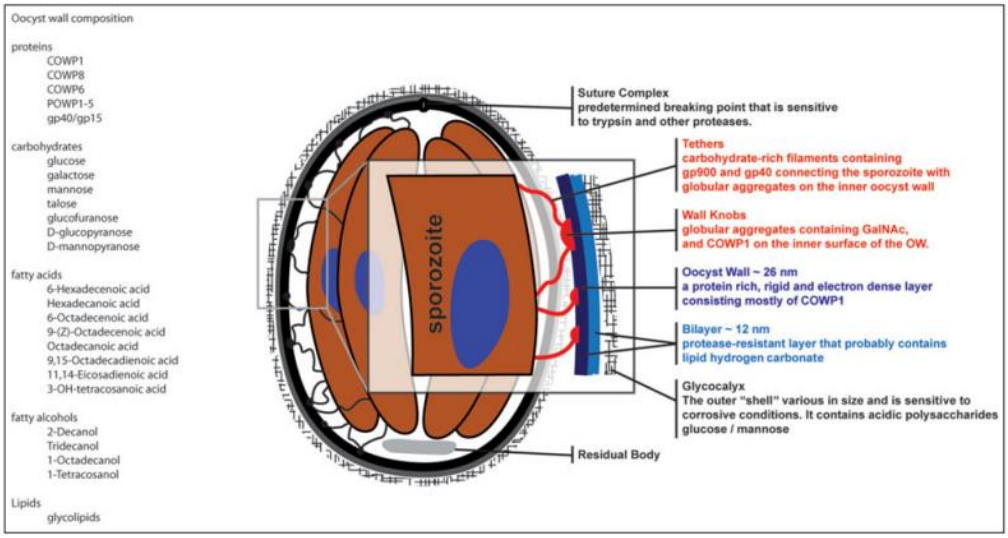

Figure 1.Oocyst wall structure and components. Source: (Lendner & Daugschies, 2014)

2.2. *C. parvum* capture element-based biosensors.

The gold standard for *Cryptosporidium* detection in environmental and recreational waters is EPA Method 1623. This method consists of several sequential steps. At first, a 10 L sample is collected and filtered with 1 µm pore size filters. Then, the materials on the filters are eluted and further concentrated by centrifugation. *Cryptosporidium* is then separated from other debris via immunomagnetic separation, where antibody-conjugated magnetic beads are used to capture the oocysts and magnetically separate them from the rest of the solution. The parasites are then eluted from the antibody-magnetic bead complex before proceeding to staining and enumeration. The recovered oocysts are then stained used FITC-labelled antibodies and 4',6-Diamidino-2-Phenylindole, Dihydrochloride (DAPI) and the sample is examined

using epifluorescence and differential interference contrast (DIC) microscopy. FITC-labelled antibodies are used to identify *Cryptosporidium* while DAPI stains serves as a measure of membrane viability and quality of the microorganisms. The quantitative and quantitative analysis is performed by trained personnel by visually scanning each slide for objects that meet the characteristics of the oocysts and by counting the total number of said objects on the slide (EPA, 2005). This method has a variable range of recovery efficiencies for *Cryptosporidium* and therefore a variable Limit of detection (LOD). It is estimated that the LOD varies between 2 to 215 oocysts/10 L (Francy et al., 2004).

To overcome some of these drawbacks, there are several biosensing techniques that have been reported in the literature from immunological techniques that involve the use of antibodies to molecular methods like PCR. While nucleic acid methods tend to be highly sensitive and specific for the detection of pathogens, they require the use of laboratory facilities and highly skilled personnel. Antigen detection-based methods usually require a smaller number of steps, since oocysts don't usually have to be lysed, which most of the time require a larger number of steps and access to laboratory reagents and equipment. This makes biosensors based on antibodies or aptamers more suitable for field testing and it could eventually make testing widely available for the general public. Therefore, the focus of this section is on recent method development based on immunological techniques or biosensors with recognition elements that bind to oocyst wall antigens, such as antibodies and aptamers. Here, current biosensors found in literature are classified into the following categories: ELISA-based methods, Western blot-based assays, surface plasmon resonance (SPR)-based sensors, electrical and electrochemical sensors and aptamer-based sensors

2.2.1. ELISA-based methods

Enzyme-linked immunosorbent assays (ELISA) are a family of tests that use antibodies as reagents and enzymes attached to them to render a color change to determine the presence of a target. These assays involve the immunoreaction or binding of antibodies with a target that is usually immobilized on a solid phase, followed by thorough washing to remove unbound antibodies and a final colorimetric enzymatic reaction carried out by the addition of a substrate (Crowther, 2009)

ELISA tests can be sorted into these different categories (Crowther, 2009):

1. **Direct ELISA:** this is the simplest ELISA, where the antigen is directly immobilized to a solid phase (normally, a 96 well ELISA plate), followed by washing to remove unbound antigen. Antibodies that bind to said antigen and are labelled with an enzyme are then added and incubated with the antigen previously immobilized into a solid phase. This is followed by thorough washing and the addition of a substrate to render a color change that can be read.
2. **Indirect ELISA:** This approach is similar to the direct ELISA. The antigen is also directly immobilized to a solid phase via adsorption, and this is followed by washing to remove unbound antigen. Primary non-labelled antibodies are then added and incubated with the antigen and followed by washing to remove unbound antibodies. After this step, secondary antibodies that bind to the primary antibodies and that are enzyme-labelled, are added, and incubated with the antigen-primary antibody mixture. After an incubation period and washing step, the chromogenic substrate is then added, and the signal is read
3. **Sandwich ELISA**: This category can be broken into two parts: direct sandwich ELISA and indirect sandwich ELISA. They work similarly to the ELISA methods described above with one difference in the antigen immobilization method: the antigen is not directly adsorbed onto a solid phase, instead, a set of antibodies called capture antibodies, are immobilized onto the solid phase and the antigen is then bound to the capture antibodies, not directly the solid phase. All the other steps, after antigen immobilization are the same to the ones described above.

Figure 2 contains a graphic comparison of the different ELISA methods.

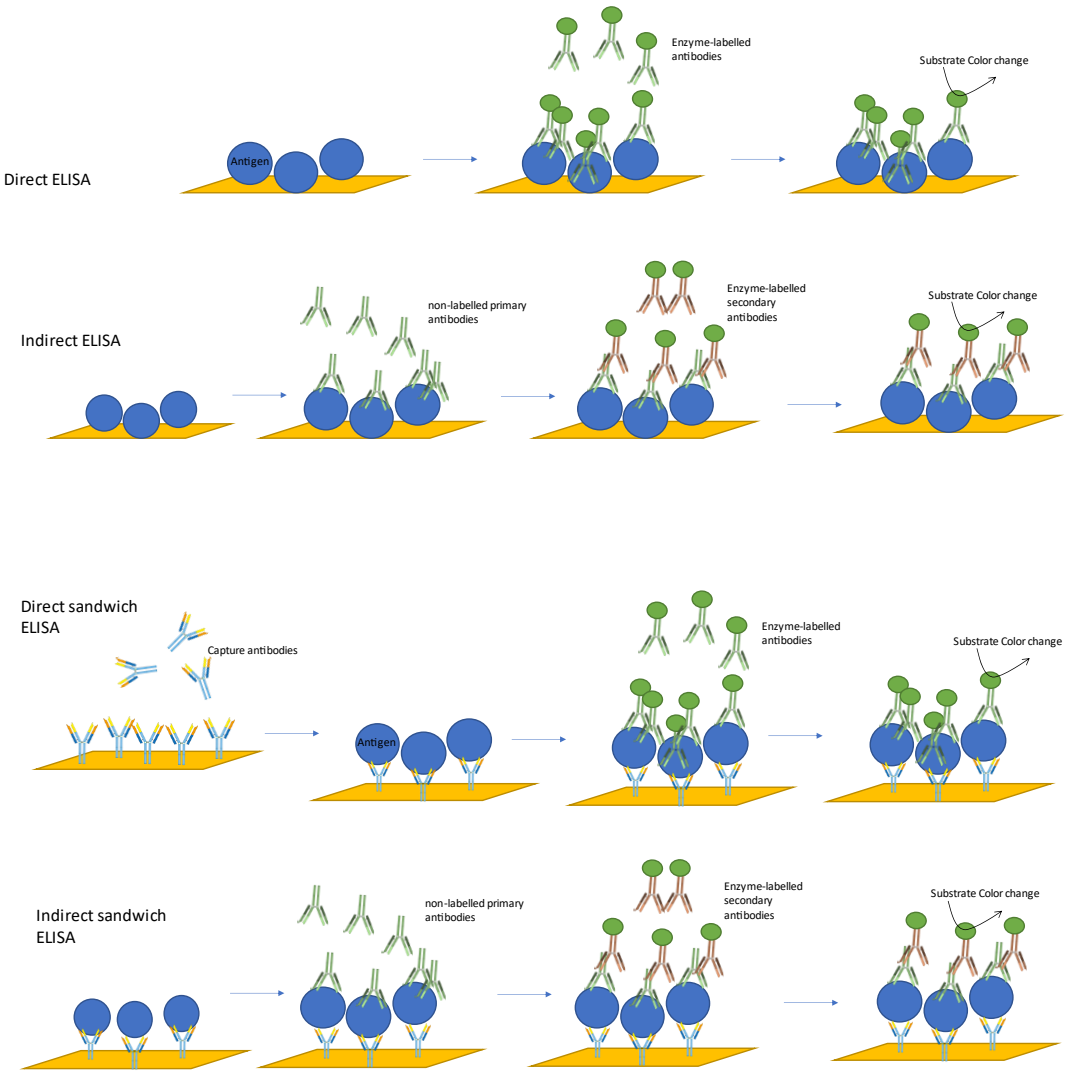

Figure 2. Graphical comparison of ELISA methods.

Numerous variations of these three main ELISA tests for *Cryptosporidium* detection have been reported in the literature. Thiruppathiraja et al., (2011) developed an electrochemical sandwich assay where capture monoclonal antibodies are immobilized into an indium tin oxide electrode and, instead of regular primary antibodies, they used a gold nanoprobe double functionalized with alkaline phosphatase (ALP) and monoclonal anti-cysts antibodies. The sandwich assay works by first incubating the sample containing target antigen with electrode-capture antibody solid phase, followed by washing, to remove unbound substances. This is followed by the incubation with the nanoprobe and extensive washing to remove unbound nanoprobe. The capture

antibody-target-nanoprobe complex is then incubated for another 10 minutes with p-nitrophenol phosphate (*p*-NPP) solution. ALP groups of the nanoprobe catalyze the hydrolysis of *p*-NPP into electroactive p-nitrophenol (*p*-NP) and differential pulse voltammetry scan is then performed. This sensor proved to be very efficient, being able to detect as few as 3 oocysts/mL with high specificity and very short processing time. By comparing the results of this method in drinking water samples using fluorescence microscopy they found that the relative standard deviation for both methods was less than 6%, indicating its high sensitivity towards *C. parvum*. However, if compared with the gold standard, EPA method 1623 has a LOD of 2-215 oocysts/10 L (2-215 $\cdot 10^{-4}$ oocysts/mL). This difference is substantial because the EPA method 1623 involves the filtration of 10 L of water. To be able to compare both methods and to have a more reliable testing protocol, filtration methods or other methods to test large quantities of water needs to be addressed.

This approach differs from a traditional direct sandwich ELISA because instead of primary enzyme-labelled antibodies, they use a nanoprobe, allowing them to attach more ALP groups into a single antibody and thus, improving the sensitivity of the sensor. It also differs from traditional ELISA in the signal emitted and read. Instead of catalyzing a colorimetric signal, ALP catalyzes an electrochemical reaction that is measured by pulse voltammetry instead of reading an absorbance. Although this approach proved to have high sensitivity towards *C. parvum* it presents some minor drawbacks such as the need for thorough washing and somewhat qualified personnel, making it difficult to be implemented for field testing or to be used by the general public.

Another ELISA-modified immunosensor was evaluated by Li, Y. et al. (2021). In this modified ELISA immunosensor, they exploit the enzymatic activity of Cas12a to obtain an amplified signal. This particular enzyme works in such a way that once it is activated by recognition of the trigger DNA, it not only cleaves the recognized site, it goes on cleaving indiscriminately any other piece of single stranded nucleic acid that is in its surrounding. By adding fluorescence reporters, which are based on a random sequence of ssDNA that have a fluorophore and a quencher, an amplified signal can be obtained; the activated Cas12a will cleave the reporters, separating the fluorophore from the quencher, which in turn, gives an amplified fluorescence signal. This sensor

relies on two sets of antibodies. First, the capture antibodies that have been immobilized onto an ELISA plate and second, the antibody-based probe. This probe uses biotin-streptavidin chemistry to attach trigger ssDNA sequences to anti-*Cryptosporidium* antibodies.

In this sensor, the target is first added to the capture antibody-coated ELISA plate and after incubation and thorough washing, the *Cryptosporidium* oocysts will be captured onto the plate. The antibody-based probe consisting of antibodies and trigger ssDNA is then added to the plate and the probe binds the captured oocysts. After an incubation period and two washes, a reaction mixture containing the CRISPR/Cas12a enzyme and excess of reporters is added. The CRISPR/Cas12 enzyme recognizes the trigger ssDNA that is linked to the antibodies in the antibody-based probe, and once it is recognized, it will cleave that piece of ssDNA and continue to cleave the surrounding quenched fluorescence reporters allowing the reporters to become unquenched. The fluorescence is then read by a plate reader. A diagram of this sensing strategy is given in Figure 3. This differs from traditional ELISA in the sense that instead of relying on one fluorescence or colorimetric reporter attached to each antibody, this method allows for several fluorescence reporters to be used, using the enzymatic activity triggered by just one antibody, producing an amplified signal. This sensor proved to be highly sensitive, being able to detect a single oocyst under optimized conditions. The sensor, compared to traditional ELISA shows an increase of 2-logs in sensitivity, from 160 oocysts to one.

This sensor was also tested in complex matrixes, including orange juice, yogurt, milk, dirt suspension and backwash mud samples from a water treatment plant (WTP). All the spiked samples in complex matrices showed higher fluorescence intensity than the sample without oocysts indicating the ability of the sensor to perform in these conditions. However, while this system could be applied to WTP samples, the sensitivity of the sensor decreased from a single cell to 10 oocysts for these samples.

This sensor proved to be highly sensitive to *Cryptosporidium* detection, down to single cell detection. Taking approximately 2.5 hours to complete, it is a simple method, like ELISA and it does not require expensive microscopy. By comparison with traditional ELISA, it proved the ability of signal amplification and superior performance by the CRISPR/Cas12a amplification strategy and in comparison, with other CRISPR/Cas

systems, this one targets surface antigens and not the organism's nucleic-acid which means that it does not require other specific steps like lysis of the cell and PCR amplification. However, as with any ELISA, it needs thorough washing to avoid interference and false positive readings. It also requires a fluorescence plate reader, which, while common, is not in every lab. Moreover, it involves multiple steps requiring somewhat trained personnel, making it harder to translate into field testing.

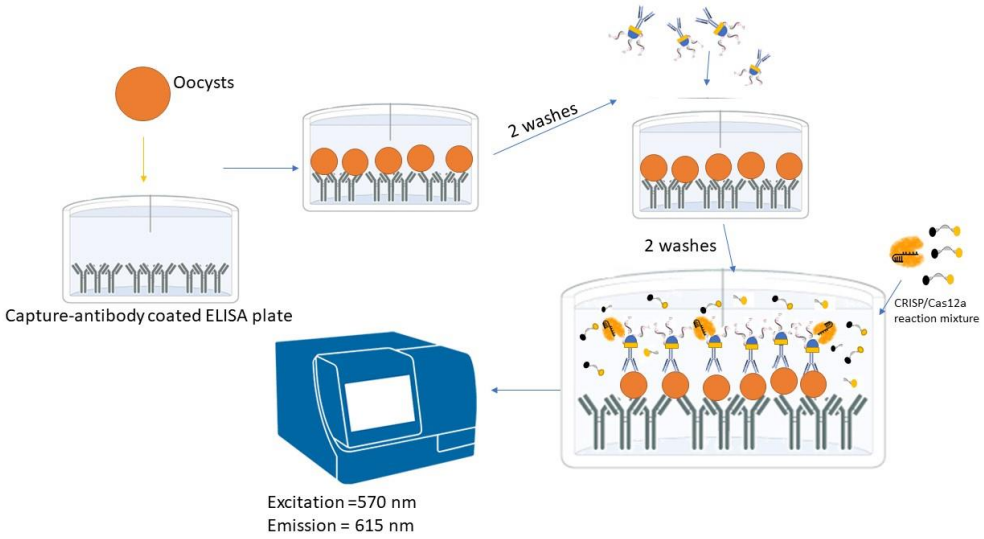

Figure 3. CRISPR/Cas12a sensing technique steps. Oocysts are first incubated with the capture antibodies and after thorough washing, the immunoprobe is added into the mixture. After binding to the oocysts, the mixture is washed to remove unbound probe and the CRISPR/Cas12a reaction mixture is added. Cas12a recognizes trigger DNA of the nanoprobe and goes into a cleaving frenzy, cleaving the fluorescence reporters as well. The fluorescence signal is then read by a fluorescence plate reader.

Laczka et al. (2013) also developed an ELISA-type biosensor where a conventional direct sandwich ELISA, based on capture polyclonal antibodies and HRP-labelled antibodies as primary antibodies is adapted to obtain a potentiometric signal. To do so, first they obtained the optimal parameters using a colorimetric direct sandwich ELISA relying on the same set of antibodies.

For the second part of this work, they modified a working electrode by coating it with capture antibodies via biotin-neutravidin chemistry. Once the capture antibodies were mounted onto the working electrode, *C. parvum* oocysts were incubated and captured by the probe, followed by the addition of HRP-labelled antibodies that bind the oocysts. The electrolyte solution contains sodium perborate, which produces hydrogen peroxide in water at low pH, and o-phenylenediamine (ODP), that acts as a

proton donor. HRP catalyzes the conversion of hydrogen peroxide into water and oxygen and OPD is converted to 2,3-diaminophenazine (DAP). The electron transfer produces an electrical potential that is measured by the electrodes. This electrical potential is proportional to the rate of enzymatic reaction mediated by HRP, which in turn, is proportional to the number of antibodies and therefore to the number of oocysts to which they bind. A diagram of this sensing scheme can be found on Figure 4.

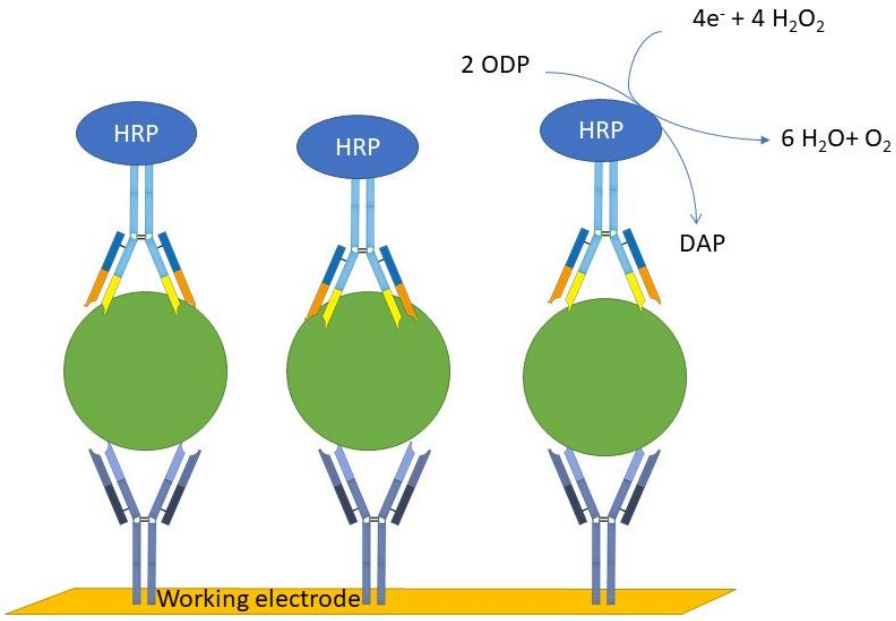

Figure 4. ELISA-modified sensing scheme. A direct sandwich ELISA is modified to have the capture antibodies immobilized into a working electrode as the solid phase. The enzyme-mediated redox reaction is measured by the electrodes instead of measuring the absorbance of an enzyme-mediated colorimetric reaction.

By using this sensing technique, they could obtain a LOD of 500 oocysts/mL, which represents a 2-fold improvement from the colorimetric method. The sensing platform gave a response in less than an hour, making it a fast and easy way of detecting *C. parvum*. This is a simple and cheap sensing platform that can be miniaturized and has the potential to detect *C. parvum* continuously, in real time. However, compared with other ELISA-modified sensors, it has a higher LOD.

In Kramer et al. (2007) the binding performance of polyclonal and monoclonal antibodies is reviewed alongside the effect of oocyst pre-treatment. The main purpose of this study was to evaluate the automation possibilities for *Cryptosporidium* detection by using systems like RAPTOR™ Plus 4S (Research International, Inc. Washington, USA). This device relies on a sandwich-like assay in which capture

antibodies are attached to the sensor, and after incubation with the sample and fluorophore-labelled antibody, the optical signal can be read.

For the evaluation of the performance of monoclonal and polyclonal antibodies, traditional ELISA assays were performed. Results showed that boiling and exposing the oocysts to a freeze and thaw cycle resulted in a 5-fold increase in the signal to noise (S/N) ratio, while bile treatment and SDS treatment to excyst the oocysts resulted in a 3-fold increase of the S/N ratio for polyclonal antibodies. Pre-treatment did not show a high difference in performance for monoclonal antibodies.

For the fiber optic-based biosensor, the LOD for polyclonal antibodies binding to boiled *Cryptosporidium* was 10^5 oocysts/mL, whereas non-boiled *Cryptosporidium* and monoclonal antibody-based assays showed a higher LOD of 10^6 oocysts/mL, showing the superior performance of pre-treating the oocysts. While this approach has a rather large LOD and it would not be compliant with EPA standards, it represents a step forward into automation for the continuous monitoring for *Cryptosporidium*.

2.2.2. Western blot-based assays

Dot-blotting refers to a series of techniques in which an antigen is first immobilized onto a membrane, followed by the detection via a molecular recognition element, such as antibodies (Stott, 1989). Western blot or immunoblot refers to a series of techniques that use antibodies to detect proteins post-electrophoresis. It usually involves the lysis of the cell and separation of proteins, followed by gel electrophoresis to separate proteins by size, transfer of the protein to a nitrocellulose membrane and visualization by an antibody labelled with an enzyme such as HRP (Shah, 2019).

Jenkins et al. (2008) used an SDS-PAGE immunoblot assay to detect *Cryptosporidium*. Instead of using antibodies that target oocyst wall proteins, their aim was to obtain a new antibody that targeted a viral symbiont present in *Cryptosporidium*, *Cryptosporidium parvum* virus (CPV) since there is a greater number of binding sites to this virus than the oocyst wall reactive proteins. After immunizing mice with recombinant CPV antigen, they used SDS-PAGE immunoblot to first obtain a specific antibody that binds to this antigen and later to determine the LOD.

The SDS-PAGE immunoblot consisted of a SDS treatment of the sample and marker proteins to denature and equalize the charge of all the proteins, followed by gel electrophoresis to separate them by molecular weight. After this, the proteins are transferred into a membrane by applying a vertical electric field. After skim milk treatment to block non-specific binding sites, the proteins are incubated with anti-CPV monoclonal antibodies, followed by washing and the incubation with secondary anti-mouse IgG ALP-labelled antibodies. After thorough washing, BCIP/NBT, which is the ALP substrate is added for a colorimetric signal.

By using this immunoblot approach they were able to detect as few as 10^2 oocysts. However, fluorescence microscopy results shows that this new antibody only binds to denatured proteins in the sporozoites walls. This means that a first pre-treatment is needed to excyst the sporozoites and a urea treatment is also needed to keep CPV protein denatured. These multiple steps make this sensing strategy tedious and moreover, highly qualified personnel and lab facilities are needed to carry out this sensing strategy, making it difficult to translate into a field-testing device.

Kniel & Jenkins (2005) used immuno dot blot to test the binding capabilities of an anti-CPV antibody for the detection of *Cryptosporidium* in fresh produce. The wash of a spiked produce sample was applied to an immuno dot-blot membrane, followed by skim milk treatment and incubation first with primary antibodies, then with biotin-labelled anti-rabbit IgG antibodies and then with avidin-ALP complex. Each step was followed by thorough washing. The addition of ALP chromogenic substrate provoked the color change. This approach proved to be highly efficient with as few as 10 oocysts being detected. Although immunoblotting is a relatively well known and established technique, the presence of somewhat trained personnel is needed. This study opens the door to *C. parvum* detection via the viral symbiont CPV, which allows targeting of a larger number of epitopes, compared with the epitopes on the oocyst wall.

In another approach, a sandwich dot-blot assay in which *Cryptosporidium* is immobilized in a nitrocellulose membrane has been developed (Thiruppathiraja et al., 2011). The oocyst-saturated membrane is incubated with gold nanoparticle probes. The gold nanoparticle probes have been dual functionalized with monoclonal anti-cyst antibodies that target the oocyst wall and alkaline phosphatase. The antibodies

selectively bind to the oocysts while alkaline phosphatase catalyze a reaction to render a color change. This sensor differs from traditional immuno-dot blot assay in the sense that they did not have to use two sets of antibodies: a primary antibody to bind to *Cryptosporidium* and a secondary ALP-labelled antibody to catalyze the colorimetric reaction. Instead, they used this gold nanoprobe. Since this probe contains more molecules of ALP per binding site compared to a single secondary antibody, the reaction is amplified, and the sensitivity was improved 500-fold.

2.2.3. Surface plasmon resonance-based sensors

Surface plasmon resonance (SPR) is a phenomenon that occurs when a photon of light hits a metal surface at a certain angle (angle of resonance). When this happens, some of the light excites the electrons in the metal surface, causing them to move and propagate parallel to the metal surface (this movement is also called surface plasmons), generating an electric field. This specific angle of resonance is highly dependant on the refractive index of the material near the surface and therefore highly sensitive to small changes in this surface. This way, measures can be obtained as changes in reflected light (Nguyen et al., 2015).

SPR-based biosensors incorporate a biorecognition element such as antibodies or aptamers that are immobilized onto the surface of a metal film where the surface plasmon occurs. When a target is present this biorecognition elements will bind to it, causing a change on the refractive properties of the surface and therefore a measurable change in the reflected light. These biosensors present valuable benefits, as they can monitor these changes in real time and they don't need labels (Phillips & Jirí Homola, 2008).

Kang et al. (2006) developed a real-time SPR sensor and improved it to achieve a lower LOD. The first approach for this sensor was to immobilize antibodies onto a chip using biotin-streptavidin chemistry. Samples containing the oocysts are injected over the conjugated surface and the changes in the SPR signal were measured. This approach allowed for real-time detection of *C. parvum* oocysts. However, it had a high LOD, of 10^6 oocysts/mL, because of the time required for the antigen-antibody complex to form.

The second approach utilized a modified flow-type SPR sensor and allowed for a much lower LOD of 10^2 oocysts/mL. In this approach, the biotinylated antibodies were first incubated with the oocysts, followed by washing by centrifugation to remove unbound oocysts. Afterwards, the *C. parvum* oocysts-antibody complexes were injected onto the streptavidin-coated SPR chip. The *C. parvum* bound biotinylated antibodies are then bound to the streptavidin on the SPR chip. This modified version, in which the binding event onto the SPR surface is not an immune reaction but a high affinity biotin-streptavidin link, improved the SPR limit of detection by four orders of magnitude compared to traditional flow-type SPR sensing. This sensing technique presented a low limit of detection for the modified version and has the potential for becoming a real time sensor.

While this was a highly sensitive sensor that could be used as a real-time sensor, specificity towards other microorganisms and debris needs to be determined for real-time monitoring of environmental samples. Since a centrifugation step is needed for the modified version, its application is likely limited to a lab setting, and it cannot be easily used for field testing.

Similarly, Kang et al. (2008) developed an SPR-based inhibition assay. In this case, unbound primary antibodies bind to secondary antibodies immobilized on the chip surface instead of relying on direct *Cryptosporidium* binding to the capture antibodies at the surface. In this case, they first developed a heterogeneous self-assembled monolayer at the end on the chips surface to reduce steric hindrance and increase the accessibility of biomolecule to the sensor surface. This self-assembled monolayer was made out mixed thiol groups bound to streptavidin at the end via EDC/NHS chemistry. Via biotin-streptavidin chemistry, which enhanced the orientation of capture antibodies, they coated the chip surface with secondary antibodies that served as capture antibodies. Oocysts and primary antibodies were first incubated together in a batch-to-batch basis. After incubation, unbound antibodies are separated from the oocysts by centrifugation and the unbound antibodies were run through the biosensor. Secondary capture antibodies will bind primary unbound antibodies, rendering a signal that was inversely proportional to the oocyst's concentration.

This sensor was able to detect oocysts in a 10^2 – 10^6 range in ideal buffer conditions. By using an inhibition assay they were able to improve the analyte binding conditions, since unlike oocysts, antibodies are hydrophilic and render a higher SPR signal. When tested in the presence of other microorganisms as well as tap and environmental water, the sensor, while able to detect *Cryptosporidium*, lost some of the sensitivity. While this approach could improve the detection signal, the limit of detection was the same as the previous SPR approach. Moreover, and inline with the previous approach, the need for a centrifugation step makes this approach only suitable for laboratory settings. While SPR sensors have the ability of becoming a real-time monitoring tool, the need for batch-to-batch incubation and centrifugation makes real-time monitoring not easily achievable on-site or in more remote locations.

2.2.4. Electrical and Electrochemical sensors

There are also a good number of biosensors that rely on electrochemical signals to obtain a response. Some of them can measure changes in the proximity of a sensor surface, in such a way that upon oocyst binding, the sensor records a change in signal. For example, in Luka et al. (2019), the researchers coated a gold electrode sensing interface with capture antibodies using Protein G chemistry, in which recombinant protein G with a thiol group was first incubated with the electrode, followed by washing and incubation with the capture antibodies. The formation of an oocyst-antibody complex produced a change in the capacitive/dielectric properties of the sensor, and this change was measurable and proportional to the number of antibodies captured.

Different dilutions of *C. parvum* oocysts were incubated with the sensor, followed by washing and drying and capacitance measurements. They measured a distinct change in capacitance for different concentrations of *Cryptosporidium* and achieved a limit of detection of 40 oocysts/mm^2 or 40 oocysts/5 µL (8,000/mL). A calibration curve measuring the relative capacitance change, with linear response in the range of 15 to 153 oocysts/mm^2 was used to quantify the number of oocysts. These measurements were also confirmed via FITC-labelled antibodies and fluorescence microscopy.

This sensor represents a quick and easy way to measure *Cryptosporidium*, compared to traditional methods. It involves a smaller number of steps compared to

EPA method 1623 and has a great potential to be used in the detection of multiple molecules and pathogens. The fact that only one set of label-free antibodies is needed also reduces production costs and complexity. Although simplified, this sensor needs a washing and drying step that should be performed by somewhat trained personnel, making field testing applications less realistic. The LOD is large, considering the low number of *Cryptosporidium* needed for infection. More tests using other microorganisms are needed to confirm the selectivity of the sensor, as well as more complex matrixes.

Similarly, Poitras et al. (2009) developed a biosensor that uses a quartz crystal microbalance with dissipation monitoring (QCM-D) as the biosensor platform. QCM-D works by measuring mass changes as well as changes of the viscoelastic properties at the surface. The sensor is excited by an alternating voltage and the subsequent resonance frequency is monitored. This frequency is affected by the mass adhering to the sensor surface, and the changes in frequency can be monitored.

For this biosensor, anti-*Cryptosporidium* capture antibodies were physically adsorbed onto a gold sensing surface. The sensing strategy consisted of physisorption of the antibodies to the gold surface, followed by incubation with the sample for 60 min and a 10 minutes rinse to remove unbound substances. Shifts in the crystal frequency were continuously monitored. An increase of the resonance frequency and energy dissipation factor was observed with an increase of time, while control experiments rendered no visible change.

This sensing platform was able to detect 10^5 oocysts/mL under clean conditions, i.e., a suspension of oocysts in PBS. However, when tested for potential interferences it was found that humic and fulvic acids, while generating a response close to clean conditions, could in some of the cases cause a slight decrease of the signal. For colloidal contaminants, tested by using latex microspheres, caused a decrease of up to 64% in signal. The effect of other pathogens was also tested using *Escherichia coli* and *E. faecalis*. The sensor showed no response to these pathogens alone. In other words, it was selective for *Cryptosporidium*, yet the sensor showed a decrease in signal when *Cryptosporidium* was in the presence of said pathogens. Although this sensor's limit of detection is rather high and more work needs to be put into improving the sensitivity, it

highlights the need for testing *Cryptosporidium* sensors against more complex matrices, including the presence of bacteria.

In Luka et al. (2022) an electrochemical, portable on-chip biosensor was developed. In this on-chip electrochemical sensor, an antibody self-assembled monolayer (SAM) was assembled onto the chip electrodes by using protein G chemistry. For that purpose, after pre-treatment of the gold chip, thiol-Protein G was first attached to the gold surface to act as the linker between the gold surface and the antibodies. Electrochemical impedance spectroscopy (EIS) was used as the electrochemical method to detect *Cryptosporidium*. In the absence of *Cryptosporidium*, $[Fe(CN)_6]^{3-/4-}$, present in the buffer, permeates and reaches the surface of the electrode where an electrochemical redox reaction provokes a measurable change of current in the surface. When the oocysts are present, an increased resistance for the permeation of $[Fe(CN)_6]^{3-/4-}$ to reach the gold chip, dampens the redox reaction. A range of 0-300 oocysts/ 5 µL was tested on this chip, proving to be a highly sensitive method, achieving a range of detection between 20-200 oocysts/ 5 µL or 4,000 to 40,000 oocysts per mL. Higher concentrations of oocysts saturated the binding sites.

Although this biosensor has the potential to be used in field testing procedures, the small amounts needed to add to the sensor (5 µL) makes the detection of large samples difficult. Some prefiltration steps would also be needed to retrieve a working number of oocysts from environmental samples. Moreover, resuspension of captured oocysts in small liquid volumes is ineffective, leaving many oocysts adhered to the filter. Larger liquid volumes need to be used for resuspension, which would make the sensor either less efficient, or it would need an extra concentration step such as magnetic beads or centrifugation.

2.2.5. Aptamer-based sensors

Aptamers are short single-stranded nucleic acids that can serve as a biorecognition element. Aptamers are selected *in vitro* via systematic evolution of ligands by the exponential enrichment (SELEX) process. This is an iterative process that takes a large, randomized oligonucleotide library and selects sequences based on their affinity for a target molecule (Tanner et al., 2018).

The aptamer mechanism of biorecognition is based on their ability to fold into a unique 3D structure in the presence of a target molecule. Analogous to antibodies, it is this specific folding that allows aptamers to bind to the targets with high affinity and specificity. This allows aptamers to be used for many applications such as therapeutic elements, reagents for affinity purification or as biosensor elements (Nakamura, 2011).

Analogous to antibodies, aptamers can fold into defined three-dimensional shapes that can bind to a wide variety of targets. They are often smaller than antibodies in size, cheaper to synthesize and easier to chemically modify. Moreover, they can bind to a wider variety of target, including non-immunogenic ones (Henri et al., 2019).

Some aptamer-based biosensors have been used for the detection of *Cryptosporidium*. In Iqbal et al. (2015), an aptamer for the detection of *C. parvum* in food was developed using the SELEX process. They performed 10 rounds of selection, starting by one round of positive selection, followed by alternating 6 rounds of positive and negative selection against *Giardia duodenalis* and three rounds of positive selection.

After aptamer selection, an electrochemical sensor was developed. A gold nanoparticle-modified screen-printed carbon electrode was coated with the aptamer. When an oocyst attached to the aptamers in the electrode, it caused an increase in the redox current that could be measured by square wave voltammetry. Upon binding, the aptamers underwent a conformational change and surface restructuring, which in turn, allowed the reagents needed for the redox reaction to penetrate more freely to the electrode, causing the increase in the redox current.

This aptasensor was used to compare the binding affinity of 14 aptamer clones selected during the SELEX process as well as to determine the limit of detection of the highest binding aptamer, R4-6. The limit of detection was shown to be 100 oocysts. *Giardia duodenalis* was used on this sensor to test the selectivity of the aptamers. It was found that the aptasensor is specific to *C. parvum*, although more research is needed to determine if the aptamer is genus-specific. The aptasensor was also tested against more complex food materials like pineapple and mango juice, and it was determined to be able to detect oocysts in those matrices.

This sensor proved to be able to detect oocysts with high sensitivity and specificity and with low processing time. However, the high complexity of the sensor makes it difficult to use in field testing and without trained personnel.

Drawing from this previous work, Iqbal et al. (2019) developed a sandwich-like assay in which 3' biotinylated R4-6 aptamer was conjugated to streptavidin-coated magnetic beads, as a concentration step. This sensing strategy used the aptasensor developed previously (Iqbal et al., 2015) to perform electrochemical measurements and using the aptamer-coated magnetic beads as a concentration step.

For this approach, in the case of environmental samples, 500 mL of spiked environmental water samples from different locations were first filtered using a flatbed filtration unit with a 0.2 µm pore size. The top of the filter was collected, centrifuged, and resuspended in 100 µL of PBS. For both PBS and environmental spiked samples, magnetic-bead conjugated aptamers were added, and the mixture was incubated for 2h at room temperature. The oocysts were then magnetically recovered from the mixture and the magnetic bead-aptamer-oocysts complex was incubated with the previously developed electrochemical aptasensor (Iqbal et al., 2015) .

By following this sensing strategy, a limit of detection of 50 oocysts was achieved, proving the efficiency of the magnetic separation step. This sensing strategy was also used in *Giardia duodenalis*, showing a high specificity towards *Cryptosporidium*. This sensor proved to be sensitive and specific towards *C. parvum* in both DPBS and water samples. Like their previous approach, the high complexity of the sensor makes it difficult to use in the field and without trained personnel.

On the other hand, Hassan et al. (2021) studied the effect of truncation on R4-6. Aptamers are usually 50-100 nucleotides long, but oftentimes, the binding region is much shorter. By reducing the length of the aptamer, they become easier and cheaper to synthesize. In this study, aptamers were conjugated to magnetic beads, by labelling the aptamer with an amine group at the 3' end and using EDC/NHS chemistry. To review the binding affinity of the previous and newly reported shorter aptamers, as well as the aptamers after conjugation with magnetic beads, aptamers were either labelled with fluorescein only at the 5' end, or double labelled with fluorescein (6-FAM) at the 5' end

and an amine group at the 3' end for conjugation. Flow cytometry was then used to determine the binding of the aptamers. After confirming the binding of the aptamer, it was found that one of the shorter aptamers, Min_Crypto2, was one with a higher binding affinity, and therefore used further. It was also found that the other half of the truncated aptamer, Min_Crypto1, also had binding properties, and they attributed this to the original aptamer having two binding domains.

Flow cytometric analysis of the three aptamers was also performed on *Giardia duodenalis* and *Cryptosporidium muris* to test the specificity of the aptamers. It was determined that Min_crypto2 conjugated with Dynabeads® showed the highest binding affinity towards *C. parvum* and the lowest non-specific binding towards *Giardia duodenalis*; however, there was cross-reactivity against *Cryptosporidium muris* and *Cryptosporidium hominis,* indicating that they could be genus-specific aptamers.

In this work, they also developed a sensing strategy that did not involve the use of flow cytometry. Using magnetic beads-functionalized aptamers and aptamers labelled with fluorescein (6-FAM) they developed a sandwich-like assay in which the oocysts were first incubated with the aptamers labelled with 6-FAM, and then washed, centrifuged, and incubated with magnetic bead-conjugated aptamers. After magnetic separation, the sample's fluorescence was determined using a plate reader. By using this sensing strategy, they determined that the LOD was 5 oocysts/ 300 µL in wastewater samples. Aptamers are much more stable long term, compared to antibodies and easier to functionalize for commercial kits. However, the need for a centrifuge and a plate reader makes it difficult to apply to field testing applications. Although they achieved a very good LOD of the spiked samples, these were only 300 µL volumes. Normally, large amounts of water (10 L by EPA method 1623) need to be processed to determine whether there is a risk to human health or not. Therefore, a pre-filtration step is needed to use this approach.

2.3. Flow cytometry and its role in *Cryptosporidium* detection.

Flow cytometry is an important tool capable of quantitative measurement on single cells or particles within a liquid suspension as they pass through one or multiple lasers. For each particle, fluorescence, and light scatter (size and complexity parameters) information is collected. It has been extensively used for routine measurements of

nucleic acid content, enzyme activity, calcium flux, membrane potential and intracellular pH. Conjugation of fluorophores (fluorescence molecules) to capture elements like antibodies has also been extensively used to specifically single out cells in a liquid stream via flow cytometry (Cram, 2002).

Conventional flow cytometers are based on three types of components: fluidics, optics and electronics. The fluidics system is based on a sheath fluid that is pressurized to deliver cells within a liquid suspension to the laser beam. Optics are comprised of excitation lasers and collection optics (detectors). Finally, the electronic systems convert the signals from the detectors into digital signals (McKinnon, 2018). The general overview of the functioning of a flow cytometer can be visualized in Figure 5.

Typically, a single cell or particle in a liquid suspension that present certain characteristics and possibly some fluorochromes is passed through one or more excitation laser beams. The fluorochromes are then excited and emit photons at their respective wavelength. These photons are then sorted by using a series of dichroic filters and bandpass filters that subdivides this light into different wavelengths. Dichroic filters allow for wavelengths that are shorter or longer than a certain number to pass while reflecting the remaining ones. Bandpass filters detect only a small window of a specific wavelength and therefore determine the wavelengths that are detected (McKinnon, 2018).

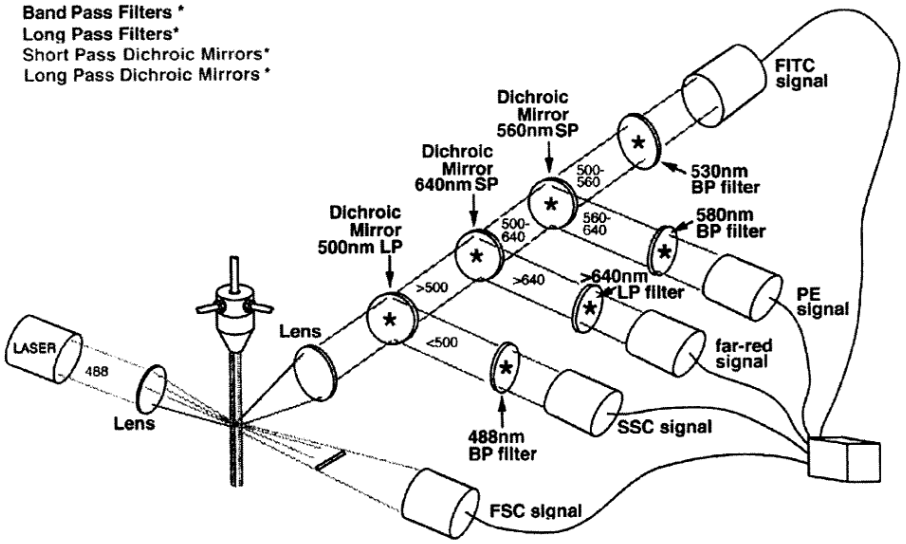

Figure 5. Functioning diagram of a conventional flow cytometer. Source: *(Cram, 2002)*

Imaging flow cytometers present themselves as a combination of conventional flow cytometry and fluorescence microscopy. It has the advantage of being able to collect morphological and fluorescence parameters of a large array of cells, while presenting the advantage of allowing for event identification through their real image (Barteneva et al., 2012).

Imaging flow cytometers work like conventional ones: a flow of monodisperse cells are run through excitation lasers; however, imaging flow cytometers are also equipped with an LED that produce transmitted light, so that a brightfield image of the cells or events can be produced. Once the events are passed through the brightfield and excitation lasers, the light collected goes through a magnification lens. After this lens, the signal is passed on to the next area, which is like conventional flow cytometry. This next area consists of a stack of filters that subdivides the signal derived from the excitation laser in different wavelengths and then this signal hits the detector. Unlike conventional flow cytometry where the detector is only able to measure a pulse profile, this detector is a CCD camera that gives a set of spectrally decomposed, spatially registered images (Andrew Filby, 2019). These mechanisms are represented in Figure 6.

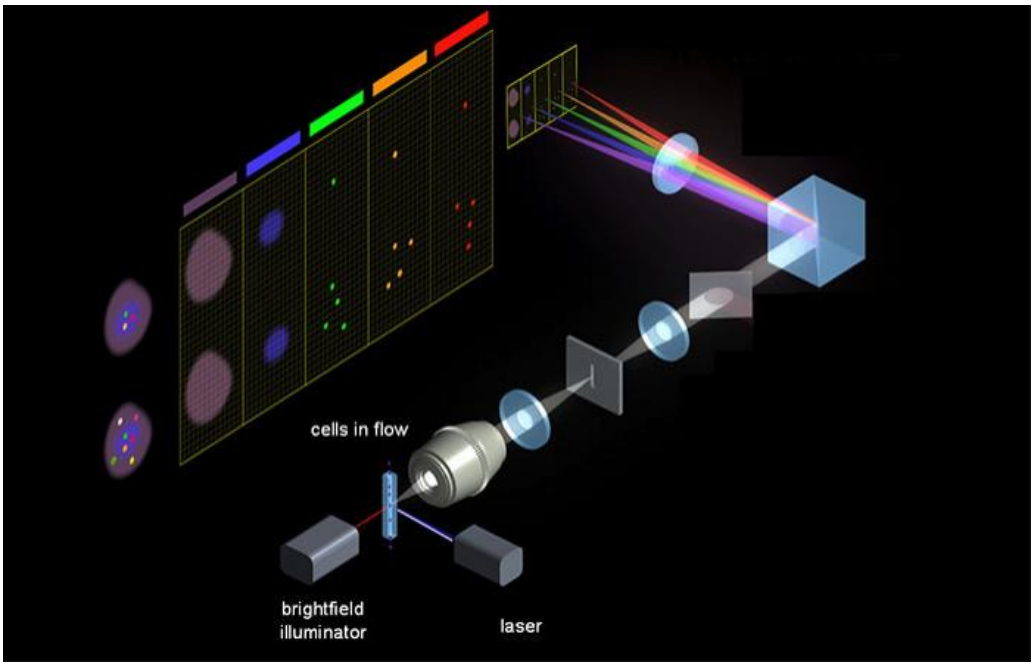

Figure 6.Functioning diagram of an imaging flow cytometer. Source: Amnis corporation

2.4. Conclusions

Cryptosporidium is a protozoan parasite that presents a wide number of characteristics that makes its detection needs peculiar. Its low infectious doses require biosensors with a very low limit of detection crucial for the detection and control of outbreaks in water systems and recreational waters.

The limits of detection range from single oocyst detection in 100 µL (10 oocyst/mL) achieved by Li et al. (2021) to 500 oocysts/mL by Laczka et al. (2013). However, while these limits of detection seem to be low, the volumes processed by these sensing techniques are in the microliters range.

To be objectively safe in the detection of *Cryptosporidium*, larger amounts of water need to be tested. EPA Method 1623 requires a 10 - 50 L sample to be filtered and processed and since the occurrence of *Cryptosporidium* in nature happens in very low concentration, filtration steps and recovery techniques need to be addressed by these biosensing platforms to make them truly suitable for the detection of *Cryptosporidium* in environmental and recreational waters. Recovery of *Cryptosporidium* from filtered samples is also an important step that could be crucial to the detection of pathogenic amounts of *Cryptosporidium* in water. Another important factor to take into consideration is the ability of these sensors to be easily deployed in the field.

Cryptosporidium was the leading cause of waterborne disease outbreaks linked to recreational water during the 2001-2010 period (*General Information for the Public | Cryptosporidium | Parasites | CDC.* 2021). This parasite is also highly resistant to traditional chlorination (Adeyemo et al., 2019). Having a biosensor that is easy to use by pools and recreational facilities staff could prevent large outbreaks linked to recreational waters. The biosensors previously described, although easier to deploy and perform than the gold standard method (which requires expert microscopy), are still bound to a lab setting. ELISA-based methods require thorough washing, which needs to be done correctly to avoid false positives, as well as proper handling of reactive agents, which are sensitive to ambient conditions.

Other biosensors also have the need for lab equipment such as plate readers, which make the field deployment difficult. While these biosensors proved to be good alternatives to EPA 1623, there is a need for these technologies to be simplified to be able to be used by the general public and there is also a need in this field for biosensors that can use easy to transport equipment or that do not require equipment at all. While some researchers addressed some of the detection issues with more complex matrices, there is also a need to address the presence of other interference materials in natural water sources to make the devices and approaches truly suitable for field testing.

3. Binding properties of inactivated *Cryptosporidium*

C. parvum is a pathogen classified as a Risk Group 2 microorganism and as such it needs Containment Level 2 facilities to work with the live parasite (Public Health Agency of Canada, 2011). This makes working with the live microorganism only available for laboratories with a Biosafety Level 2 classification. To overcome this and/or to make it safer to handle this pathogen, inactivated *C. parvum* can be used. Commercially available inactivated *Cryptosporidium* are inactivated either by suspension in 5% formalin, heat-treated (15 minutes, 70 ºC) or freeze-treated (24 hours, between -20 to -15 ºC) (Waterborne, INC). Other inactivation methods include desiccation. Robertson et al. (1992) assessed *Cryptosporidium* viability after air-drying a sample containing 10^6 oocysts and concluded that after 4 or more hours of drying, the samples had no viable *Cryptosporidium*, implying a log 6 reduction in viability. Moreover, desiccation, alongside heat-treatment and freeze-treatment are listed as physical inactivation methods in the pathogen safety data sheet provided by health Canada (Public Health Agency of Canada, 2011).

Inactivation processes can, however, change the way different binding elements such as aptamers and antibodies bind to their target. Formalin fixation causes the denaturation and cross-linking of proteins that could lead to either a change in the epitopes (antibody binding sites of a target), modification of the epitopes by direct binding to them or a blocking of the epitopes (Otali et al., 2009). Moreover, Li, T. et al. (2021) studied the effect of heat treatment on the antigenicity of β-conglycinin and determined that heat treatment can affect the antigenicity of the protein by changing its structure.

Usukura (1993) proposed freeze treatments as an alternative fixation method for retinal cells as it can retain the antigenicity of the cell proteins as well as the overall structure. Moreover, Phillip et al. (1984) studied the effect of antigenicity of sperm cells after freezing and thawing and found no significant removal of surface proteins from the cell structure.

While Boi et al. (2016) mention that drying of tissues would in general cause some loss of antigenicity, Jennens (1954) conclude that drying processes do not seem

to damage bacterial antigens and Ho et al. (2009) found that red blood cells are well preserved via desiccation and maintain the necessary antigen-antibody reactions for cell surface markers.

In this Chapter, different methods of inactivation and different binding elements have been studied to assess the influence of inactivation procedures on cell surface changes and binding properties, as well as their influence on the LOD. More specifically, this chapter focuses on studying: the effects of inactivation processes on limits of detection via antibody binding; the effects of inactivation processes on antibody binding; and the binding properties of aptamers to inactivated *Cryptosporidium*.

1. Effects of inactivation processes on limits of detection via antibody binding

The objective of this part of the study was to determine whether the process of inactivation affects the surface structures of the oocysts and thus, the binding capabilities of Horseradish peroxidase (HRP) labelled polyclonal antibodies to *C. parvum* and therefore the limit of detection achievable by this method. Various inactivation methods were examined: heat-treatment, freeze-treatment and formalin-treatment. Live *Cryptosporidium* was used as the control.

To test the binding of antibodies to *Cryptosporidium*, HRP-labelled antibodies were used and a modified ELISA assay was used to determine a limit of detection but instead of binding the oocysts to a solid phase, removal of unbound antibodies was performed by centrifugation. Briefly, 10- fold dilutions of oocysts were made in microcentrifuge tubes and equal amounts of HRP-labelled antibodies were added to each vial. After incubation and removal of unbound antibodies by centrifugation, samples were transferred to a 96-well plate and TMB was added. The HRP present in the antibodies bound to the oocysts catalyzed the TMB colorimetric reaction. A graphic summarizing this assay is presented in Figure 7.

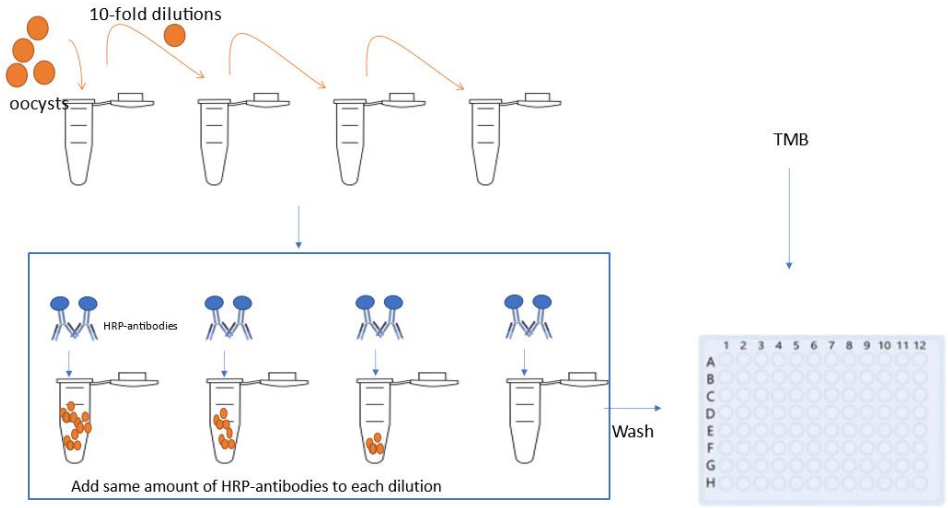

Figure 7. Graphical representation of the approach taken to determine the limit of detection via the use of HRP-labelled antibodies

2. Effects of inactivation processes on antibody binding

This work was done to further explore the effect of inactivation processes on *C. parvum* and the integrity of the binding mechanisms between oocysts and antibodies in a variety of inactivation procedures.

Two different protocols for immunostaining were performed. In protocol 1 live oocysts are first inactivated via different methods: desiccation, formalin inactivation, freeze treatment and heat treatment. After the inactivation process, oocysts are incubated with the antibodies and binding is assessed via flow cytometry.

The second protocol binds the antibodies to the oocysts first and then the samples undergo the different inactivation processes. Binding is again assessed via flow cytometry. The aim of the different protocols is to determine whether there is a protective role on the antigens by securing the binding first or, on the other hand, the inactivation process negatively affects the integrity of the antibodies or the antibody-antigen bond.

3. Binding properties of aptamers to inactivated *Cryptosporidium*

The objective of these experiments was to determine whether the inactivation of *Cryptosporidium* affects structures that are critical to aptamer binding. Since aptamers bind to a wide array of targets, including non-immunogenic ones, binding of

antibodies does not necessarily mean that the structures necessary for aptamer binding are conserved during inactivation.

To test the binding of *Cryptosporidium*, two procedures were tested. First, the live *Cryptosporidium* was inactivated and then, the aptamers were added. The second procedure was to first bind the aptamers to the live *Cryptosporidium* and afterwards different inactivation processes were tested.

To test this binding, R4-6 aptamer labelled with fluorescein (6-FAM) on the 5' end was used and like the previous antibody procedure, flow cytometry is performed to assess the binding as a function of the measured fluorescence intensity.

3.1. Materials and Methods

Both live and formalin-inactivated *Cryptosporidium* were acquired from Waterborne INC through its supplier in Canada, Cedarlane Laboratories. Polyclonal IgG Anti-*Cryptosporidium* HRP-labelled antibodies were purchased from GeneTex Inc. (Catalog number: GTX36458). Polyclonal IgG Anti-*Cryptosporidium* FITC-labelled antibodies were purchased from GeneTex Inc. (Catalog number: GTX36306). Phosphate-buffered saline (PBS, 10 X), pH= 7.4 was bought from Alfa Aesar and further diluted to 1X in deionized water (DI water). 3,3',5,5'-Tetramethylbenzidine (TMB) was purchased from Sigma-Aldrich (Cat. No :860336). All other reagents were of analytical grade. Aptamers labelled with fluorescein (6-FAM) at the 5' end were obtained from Integrated DNA Technologies (IDT) The aptamer sequence used was R4-6 (Table 3).

3.1.1. Heat-treatment for *Cryptosporidium* inactivation

110 µL of live *Cryptosporidium* stock solution (10^8 oocysts / 8 mL) was placed in a 1.5 mL microcentrifuge tube and centrifuged at 15000 x g for 5 minutes. The supernatant was discarded, and the pellet was resuspended in 1X PBS (pH=7.4). The microcentrifuge tube was placed in a hot water bath at 80 ºC for 20 minutes, before being cooled down to room temperature.

3.1.2. Freeze-treatment for *Cryptosporidium* inactivation

110 µL of live *Cryptosporidium* stock solution (10^8 oocysts / 8 mL) was placed in a 1.5 mL microcentrifuge tube and it was centrifuged at 15000 x g for 5 minutes. The supernatant was discarded, and the pellet was resuspended in 1X PBS (pH=7.4). The

microcentrifuge tube was then placed in the freezer between -21 to -15 ºC for 24 hours. After that period, it was thawed to room temperature.

3.1.3. Formalin-treatment for *Cryptosporidium* inactivation

Formalin 5% was prepared in PBS (1X, pH=7.4). Oocysts (10^8 oocysts / 8 mL) were centrifuged and resuspended in formalin 5% solution and left to incubate for at least 24 hours prior to use at 4ºC.

3.1.4. Desiccation for *Cryptosporidium* inactivation

100 µL of oocysts ($1.25x10^7$ oocysts/mL) were placed on glass slides and left to dry overnight at room temperature. The oocysts were collected and suspended in buffer by running 4 mL of DPBS over the glass slide and collecting the liquid, followed by a concentration step by centrifugation (5 min at 15,000 g).

3.1.5. Binding test of HRP-labelled polyclonal antibodies

Different concentrations of oocysts (10^8, 10^7 ,10^6 ,10^5 ,10^4 ,10^3 and 0 oocysts/mL for formalin-inactivated *Cryptosporidium* and 10^7 ,10^6 ,10^5 ,10^4 ,10^3 and 0 oocysts/mL for the rest of the samples) were incubated with 1 µg/mL of anti-*Cryptosporidium* HRP-labelled antibody for 1 hour in microcentrifuge tubes.

Solutions were washed twice by centrifuging the samples at 15000 x g for 5 minutes, discarding the supernatant and resuspending the pellet in PBS 1X (pH= 7.4). The final resuspension was transferred to a 96-well plate and TMB was added. Results were recorded after 10 minutes. Experiment was performed at room temperature.

3.1.6. Binding protocol 1 for FITC-labelled antibodies

100 µL of FITC-labelled antibodies at a concentration of 5 µg/mL were added to 100 µL of 10^6 inactivated oocysts and incubated for an hour on a shaker. After the incubation period, tubes were centrifuged at 15,000 x g for 5 minutes and the supernatant was discarded. The pellet was resuspended in 200 µL of PBS 1X and taken to a flow cytometer (BD Accuri™ C6 Plus, excitation at 488 nm). Emission was recorded in the green fluorescence range (FITC). Experiment was performed at room temperature.

3.1.7. Binding protocol 2 for FITC-labelled antibodies

100 µL of 10^6 oocysts were incubated with FITC-labelled antibodies at a concentration of 5 µg/mL for one hour on a shaker. After the incubation period, various inactivation procedures were performed on the samples. To remove unbound antibodies, vials were centrifuged at 15,000 x g for 5 minutes and the supernatant was discarded. The pellet was resuspended in 200 µL of DPBS and taken to a flow cytometer (BD Accuri™ C6 Plus, excitation at 488 nm). Emission was recorded in the green fluorescence range (FITC). Experiment was performed at room temperature.

3.1.8. Binding protocol 1 for (6-FAM)-labelled aptamers

100 µL of R4-6 aptamer at a concentration of 50 µM was added to 100 µL of 10^6 of inactivated oocysts and incubated for an hour on a shaker. After the incubation period, vials were centrifuged at 15,000 x g for 5 minutes and the supernatant was discarded. The pellet was resuspended in 200 µL of DPBS and taken to a flow cytometer (BD Accuri™ C6 Plus, excitation at 488 nm). Emission was recorded in the green fluorescence range (FITC). Experiment was performed at room temperature.

3.1.9. Binding protocol 2 for (6-FAM)-labelled aptamers

100 µL of 10^6 oocysts were first incubated with 100 µL of R4-6 aptamer at a concentration of 50 µM for one hour in a shaker. After the incubation period, various inactivation procedures were performed on the samples. To remove unbound aptamers, vials were centrifuged at 15,000 x g for 5 minutes and the supernatant was discarded. The pellet was resuspended in 200 µL of DPBS and taken to a flow cytometer (BD Accuri™ C6 Plus, excitation at 488 nm). Emission was recorded in the green fluorescence range (FITC). Experiment was performed at room temperature.

3.1.10. *E. coli* negative control assays

E. coli strain ATCC 10798 was grown on laurel sulphate broth for 24 hours at 37 ºC. After 24hours it was centrifuged at 5,000 g for 5 minutes and resuspended in PBS 1X + Formalin 5%. This suspension of *E. coli* was used for all the negative control experiments. *E. coli* was then stained according to Binding protocol 1. Experiment was performed at room temperature.

3.1.11. Flow cytometry

A minimum of 5,000 events were collected with the ImageStream® X Mk II Imaging Flow Cytometer and 10,000 events with the BD Accuri™ C6 Plus. Samples run on the ImageStream ® X Mk II Imaging Flow Cytometer were restricted to those that were formalin-inactivated by a commercial supplier. Analysis of flow cytometry data was done with the free online software floreada.io: https://floreada.io/. This software allows for the processing data of flow cytometry (.fcs) files.

To analyze the data, the first step was to gate or select the oocyst population in a front versus side scatter plot (FSC -vs- SSC). The gating process consisted of selecting a grouping of events in a scatter plot that represented the population of cells of interest. Cells exhibit certain unique characteristics such as size and granularity, which makes them form a distinct population in this type of scatter plot.

3.2. Results and Discussion

3.2.1. Studying the effects of inactivation processes on visual and absorbance-based limits of detection following antibody binding

3.2.1.1. Live Cryptosporidium oocysts

Following the procedures shown in Figure 7, the results recorded in each microwell plate visually, as well as the absorbance values registered via spectrophotometry are shown in Figures 8 and 9.

Figure 8. Visual limit of detection for live Cryptosporidium using HRP-labelled antibodies. A blue color indicating the presence of oocysts is shown.

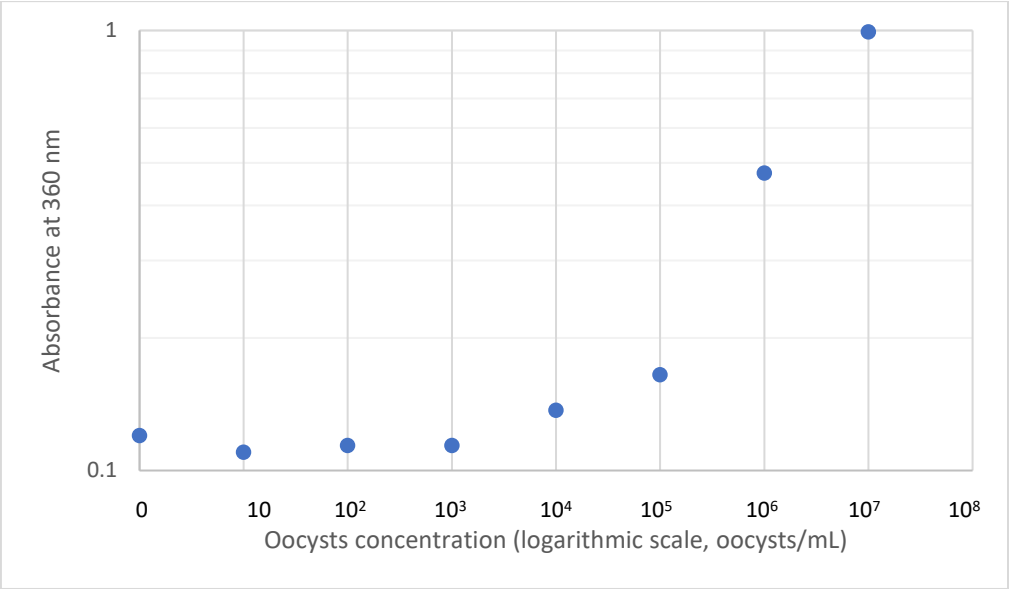

Figure 9. Detection of live Cryptosporidium obtained through absorbance. Absorbance at 360 nm as a function of oocyst concentration is shown.

The limit of detection was determined visually and through absorbance. However, since the main focus of these thesis is the future use of these antibodies and techniques for a colorimetric biosensor easy to use by the general public, the visual limit of detection was taken as the main parameter in further discussion. For the visual approach, the limit of detection would be what the naked eye can easily distinguish as signal. This LOD is 10^5 oocysts/mL for live oocysts.

Results for absorbance are given on a logarithmic scale. For these experiments these curves start in a plateau, in which absorbance is undistinguishable from point to point, until some detection can be achieved, which translates in a colorimetric blue signal and an increase in the absorbance at 360 nm, this increase then proceeds to be rather lineal.

To determine the limit of detection through absorbance, the signal-to-noise ratio (S/N) (obtained as the ratio between the absorbance peak at 360 nm for each oocyst concentration divided by the absorbance peak at 360 nm for the control) was calculated. For all the cases a S/N equal or superior to 1.3 was chosen to be the limit of detection. This threshold was chosen because points contained in them were considered reliably different from the control. The results for signal to noise ratio and the limit of detection obtained through absorbance is presented in Table 1.

Table 1. Determination of the signal to noise ratio for live Cryptosporidium

Oocyst concentration (oocysts/ mL)	Absorbance at 360 nm	Signal-to-noise ratio
10^7	0.992	8.27
10^6	0.474	3.95
10^5	0.165	1.38
10^4	0.137	1.14
10^3	0.114	0.95
10^2	0.114	0.95
10	0.11	0.92
0	0.12	1.00

The limit of detection, corresponding to the minimum value with a S/N equal or superior to 1.3, corresponds to 10^5 oocysts/mL for live oocysts.

3.2.1.2. Formalin-inactivated Cryptosporidium oocysts

Following the procedures shown in Figure 7, the results recorded in each microwell plate visually, as well as the absorbance values registered via spectrophotometry are shown in Figures 10 and 11.

Figure 10.Visual limit of detection for formalin-inactivated Cryptosporidium using HRP-labelled antibodies. A blue color indicating the presence of oocysts is shown.

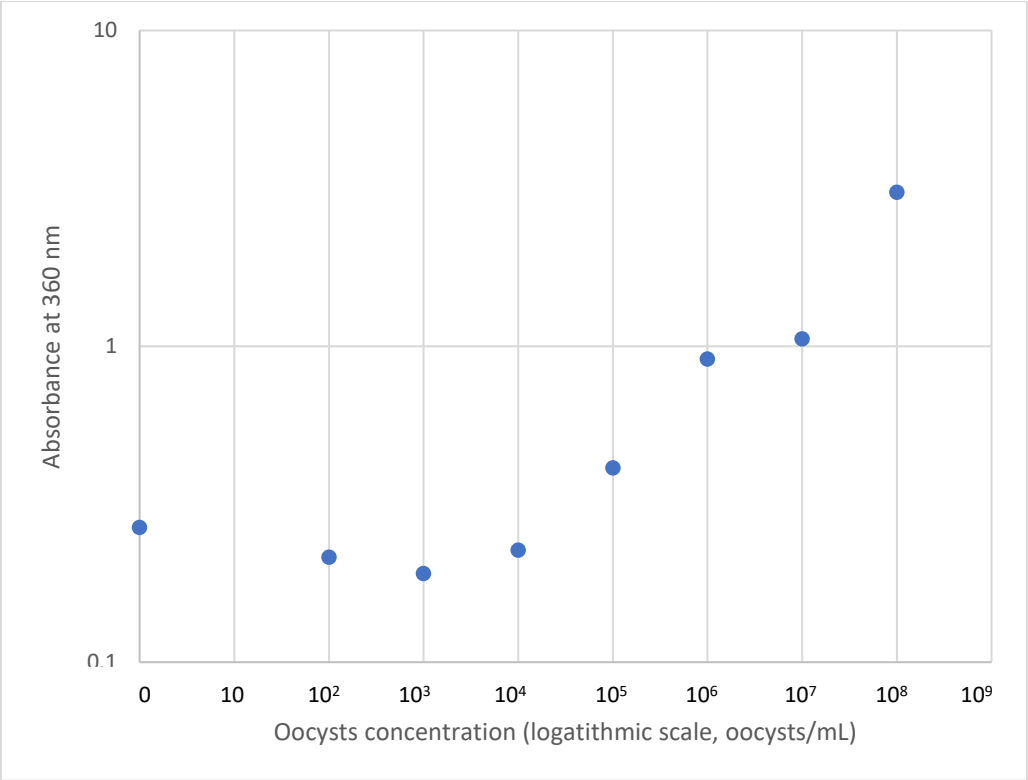

Figure 11.Limit of detection for formalin-inactivated Cryptosporidium obtained through absorbance. Absorbance at 360 nm as a function of oocyst concentration is shown

These results show that the visual limit of detection is 10^5 oocysts/mL. The S/N ratio is also calculated and shown in Table 2.

Table 2.Determination of the signal to noise ratio for formalin-treated Cryptosporidium

Oocyst concentration (oocysts/ mL)	Absorbance at 360 nm	Signal-to-noise ratio
10^8	3.07	11.51
10^7	1.05	3.95
10^6	0.91	3.41
10^5	0.41	1.54
10^4	0.22	0.84
10^3	0.19	0.71
10^2	0.21	0.80
0	0.26	1

The limit of detection, corresponding to the minimum value with a S/N equal or superior to 1.3, corresponds to 10^5 oocysts/mL for formalin-treated oocysts.

3.2.1.3. *Heat-treated Cryptosporidium oocysts*

Following the procedures shown in Figure 7, the results recorded in each microwell plate visually, as well as the absorbance values registered via spectrophotometry are shown in Figures 12 and 13.

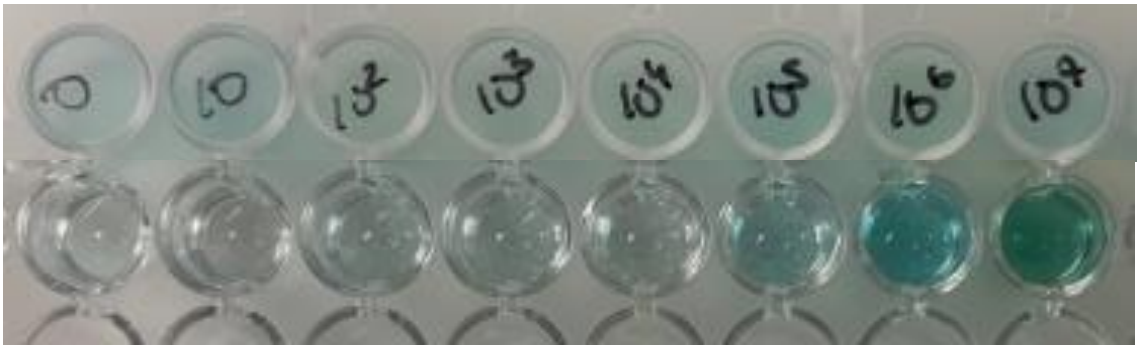

Figure 12.Visual limit of detection for heat-inactivated Cryptosporidium using HRP-labelled antibodies. A blue color indicating the presence of oocysts is shown.

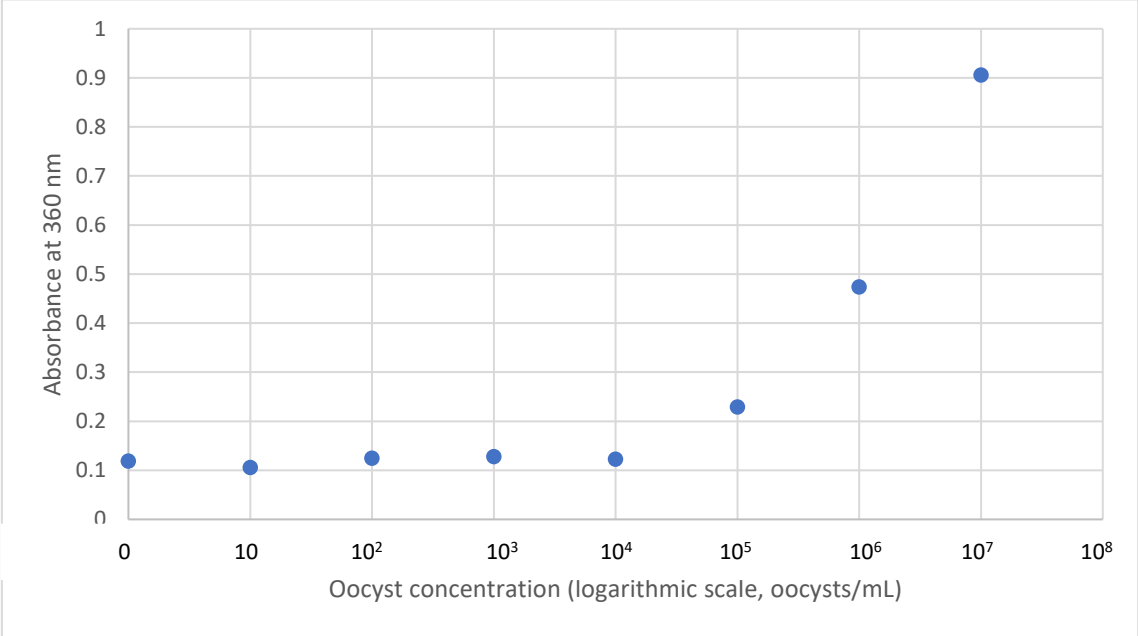

Figure 13. Limit of detection for heat-inactivated Cryptosporidium obtained through absorbance. Absorbance at 360 nm as a function of oocyst concentration is shown

Like the other results, these results show that the visual limit of detection is 10^5 oocysts/mL.

Table 3 summarizes the absorbance at 360 nm for each point and the S/N for heat-treated oocysts

Table 3.Determination of the signal to noise ratio for heat-treated Cryptosporidium

Oocyst concentration (oocysts/ mL)	Absorbance at 360 nm	Signal-to-noise ratio
10^7	0.91	7.61
10^6	0.47	3.98
10^5	0.23	1.92
10^4	0.12	1.03
10^3	0.13	1.08
10^2	0.13	1.05
10	0.11	0.89
0	0.12	1.00

The limit of detection, corresponding to the minimum value with a S/N equal or superior to 1.3, corresponds to 10^5 oocysts/mL for heat-treated oocysts.

3.2.1.4. Freeze – treated Cryptosporidium oocysts

Following the procedures shown in Figure 7, the results recorded in each microwell plate visually, as well as the absorbance values registered via spectrophotometry are shown in Figures 14 and 15.

Figure 14.Visual limit of detection for freeze-inactivated Cryptosporidium using HRP-labelled antibodies. A blue color indicating the presence of oocysts is shown.

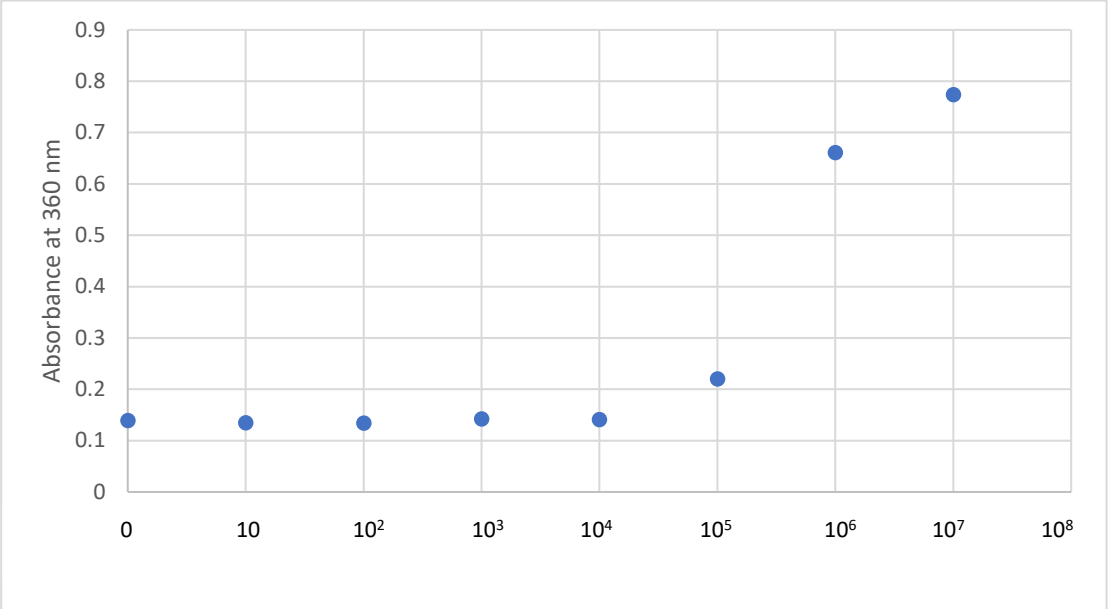

Figure 15. Limit of detection for freeze-inactivated Cryptosporidium obtained through absorbance. Absorbance at 360 nm as a function of oocyst concentration is shown

Like the other results, these results show that the visual limit of detection is 10^5 oocysts/mL. Table 4 summarizes the absorbance at 360 nm for each point and the S/N for freeze-treated oocysts

Table 4.Determination of the signal to noise ratio for freeze-treated Cryptosporidium

Oocyst concentration (oocysts/ mL)	**Absorbance at 360 nm**	**Signal-to-noise ratio**
10^7	0.77	5.57
10^6	0.66	4.76
10^5	0.22	1.58
10^4	0.14	1.01
10^3	0.14	1.02
10^2	0.13	0.96
10	0.14	0.97
0	0.14	1.00

The limit of detection, corresponding to the minimum value with a S/N equal or superior to 1.3, corresponds to 10^5 oocysts/mL for freeze-treated oocyst.

3.2.1.5. *Overall summary of results obtained using HRP-labelled antibodies*

There seems to be no apparent influence of the inactivation processes on the LOD. In live, heat-inactivated, freeze-inactivated and formalin-inactivated oocysts, the LOD achieved was 10^5 oocysts/mL, or 10^4 oocysts total (because only 100 µL of sample was used). Compared with other reported methods in which antibodies are used, this LOD was rather high.

Table 5 presents a comparison of the limit of detection achievable via HRP-labelled antibodies to oocysts inactivated via different procedures.

Table 5. Limit of detection comparison for different inactivation methods.

Inactivation method	Limit of detection achieved (oocysts/mL) via naked-eye detection	Limit of detection achieved (oocysts/mL) via absorbance
None (live *Cryptosporidium*)	10^5	10^5
Formalin inactivation	10^5	10^5
Heat treatment	10^5	10^5
Freeze treatment	10^5	10^5

3.2.2. Effects of inactivation processes on antibody binding analyzed via flow cytometry

For the samples explored in this Chapter, there was only one clear population depicted in the FSC-vs – SSC plot that corresponded to the oocysts. Gates were kept consistent for all samples within the same inactivation method. Figure 16 shows the gated population within the total of the events in the FSC- vs – SSC plot.

For each of the inactivation methods, three types of samples were run on the flow cytometer. First, an unstained sample of the inactivated pathogen served as a control to check the autofluorescence and other characteristics of the oocysts before addition of the antibodies. Second were the samples that underwent Protocol 1 described in the method section. That is, samples that were first inactivated and then subjected to the binding agent. Third were the samples that followed Protocol 2 in which oocysts are first bound to antibodies and then inactivated.

For each inactivation method, histograms showing the green fluorescence intensity vs the number of events were compared. Since the antibodies are labelled with FITC, the binding of the antibodies can be assessed by measuring the green fluorescence intensity of each event. Oocysts with a larger number of antibodies attached to them will show a higher fluorescence intensity, given by the FITC group attached to each antibody. Since flow cytometry collects information of the fluorescence intensity of each event (in other words, of each oocyst), this information of fluorescence intensity is best represented in a histogram, as the events will have a similar but not equal fluorescence intensity. For populations that are stained as expected, with a similar fluorescence intensity, a thin, gaussian curve is expected. For unequally stained populations, this curve can vary and have multiple peaks or can be spread out. Differences between the mean and median of fluorescence intensity are also useful to determine if these populations are similarly stained or unequal, since a mean and median that are close to each other usually imply that all the gated events have a similar fluorescence intensity.

3.2.2.1. Desiccated Cryptosporidium oocysts

Gating of the oocyst population was made by taking the cluster population found in the control. For all the other samples, the same gate was applied. This gate is shown in Figure 16.

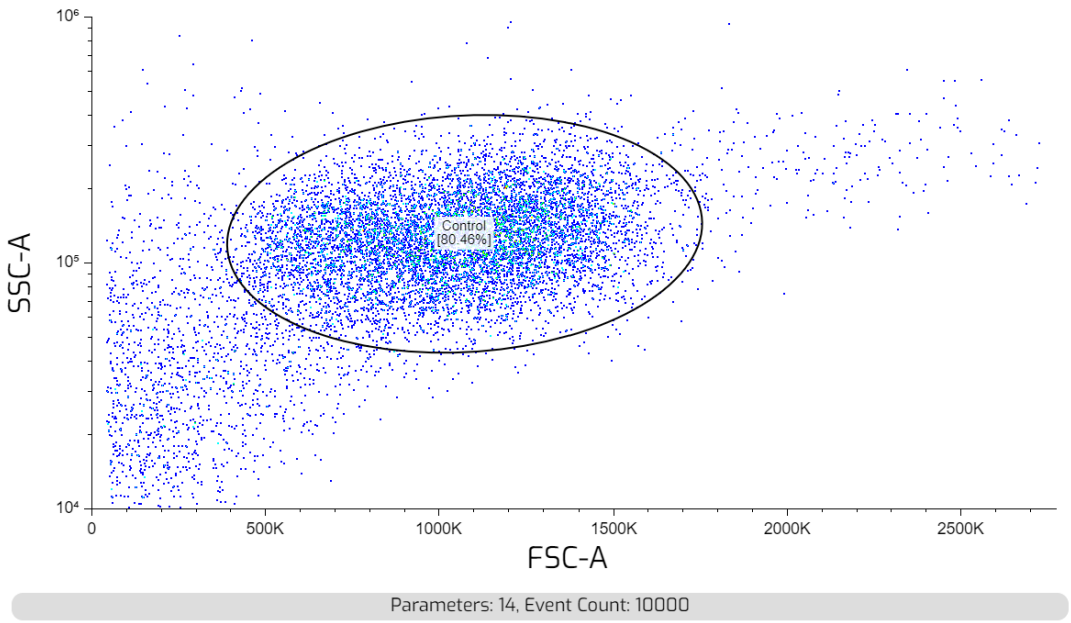

Figure 16. Forward versus side scatter plot for a control sample containing unstained oocysts. Gating process is depicted as a black oval line around the population of interest

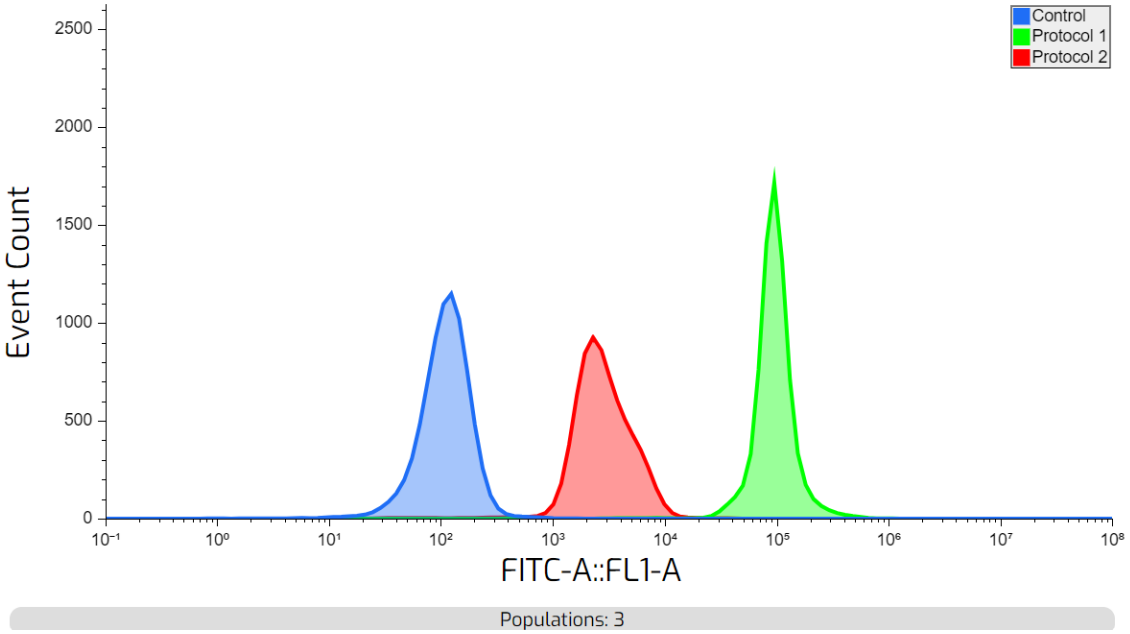

Figure 17. Histograms comparing the fluorescence intensity for an unstained control (blue), a sample stained with antibodies following Protocol 1 (first, inactivation, then staining - Green) and protocol 2 (first, staining, then inactivation – Red) for a sample inactivated via desiccation.

For the desiccation method, the binding of the antibodies is clearly seen, as the events from the Protocol 1 (green) and Protocol 2 (red) samples had a significantly higher fluorescence intensity (various orders of magnitude) than the control (blue) –

(Figure 17). However, Protocol 1, in which oocysts were first inactivated and then bound to the antibodies, yielded higher fluorescence intensities than Protocol 2, in which the desiccation process was done after the antibody binding. It could be that the absence of liquid medium interfered with the antigen-antibody interactions or with the antibody stability and ability to remain in its folded state.

3.2.2.2. *Heat-treated Cryptosporidium oocysts*

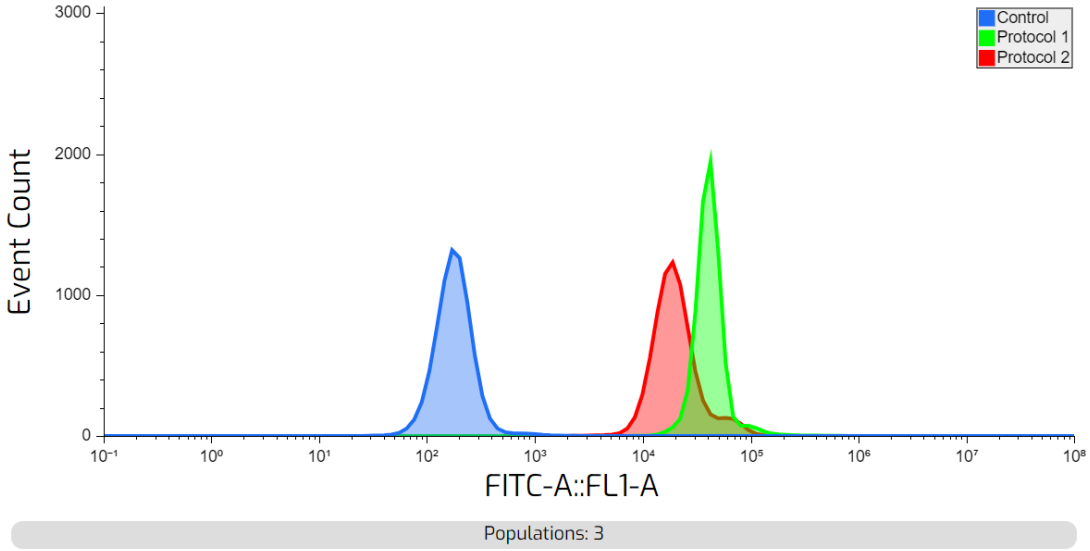

Figure 18.Histograms comparing the fluorescence intensity for an unstained control (Blue), a sample stained with antibodies following Protocol 1 (first, inactivation, then staining - Green) and Protocol 2 (first, staining, then inactivation - Red) for a sample inactivated via heat-treatment

For the heat-treated samples, binding of the antibodies occurred, as samples-stained following Protocol 1 (green) or Protocol 2 (red) had a much higher fluorescence intensity than the control, unstained sample (blue) – (Figure 18). For the heat-treated samples it seems that Protocol 2 had lower fluorescence intensity compared to Protocol 1. This is likely because the heating process after binding causes the denaturation of some of the antibodies.

3.2.2.3. *Freeze-treated Cryptosporidium oocysts*

For the freeze-treated samples, binding of the antibodies occurred, as samples that were stained following Protocol 1 (green) or Protocol 2 (red) had a much higher fluorescence intensity than the control, unstained sample (blue) – (Figure 19). There is not a significant difference between Protocol 1 and 2, which indicates that the freezing process does not significantly interfere with the antibody binding or stability.

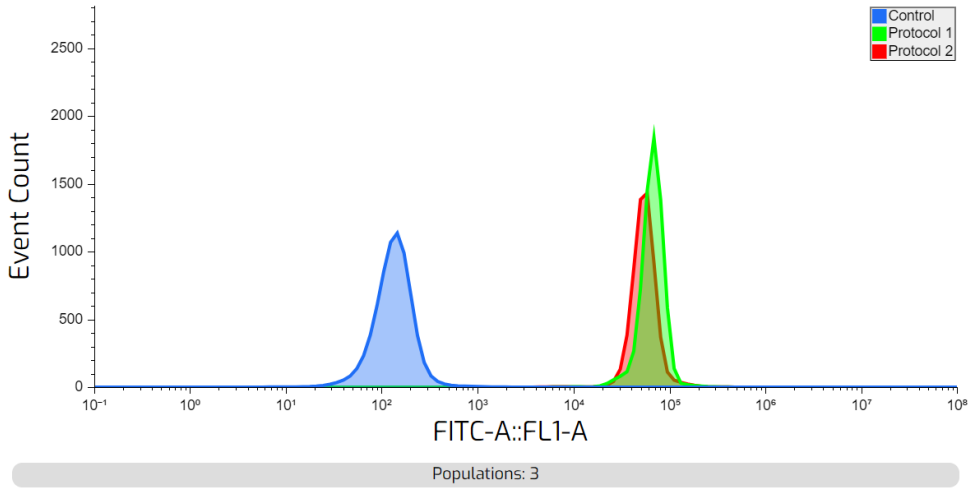

Figure 19.Histograms comparing the fluorescence intensity for an unstained control (Blue), a sample stained with antibodies following protocol 1 (first, inactivation, then staining - Green) and protocol 2 (first, staining, then inactivation - Red) for a sample inactivated via freeze-treatment

3.2.2.4. Formalin-inactivated Cryptosporidium oocysts

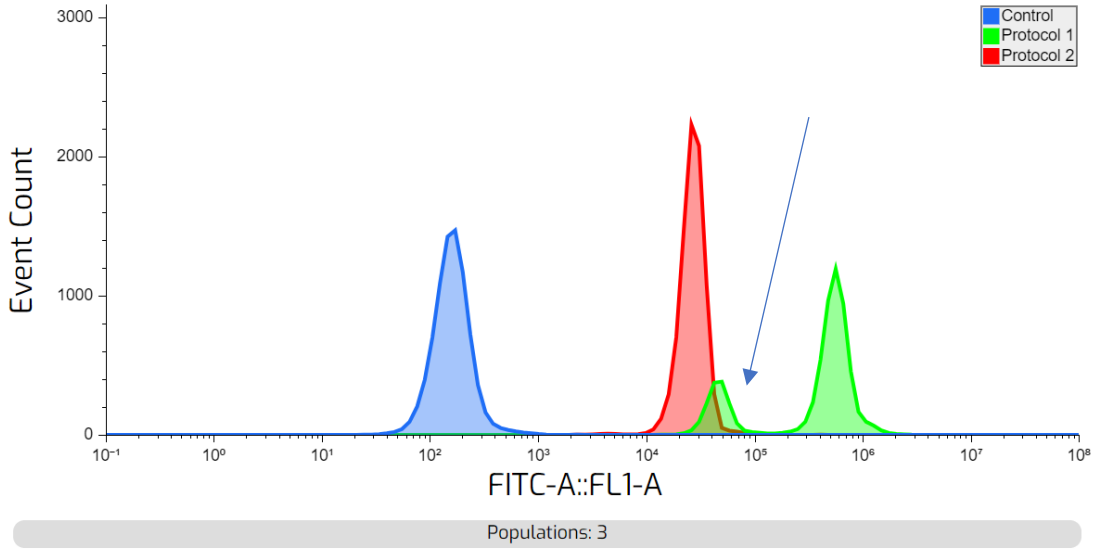

Figure 20. Histograms comparing the fluorescence intensity for an unstained control (Blue), a sample stained with antibodies following Protocol 1 (first, inactivation, then staining - Green) and Protocol 2 (first, staining, then inactivation - Red) for a sample inactivated via formalin-treatment

Comparing the fluorescence intensity of samples that were stained following Protocol 1 (green) or Protocol 2 (red) with the control, the binding of the antibodies could be observed (Figure 20). For samples stained with Protocol 1, the fluorescence peak is considerably higher than any other sample catalogued in this Chapter and it is

also significantly higher than the sample following Protocol 2. It could be that the use of formalin after binding negatively interferes with the binding ability of the antibodies or that formalin affects FITC, resulting in a reduced intensity.

Moreover, it is also worth noting that some of the oocysts that were stained following Protocol 1 belong in a subpopulation where the fluorescence intensity is closer to those stained with Protocol 2 (represented as a blue arrow in Figure 20) . This could indicate that the staining process was not equal across all oocysts.

3.2.2.5. E. coli negative control

A negative control using *E. coli* inactivated by suspension in 5 % formalin was performed to determine whether the fluorescence intensity displayed by the oocyst-stained samples was due to specific antigen-antibody interactions or if, on the other hand, was the result of non-specific interactions and background noise.

Since *E. coli* is different in size and granularity with respect to *Cryptosporidium*, a new gate around this population was done. This gate was collected following the same strategy as with *Cryptosporidium*, by taking the cluster population found in the unstained control that was known to contain the bacteria. Figure 21 shows the FSC – vs – SSC plot and the gate around the *E. coli* population.

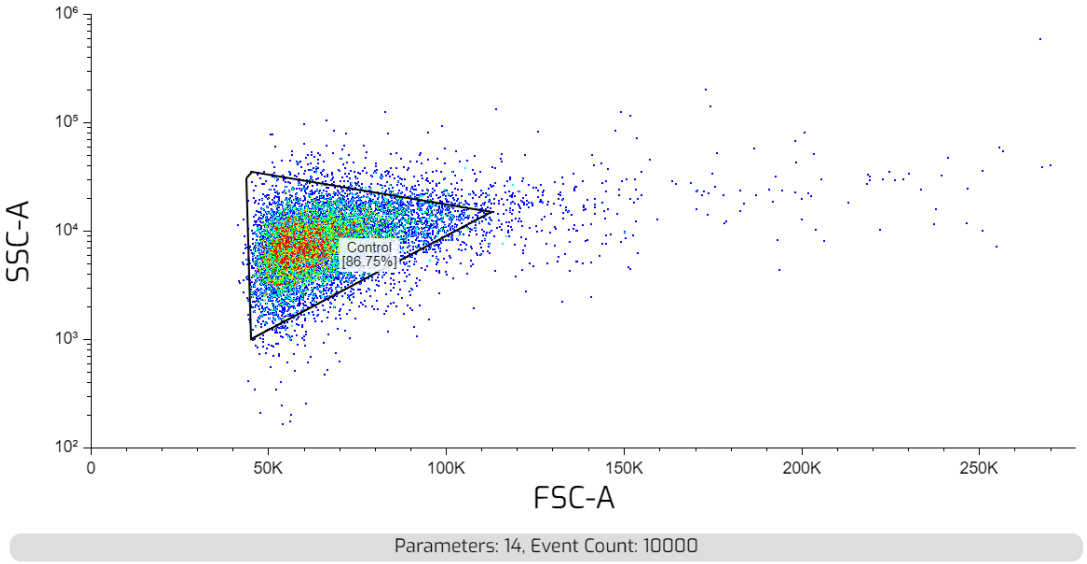

Figure 21. Forward versus side scatter plot for a control sample containing unstained E. coli. Gating process is depicted as a black triangular line around the population of interest

As with the *Cryptosporidium* samples, the histograms showing the green fluorescence intensity -vs- number of events were compared and fluorescence intensity was used as a measure of antibody binding.

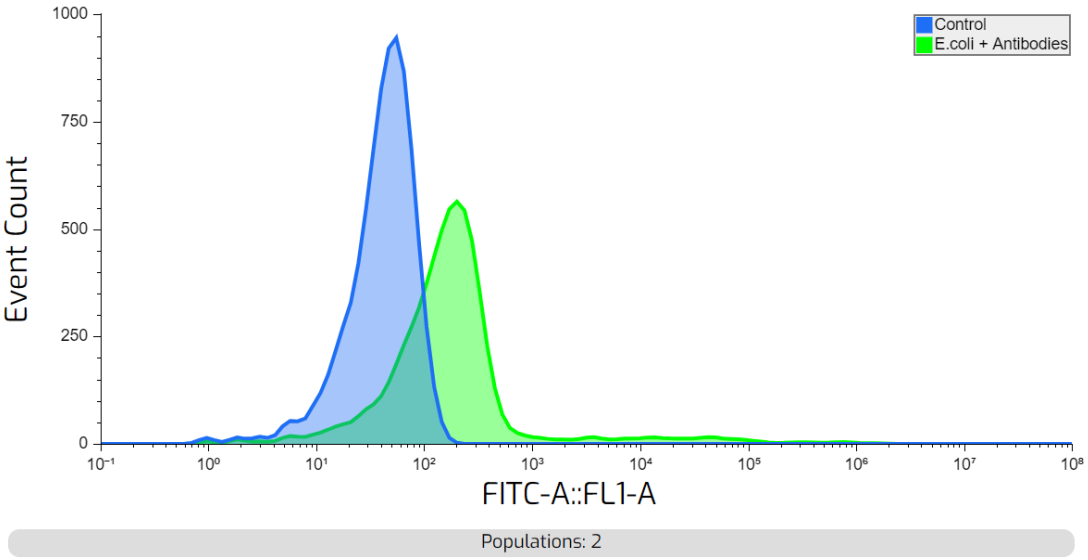

Figure 22. Histograms comparing the fluorescence intensity for an unstained E. coli control and a sample stained with antibodies

Although there was a difference between control and stained samples, indicating some level of unspecific binding or background noise, this signal was significantly lower than stained *Cryptosporidium*, indicating antibody binding is preferential to *Cryptosporidium*. Moreover, it is worth noting that the antibodies used were polyclonal antibodies. These antibodies bind to a wider range of epitopes, making them less specific than monoclonal antibodies.

3.2.2.6. Overall summary of results obtained with FITC-labelled antibodies

The mean and median of green fluorescence intensity of the gated samples populations were collected and are displayed in Figure 23 and Table 6. Standard deviations were calculated and corrected according the procedures described in Appendix I. These values seem to suggest that most samples follow a gaussian distribution except for the formalin-treated, protocol 1 sample, due to the two peaks observed in the histogram.

Table 6.Comparison of the mean and median of fluorescence intensity for different inactivation methods following protocol 1 (first inactivation, then staining) and protocol 2 (first staining, then inactivation) and a negative control with E. coli

Sample		Mean	Median	Standard Deviation
Desiccation	Control	130	120	68
	Protocol 1	114,139	104,927	53,064
	Protocol 2	3,594	2,858	2,132
Formalin	Control	183	170	83
	Protocol 1	516,142	586,491	320,482
	Protocol 2	30,292	30,161	6,967
Heat-treatment	Control	206	189	101
	Protocol 1	48,705	45,417	17,788
	Protocol 2	25,097	20,755	15,913
Freeze-treatment	Control	155	144	79
	Protocol 1	74,957	75,173	17,299
	Protocol 2	62,636	60,360	17,876
E.coli	*Control*	48	46	28
	Protocol 1 - stained	5,422	148	11,570

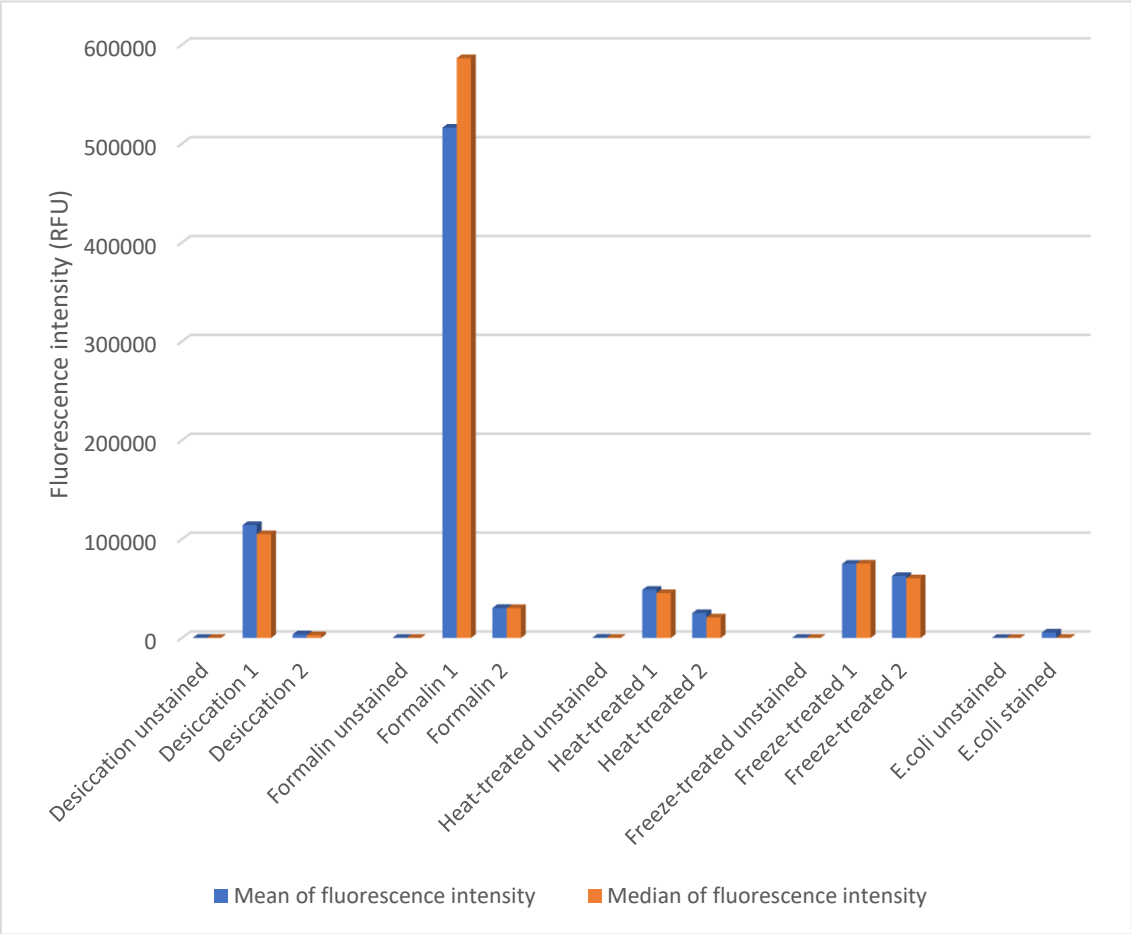

Figure 23. Diagram showing a comparison of the mean and median of fluorescence intensity for different inactivation methods following protocol 1 (first inactivation, then staining) and protocol 2 (first staining, then inactivation) and a negative control with E. coli

The antibodies used seem to have the highest affinity for formalin-inactivated *Cryptosporidium*, with Protocol 1 yielding the highest fluorescent intensities. While other procedures like desiccation and freeze-treatment also showed significant shifts in fluorescent intensities, even labelled heat-treated *Cryptosporidium* showed a higher fluorescence intensity compared to the unstained samples. No benefit to performing the staining on the live oocysts prior to inactivation was observed. In most cases, the data shows that staining the oocyst prior to inactivation had less than optimal results.

Heat-treated oocysts seem to have the lowest binding affinity of all the samples tried. It could be that heat-treatment is detrimental to the stability of the antigens on the oocyst surface or that this process affected the necessary structures needed for antibody binding.

3.2.3. Binding properties of aptamers to inactivated *Cryptosporidium*

The gating process was similar to that used for the antibody binding, by taking a control sample (oocysts inactivated by desiccation) where *Cryptosporidium* is known to be present and where no other significant amounts of counting beads or microorganisms are present in the samples and taking a gate around the most visible clear population (Figure 24).

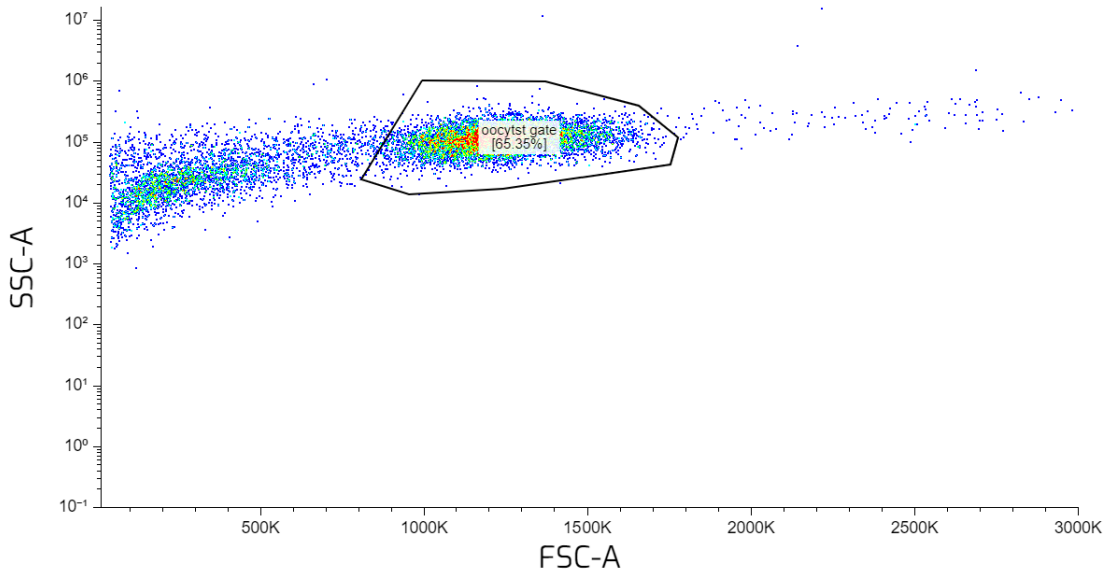

Figure 24. Forward versus side scatter plot for a control sample containing unstained oocysts. Gating process is depicted as a black oval line around the population of interest

3.2.3.1. Desiccated Cryptosporidium oocysts

As with the antibody samples, histograms showing the green fluorescence intensity emitted by the FITC-conjugated-aptamers were chosen to best represent the aptamer binding.

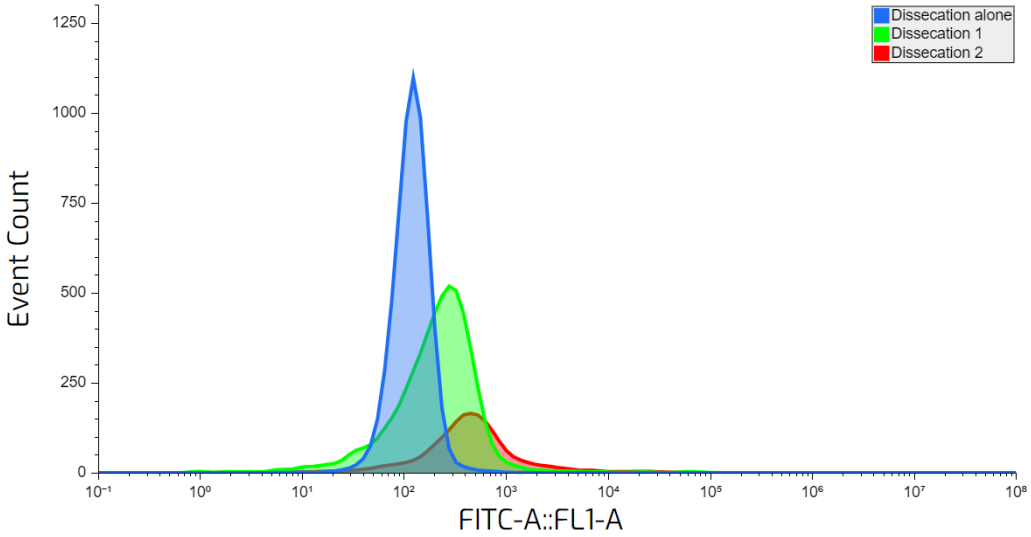

Figure 25. Histograms comparing the fluorescence intensity for an unstained control (Green), a sample stained with aptamers following Protocol 1 (first, inactivation, then staining - Red) and Protocol 2 (first, staining, then inactivation - Blue) for a sample inactivated via desiccation.

For the desiccation procedure, there was a slight shift in the fluorescence intensity of oocysts stained with aptamers following Protocol 1 (green) or Protocol 2 (red), compared to the control (blue) – (Figure 25). However, this shift was quite small compared to those stained with antibodies. There was no significant difference between both protocols.

3.2.3.2. Formalin-inactivated Cryptosporidium oocyst

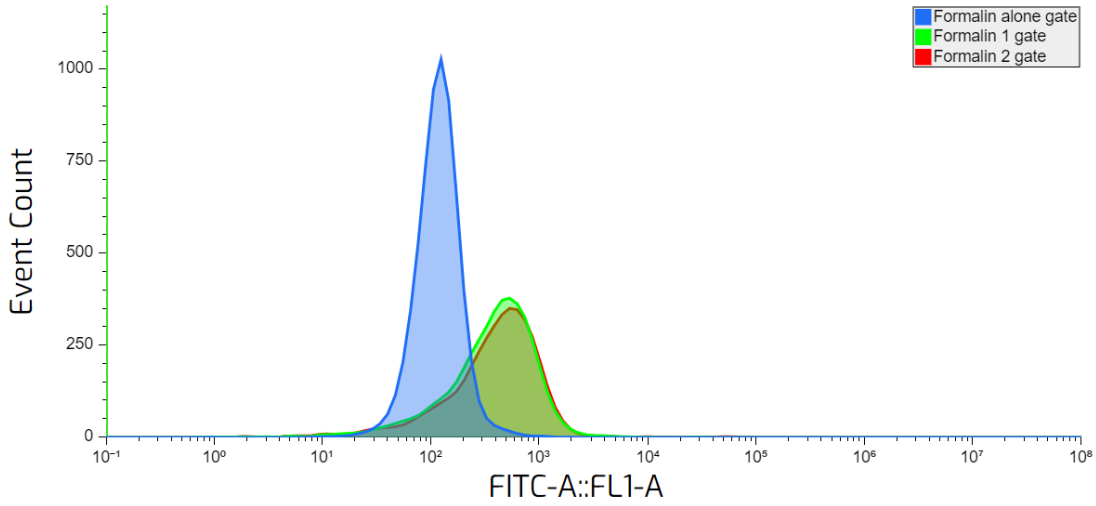

Figure 26. Histograms comparing the fluorescence intensity for an unstained control (Blue), a sample stained with aptamers following Protocol 1 (first inactivation, then staining - Green) and protocol 2 (first staining, then inactivation - Red) for a sample inactivated via formalin-treatment

Results for formalin-treated oocysts were similar to those obtained for the desiccation method (Figure 26). While there was a slight shift in fluorescence intensity of oocysts stained with aptamers following Protocol 1 (green) or 2 (red), compared to the control (blue), this shift was quite small compared to those stained with antibodies. No significant difference between the staining protocols was observed.

3.2.3.3. Heat-treated Cryptosporidium oocysts

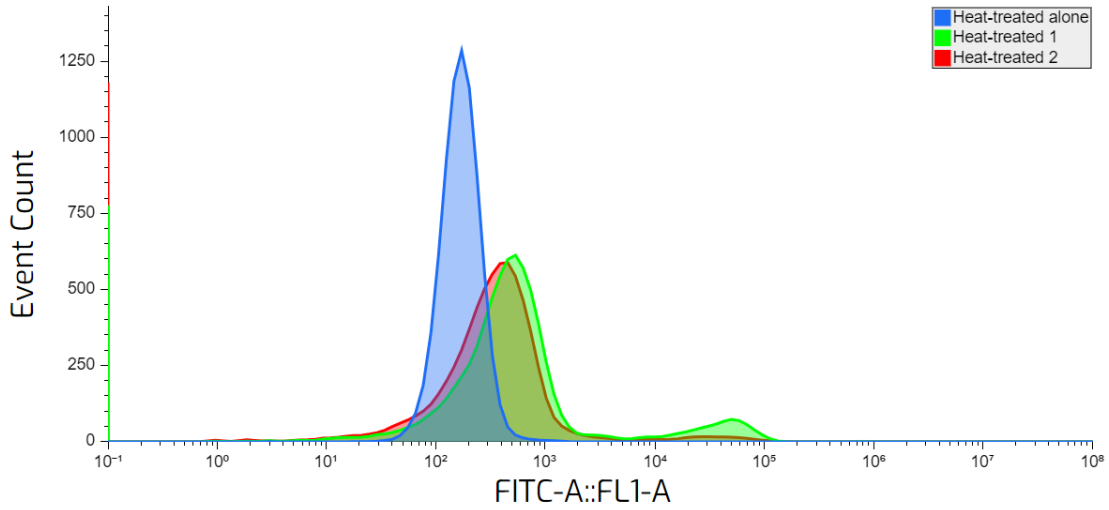

Figure 27.Histograms comparing the fluorescence intensity for an unstained control (Blue), a sample stained with aptamers following Protocol 1 (first, inactivation, then staining - Green) and Protocol 2 (first, staining, then inactivation - Red) for a sample inactivated via heat-treatment

For the heat-treated oocysts, the majority produced only a small shift in fluorescence intensity; however, for a small subpopulation of the oocysts-stained following Protocol 1, a significantly higher fluorescence intensity was observed (Figure 27). The appearance of this subpopulation could mean that the inactivation process was not complete and that not all the oocysts conserved the same structures after the inactivation procedure. The appearance of this subpopulation is further explored in Chapter 5.

3.2.3.4. *Freeze-treated Cryptosporidium oocysts*

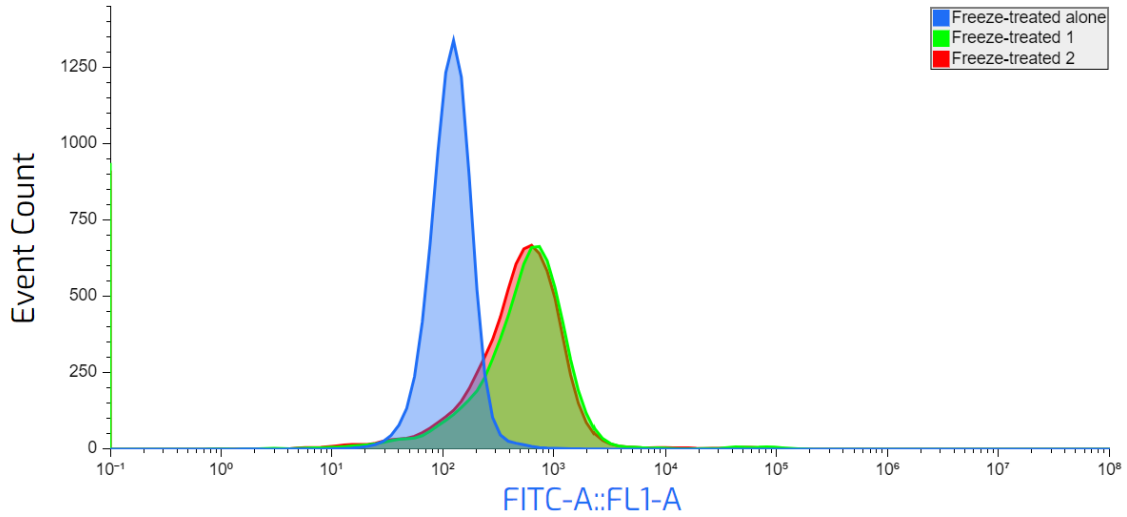

Figure 28.Histograms comparing the fluorescence intensity for an unstained control (Blue), a sample stained with aptamers following Protocol 1 (first, inactivation, then staining - Green) and protocol 2 (first, staining, then inactivation - Red) for a sample inactivated via freeze-treatment

The results for the freeze-treated oocysts were similar to the other samples with only a slight shift in fluorescence intensity (Figure 28). No difference was observed between Protocol 1 or Protocol 2.

3.2.3.5. *E. coli negative control*

A negative control using *E. coli* inactivated by suspension in 5% formalin was performed to determine whether the fluorescence intensity displayed by the oocyst-stained samples were due to specific interactions or if, on the other hand, were the result of non-specific interactions and background noise. The *E. coli* sample used gates that were consistent with the *E. coli* samples stained with antibodies. The green fluorescence histogram of the events gated was also used to assess the aptamer – cell interactions. Figure 29 shows the histogram that compares *E. coli* unstained and fluorescein-labelled aptamer-stained fluorescence intensity.

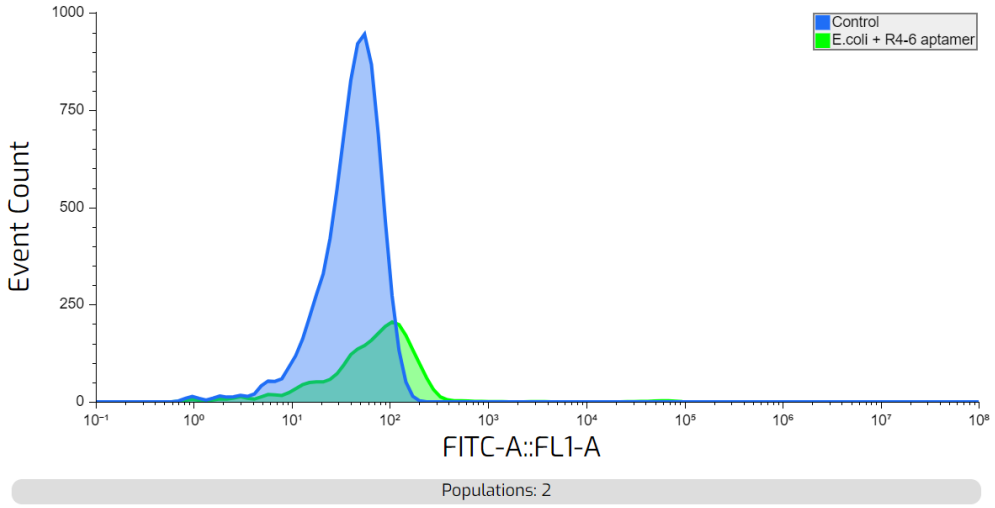

Figure 29.Histograms comparing the fluorescence intensity for an unstained control and a sample stained with aptamers as a negative control with E. coli

A small shift in fluorescence intensity of the stained sample was observed, though the shift was not significant.

3.2.3.6. Overall summary of results obtained with (6-FAM)-labelled aptamers

The mean and median of the fluorescence intensities were taken for each procedure (Table 2) and a histogram showcasing these results is shown in Figure 30. There seems to be a slight increase in the mean of fluorescence intensity from binding Protocols 1 and 2 compared with the control. This shift in fluorescence intensity seems to be highest for heat-treated oocysts. However, the mean and median of fluorescence intensity of heat-treated oocysts are very distant, indicating that the population does not show an expected thin, gaussian curve in fluorescence intensity. Moreover, Figure 27 shows a second subpopulation for the heat-treated samples processed using Protocol 1. This could be because of the inactivation process, since it could be that the process affected some oocysts differently. Standard deviations were also obtained following procedures described in Appendix I. Corrected standard deviation shows that for the heat-treated oocysts distributions are not gaussian, this represents the two peaks that were observed in past histograms and this effect will be further explored in next chapters.

Table 7. Comparison of the mean and median of fluorescence intensity for different inactivation methods using both aptamer staining protocols and a negative control with E. coli

Sample		Mean of fluorescence intensity	Median of fluorescence intensity	Standard deviation
Desiccation	Control	129	136	60
	Protocol 1	496	212	405
	Protocol 2	1,028	428	2,968
Formalin	Control	137	125	77
	Protocol 1	534	333	474
	Protocol 2	556	344	459
Heat-treatment	Control	191	179	88
	Protocol 1	4,562	460	15,703
	Protocol 2	1,409	316	8,384
Freeze-treatment	Control	136	126	61
	Protocol 1	1,272	563	671
	Protocol 2	872	502	669
E.coli	*Control*	49	46	27
	Protocol 1 - stained	262	39	72

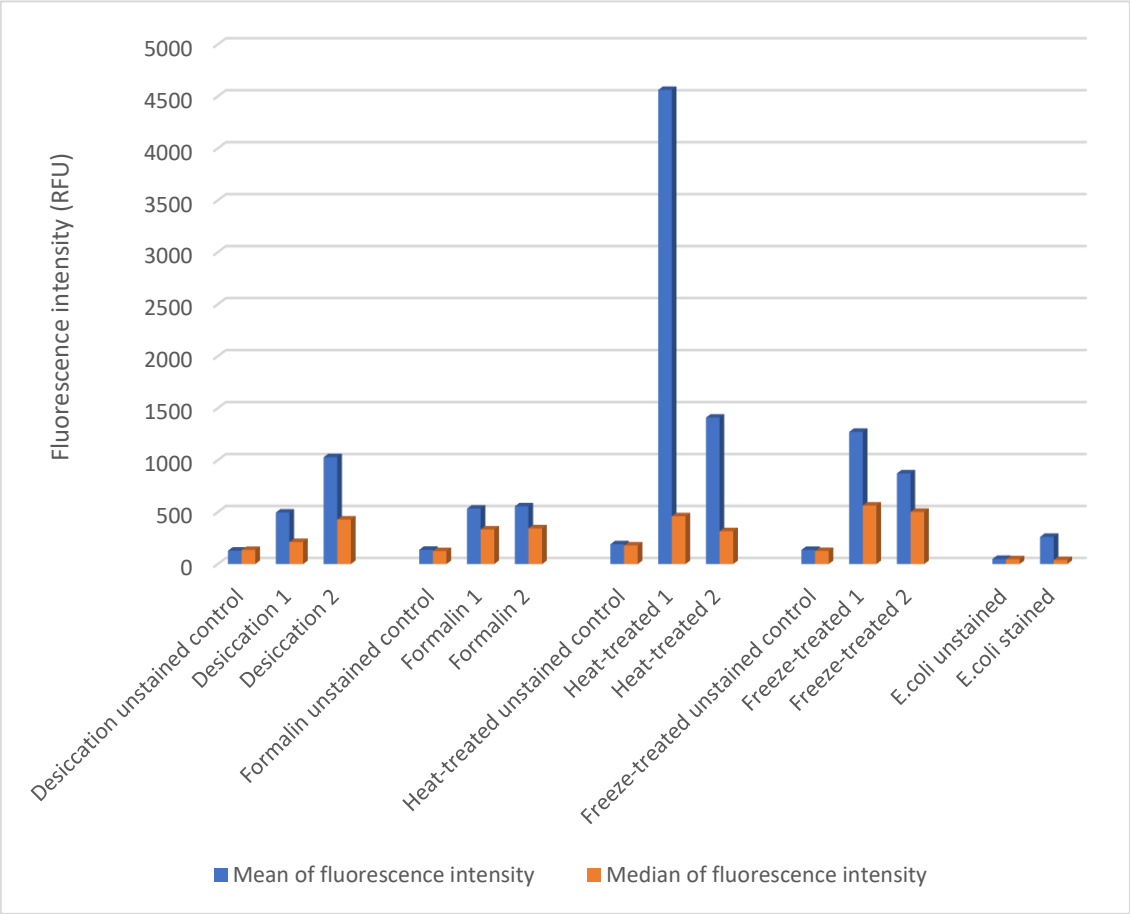

Figure 30. Diagram showing a comparison of the mean and median of fluorescence intensity for different inactivation methods using both aptamer staining protocols and a negative control with E. coli

There is also no pattern or correlation between binding Protocols 1 and 2. While binding Protocol 2 seemed to work slightly better for formalin-inactivated and desiccated samples, Protocol 1 showed a higher mean of fluorescence intensity for freeze and heat-treated oocysts.

Moreover, while there was a small shift in fluorescence intensity, the median of fluorescence intensity did not change as dramatically as with samples stained with antibodies. This could indicate that aptamer binding under these conditions was much weaker than antibody binding or could have been a function of the fluorescent molecule (FITC vs. 6-FAM).

3.3. Conclusions

While inactivation methods could play a significant role in the ability of molecules to bind to their target, it was found that for targeting oocysts, the inactivation did not play a significant role when using colorimetric or fluorescence-based methods. In determining a LOD via HRP-labelled antibody binding, the same LOD was achieved for the live and inactivated samples. However, when using a more sensitive technique, such as flow cytometry, a greater difference between inactivation methods was observed. Using flow cytometry and FITC-labelled antibodies, formalin-inactivated *Cryptosporidium* yielded the greatest response compared to other methods of inactivation.

Aptamer-binding showed a significantly lower binding affinity compared to antibodies. Heat-treated *Cryptosporidium* showed a higher mean of fluorescence intensity than other methods of inactivation. However, this increase in the mean was the result of a subpopulation showing higher binding affinity. It could be that the heat-treatment that these oocysts underwent did not affect all the oocysts equally, causing these differences in fluorescence intensity between events.

It was also found that there was no benefit in performing the antibody-binding step prior to inactivation. Antibody-binding seems to be negatively affected when undergoing inactivation procedures while aptamer binding showed no significant difference between procedures.

4. Effect of different aptamer sequences on binding affinity of inactivated *Cryptosporidium*

4.1. Introduction

Several different aptamers that bind *Cryptosporidium* oocysts have been reported in literature. Given that not all aptamers necessarily bind to the same site on an oocyst, it is possible that the aptamer chosen in the previous chapter was not optimal for the procedures used. The inactivation process could be modifying some of the structures to which these aptamers attach. Previous results performed with polyclonal antibodies seemed to demonstrate that some structures are conserved during the inactivation process, as polyclonal antibodies do show binding affinity. Aptamers bind to a wide diversity of targets, even non-immunogenic ones, which means that they do not need to necessarily bind to the same epitopes that polyclonal antibodies do. In Zheng et al. (2015) where they performed SELEX to find an aptamer against inactivated *Vibrio alginolyticus*, it was noted that while some aptamers were only able to bind inactivated *Vibrio alginolyticus,* others were able to bind to both live and inactivated cells, indicating that the target of the aptamer was likely a structure that was not altered through the inactivation process.

In Iqbal et al. (2015), several aptamers with high affinity were found through the SELEX process. They chose R4-6, but other aptamers showed high affinity compared to the control as well. Since the assays with polyclonal antibodies seemed to indicate that some structures are conserved during the inactivation process, it could be that a different aptamer could target a different structure that is conserved during the inactivation process. Moreover, if found, having an aptamer that can only bind to live and another one that can bind to inactivated could be used as a potential tool to discriminate between viable and non-viable organisms. Since aptamers present a defined fold that can recognize a specific target, it could be possible that the more different the folded structure, the more probability there is for an aptamer to bind to a different target within the same cell. To assess how different the folded structure of each different aptamer is from aptamer R4-6, a protocol similar to what it is described in Cowperthwaite & Ellington (2008) was followed. First, the secondary structure of

each aptamer was determined. Using the RNA structure software provided at https://rna.urmc.rochester.edu/RNAstructureWeb/, the secondary structure is the structure that has the lowest free energy for the sequence of interest. The secondary structures were converted to dot and bracket notation using the same software. Dot and bracket notation is a way of representing a secondary structure. In this notation, open parentheses indicate that the base is paired to another base ahead of it. Closed parentheses indicate that a base is paired to another base behind it. Dots indicate unpaired bases. This is used to represent structures.

In Cowperthwaite & Ellington (2008), the Hamming distance is used as a way to compare the structural differences between two structures expressed in dot-bracket notation. The Hamming distance is a tool used in coding where two strings of the same length are compared by counting the number of substitutions necessary to turn one string into the other. However, since not all reported sequences in Iqbal et al. (2015) have the same length, the Levenshtein Distance was used to compare the dot and bracket notation strings of characters. The Levenshtein Distance is similar to the Hamming distance, but allows for insertion and deletion of characters, which makes the comparison between two strings of different lengths possible.

Four different aptamers were chosen this way to maximize the possibility of one of them binding to inactivated *Cryptosporidium*. All aptamers were compared to the parent aptamer (R4-6) and then with each other. Results from this comparison are presented in Table 8.

Table 8. Levenshtein distance and binding affinity comparison for different aptamer sequences and aptamer selection

Aptamer name	Full sequence	Dot-bracket notation	Distance from R4-6	Distance from R4-8	Distance from R8-5	Distance from R4-1	Binding affinity (current change)
R4-6	CTC CTC TGA CTG TAA CCA CGG TGG TCC CGC AAA ATG CAC GAC GAG TCT TGC TTC TGA TCT GCA TAG GTA GTC CAG AAG CC	.....((((((.((((...)))).(((...))).)).)))..(((((((..(((....)))).)).))))).	0	45	35	38	179
R1-4	CTCCTCTGACTGTAACCACG AGA TTG CGG ATT GCC CAC GTG GAA AGT GAT TTG TTC GTC CG GCATAGGTAGTCCAGAAGCC	....(((((((...(((.((.....)).(((((.(((...(((....))).)))..)))))..)))))).)))))....	38	29	18	37	155
R4-1	CTCCTCTGACTGTAACCACG TCT TGG GGC AGG CAT GAG GTG TGG CAG AGG TAA GGG ATA A GCATAGGTAGTCCAGAAGCC	..((((((.((((..(((.....))).)))).(((.....))).)))))).....((....))....	38	32	34	0	150
R4-3	CTCCTCTGACTGTAACCACG CAC ACA AAC TGA ATT CTC AGG ATG TGG TGA TGG TTT GCA T GCATAGGTAGTCCAGAAGCC	....(((((((((.((((((..((((((..((((....))))..)))).)).))))))((....))....))))))).))))....	30	34	27	36	150
R4-8	CTCCTCTGACTGTAACCACG CTA GGT CAC GCT TAG GAT GAA TAA CGC CCT CTT GGT TAC A GCATAGGTAGTCCAGAAGCC	..(((.((.((((((((((.((.....)).((.(((.....))).)).)))))))))).))).))).....	45	0	32	32	167
R4-9	CTCCTCTGACTGTAACCACG CTC TGT GGC GCT TGG GAT CAA CGG CCT CTT GGT TAC G GCATAGGTAGTCCAGAAGCC	..(((.((.((((((((((((....)))).((((.((.....)).)).).)))))))))).))).))).....	41	12	34	32	152
R4-12	CTCCTCTGACTGTAACCACG ATT GTG ACT GTG AAG GTC CAG ATT GGG CAA TCC GTT GTA A GCATAGGTAGTCCAGAAGCC	....(((((((...(((.((((((..(((.....)))(((...))).)))).)).((....))..)))))).)))))....	34	36	23	35	158
R4-14	CTCCTCTGACTGTAACCACG CGG TAC CGG CCT ATT CAT ACT TGA AAC CTG CAC TCT TAA T GCATAGGTAGTCCAGAAGCC	....((((((((((.((....)))))...(((.((((....)))).....((((.......)))).)))..))).))))....	28	35	26	34	161
R8-2	CTCCTCTGACTGTAACCACGT CTTCCGTAGCGTCAGTGTAGTGCCTCAAATCGCAATGT GC ATAGGTAGTCCAGAAGCC	....(((((((...((((((.....))).(((.........)))).....((.(((...))))).)))))).)))))....	31	34	24	35	145
R8-2B	CTCCTCTGACTGTAACCACG ACA GGA GTA GGC GTT AAC ATA GGG CCG TGT CGG TTG TCA G GCATAGGTAGTCCAGAAGCC	..(((.((.(((.((((((.((....)).(((.(((...))).)))..)).))))..))).)).))).....	39	16	32	29	167
R8-5	CTCCTCTGACTGTAACCACG CCC CAG TGA CGG GTA GCA GAG CGT CCA CAG TTT TCC TGT AT GCATAGGTAGTCCAGAAGCC	....(((((((...(((..((((.......)))).(((((...)).((((.....)))).)))...)))))).)))))....	35	32	0	34	162

Aptamers R4-8, R4-12, R8-5 and R4-1 were chosen as possible alternatives to evaluate the binding properties of inactivated oocysts.

4.2. Materials and Methods

Aptamers labelled with 6-FAM at the 5' end were obtained from Integrated DNA Technologies (IDT). Formalin-inactivated *Cryptosporidium* was obtained from Waterborne; Inc. DPBS was obtained from Sigma-Aldrich (Catalog number: D8662). All other reagents were of analytical grade. Imaging flow cytometry was performed with a ImageStream ® X Mk II Imaging Flow Cytometer. Excitation laser used was 488 nm and the emission was recorded in channels 1 to 5 corresponding to blue, green, yellow, orange and red fluorescence emission. Channel 6 corresponds to the side scatter. However, only Channel 6 and Channel 2 are relevant for this purpose as fluorescein has an emission peak of 520 nm, corresponding to green fluorescence.

To evaluate the binding ability of the different aptamers, the same procedure was followed for each aptamer. Briefly, 100 µL of formalin-treated *Cryptosporidium* with a concentration of 1.25 x 10^8 oocyst/mL and 100 µL of heat-treated *Cryptosporidium* with a concentration of 1.25 x 10^5 oocysts/mL were washed twice in DPBS by centrifugation at 5,000 g for 5 minutes. The oocysts were then diluted further to 2.5x10^6 for the formalin-treated *C. parvum* and 1.25x10^5 for the heat-treated *C. parvum*. 5' 6-FAM labelled aptamers were reconstituted in DI water to a final concentration of 100 µM. 100 µL of aptamers were diluted to 50 µM in DPBS and heated for 10 min at 90ºC followed by cooling down at room temperature for 15 minutes. 20 µL of 50 µM of each aptamer were added to 100 µL of each kind of inactivated *C. parvum*. The mixture was incubated together for 1 hour followed by two washes by centrifugation at 5,000 x g for 10 minutes.

4.3. Results and Discussion

4.3.1. Formalin-inactivated *Cryptosporidium* oocyst

Since imaging flow cytometry requires the use of reference beads, additional gating is necessary to distinguish events that are *Cryptosporidium* from events that correspond to reference beads or other debris. As mentioned in Chapter 3, the gating process consisted of selecting a series of points in a scatter plot that represented the

population of cells of interest, leaving other points that represent events other than the cells of interest, out of further analysis. Cells exhibit certain characteristics unique to them such as size and granularity, which makes them form a distinct population in a scatter plot. There are also other helpful markers such as autofluorescence that can aid with the gating process, as autofluorescence can help distinguish the cells of interest from other populations. In this work, since formalin-inactivated *Cryptosporidium* showed an increase in autofluorescence that other counting beads and debris did not and since the reference beads showed a high side scatter, the gating process was done based on these characteristics.

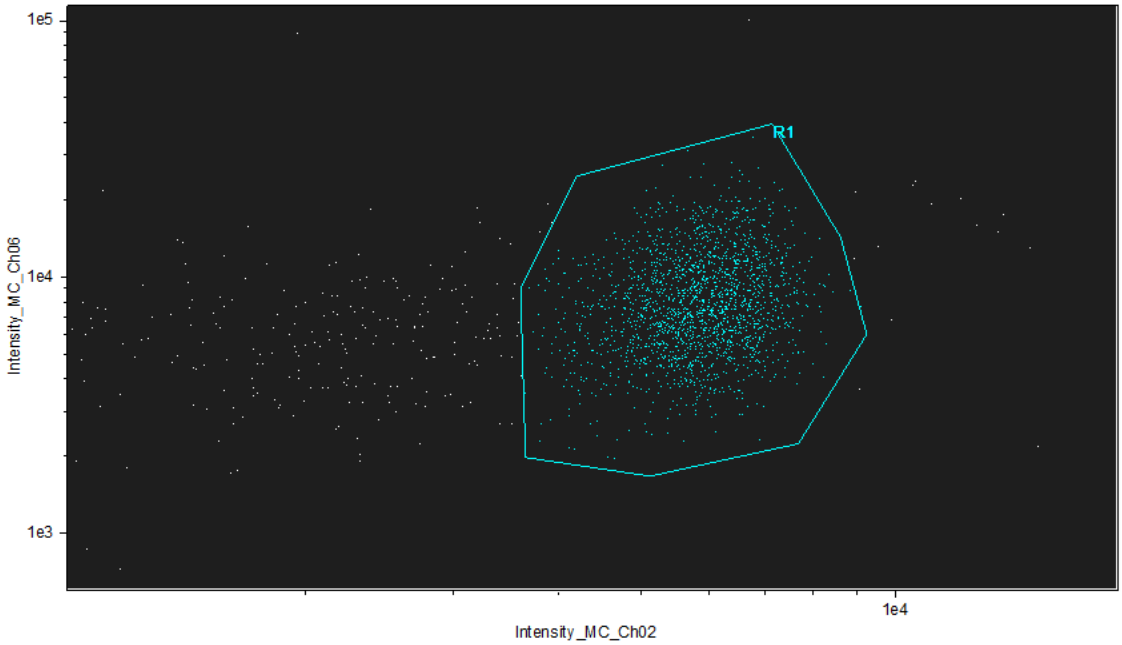

Figure 31. Dot plot showing side scatter (Intensity_MC_Ch06) versus green fluorescence intensity (Intensity_MC_Ch02) with the oocyst's population showing autofluorescence gated

First, a population is selected as shown in Figure 31, where the Intensity_MC_Ch06 correspond to the side scatter and Intensity_MC_Ch02 correspond to the green fluorescence intensity. However, this is not yet the gate created according to size. This plot was used to find the events that showed high autofluorescence as a way to locate the oocysts. Once these points were found, referred to in Figure 31 as population R1, these points were then transferred to a pseudo-forward vs side scatter (FSC -vs- SSC) plot of the event and a new gate was created around them, this time, according to size (Area_M01) and granularity (Intensity_MC_Ch06). Figure 32 shows the gate that corresponded to the oocysts.

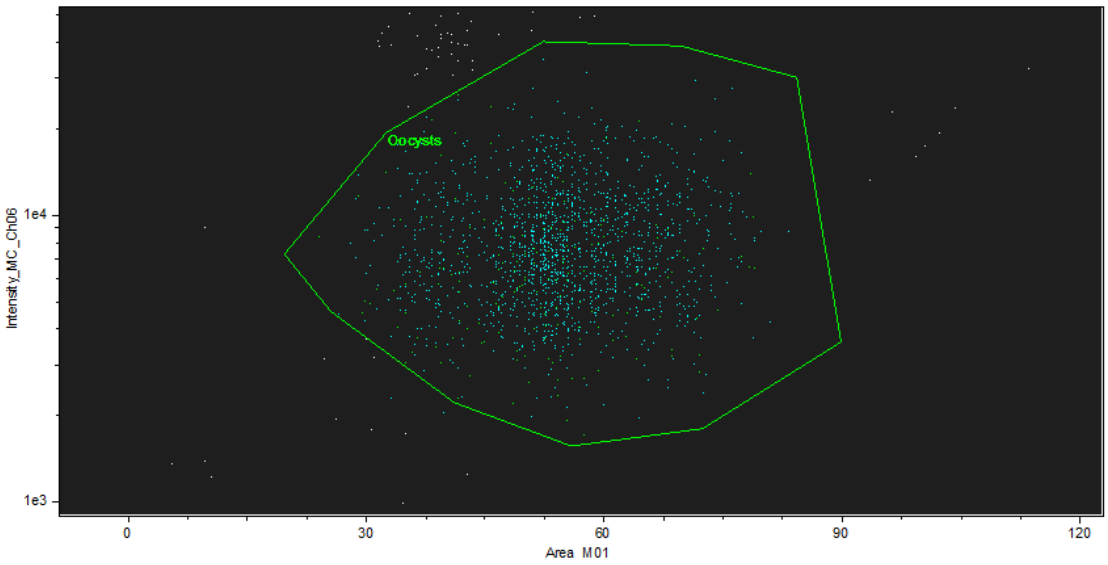

Figure 32. Pseudo front-vs side scatter plot with the oocyst's population gated by size, using its autofluorescence to distinguish this population

This gate remained consistent for all subsequent samples. The accuracy of the gate was confirmed by examining the images recorded for each event (Figure 33). The majority of the images captured during flow cytometry were consistent with images of *Cryptosporidium* in size and shape.

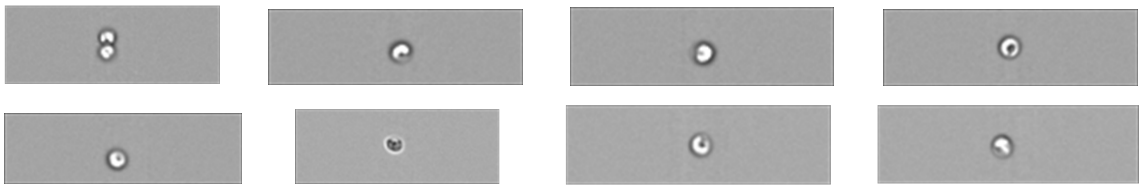

Figure 33. Brightfield images of the events gated as oocysts

Using consistent gates, the fluorescence intensity of the oocyst population was determined for each aptamer. In Table 9, a summary of the mean and median of fluorescence intensity is shown. Standard deviations were obtained as illustrated in Appendix I.

Table 9. Mean and median of fluorescence intensity shown by the oocysts stained with different aptamers for formalin-treated oocysts

Sample	Mean	Median	Standard Deviation
Oocysts alone	5,490	5,748	1,378
R4-1	16,552	6,469	37,021
R4-6	7,397	6,038	3,052
R4-8	23,224	6,556	49,196
R4-12	33,372	6,923	65,5680
R8-5	16,872	6,389	34,409

As shown in Table 9, all samples but the R4-6 aptamer bound oocysts have a significantly higher mean fluorescence intensity compared to the oocysts alone. However, the median of fluorescence intensity remained similar for all the samples. Moreover, most samples (except R4-6 and oocysts alone) had a significant difference between the mean and median fluorescence intensity and standard deviations values that suggest that distributions are not gaussian and therefore not all the events showed similar fluorescence characteristics. This is indicative that the aptamer binding and thus the fluorescence affected oocysts differently across the selected population.

Examining the histogram of fluorescence intensity, it is noticeable that for most of the oocysts in all the samples, the mean of fluorescence intensity is that of autofluorescence (main peak). However, there seems to be a subpopulation within the oocyst gate that shows high fluorescence intensity (marked with an arrow in Figure 34.

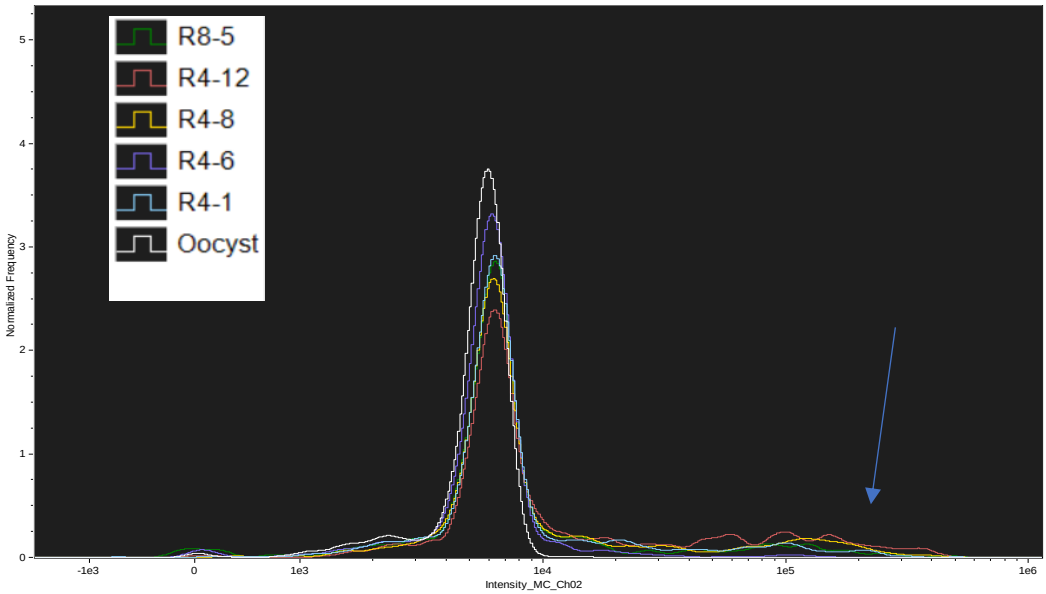

Figure 34. Histograms comparing the fluorescence intensity of unstained oocysts samples and samples stained with different aptamers

This subpopulation represents between 1.22 % (for aptamer R4-6) to 19.1% (for aptamer R4-12) of the total oocyst population (subpopulation marked with a blue arrow). The brightfield image of the subpopulation showing high fluorescence intensity is shown in Figure 35.

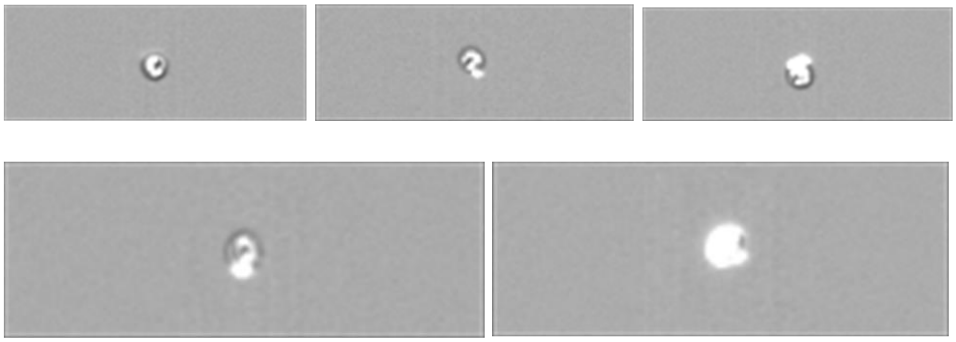

Figure 35. Brightfield images of the events in the high-fluorescence subpopulation

Some of the events were visually categorized as *Cryptosporidium* oocysts by comparison with other *Cryptosporidium* images obtained in the literature (see Figure 36), while others had a generic, round shape that could indicate that they were either stained reference beads or oocysts whose image is not so clearly distinguished due to

the high fluorescence signal given by the aptamers. Some of the events were completely out of focus.

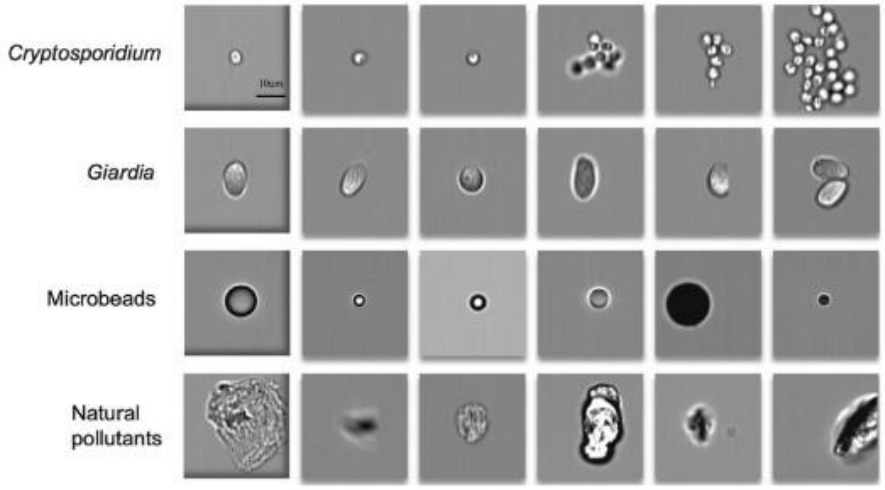

Figure 36. Images of Cryptosporidium, Giardia, Microbeads and debris found in literature. Source: (Luo et al., 2021)

It is possible that these rare events corresponded to either non-specific interactions of the aptamers or it could be that the inactivation processes were not as homogeneous, leaving most of the oocysts with a modified cell surface in which aptamers cannot bind while some oocysts are able to maintain those structures that are critical for aptamer binding.

4.3.2. Heat-treated Cryptosporidium oocysts

Like previous experiments, the fluorescence intensity for each sample was taken as shown in Table 10.

Table 10. Mean and median of fluorescence intensity shown by the oocysts stained with different aptamers for formalin-treated oocysts

Sample	Mean	Median	Standard Deviation
HT oocysts alone	278	130	305
R4-1	140,507	123,176	94,754
R4-6	50,408	2,196	80,341
R4-8	124,652	111,792	78,005
R4-12	172,804	148,155	99,208
R8-5	168,706	147,583	105,207

Almost all samples had an increased fluorescence intensity compared to the control which consisted of a sample without aptamers (oocysts alone). All samples but the R4-6 had a mean and median of fluorescence intensity that were relatively close and a standard deviation that suggest a gaussian distribution.

It is also worth noting that heat-treated oocysts displayed a much lower autofluorescence compared with formalin-treated oocysts. This is because reactive groups in formalin can cause Schiff acid-base reactions with amine groups (which in this case would be present in the oocysts membrane proteins) resulting in adducts that are highly fluorescent (Kajimura et al., 2016).

For the R4-6 bound oocysts, the mean and median of fluorescence intensity varied almost 20-fold. By taking a closer look at the histogram associated with this sample (Figure 37), it is noticeable that similar to the histograms obtained for formalin-inactivated *Cryptosporidium*, there are two subpopulations, one that would correspond to no fluorescence at all and the other one that displays a higher fluorescence intensity.

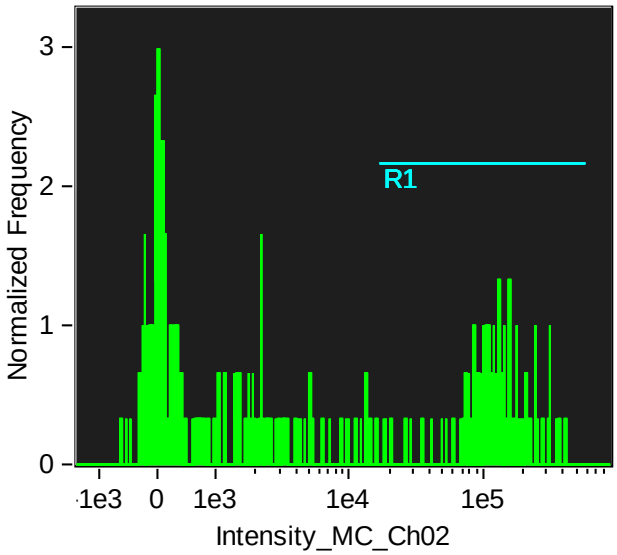

Figure 37. Histogram showing the fluorescence intensity of heat-treated oocysts stained with aptamer R4-6

Similar to the formalin-inactivated oocysts, the brightfield images of the higher intensity population, represented in Figure 37 as the threshold named R1 were taken and they are displayed in Figure 38.

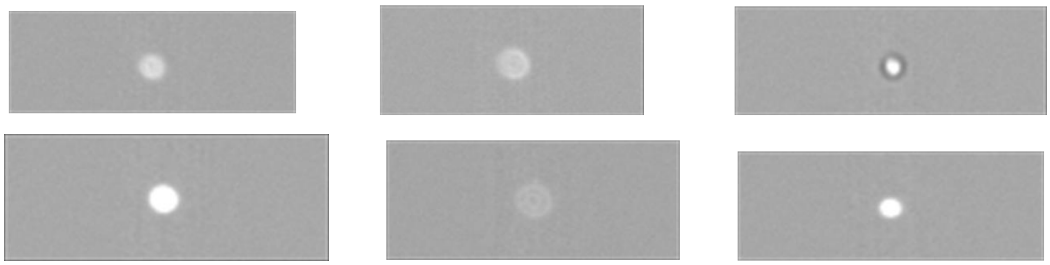

Figure 38. Brightfield image of the events included in the subpopulation with higher fluorescence intensity

By comparison with the oocyst images obtained from literature (Figure 36), there were no unequivocal images of an oocyst in this subpopulation; however, many round shapes, which resembled *Cryptosporidium*, were found. It could be because the high fluorescence signal makes *Cryptosporidium* images appear blurry, or it could be that the similarly round-shaped counting beads are adsorbing some of the aptamers via non-specific interactions, giving a high fluorescence signal.

Similarly, brightfield images of the population with lower fluorescence signal were taken. By comparison with well-established pictures of *Cryptosporidium* obtained in the literature, there was not a clear population that was mostly oocysts. There were

a few events within the gate whose shape highly resembled that of oocysts but there were also a sizable number of events that resembled counting beads, debris and events that are out of focus (Figure 39).

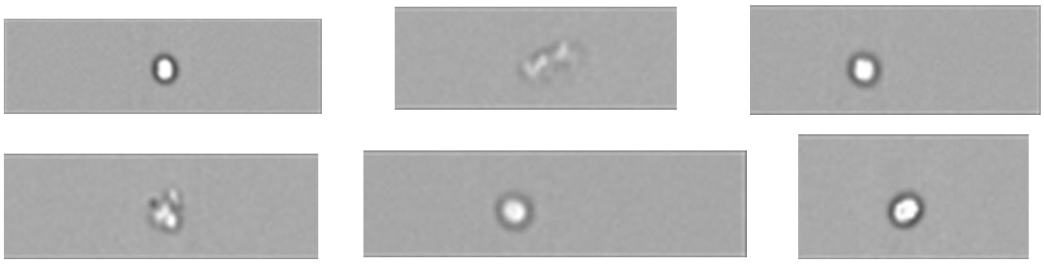

Figure 39.Brightfield image of the events included in the subpopulation with lower fluorescence intensity

For the rest of the samples, the imaging results were similar, they were either too bright to determine that they were clearly oocysts or out of focus.

Moreover, for the heat-treated oocysts, the gates did not gather a clear population distinguishable from beads as the formalin-treated ones did. Instead, they just gathered events that seemed to be in an event continuum (Figure 40).

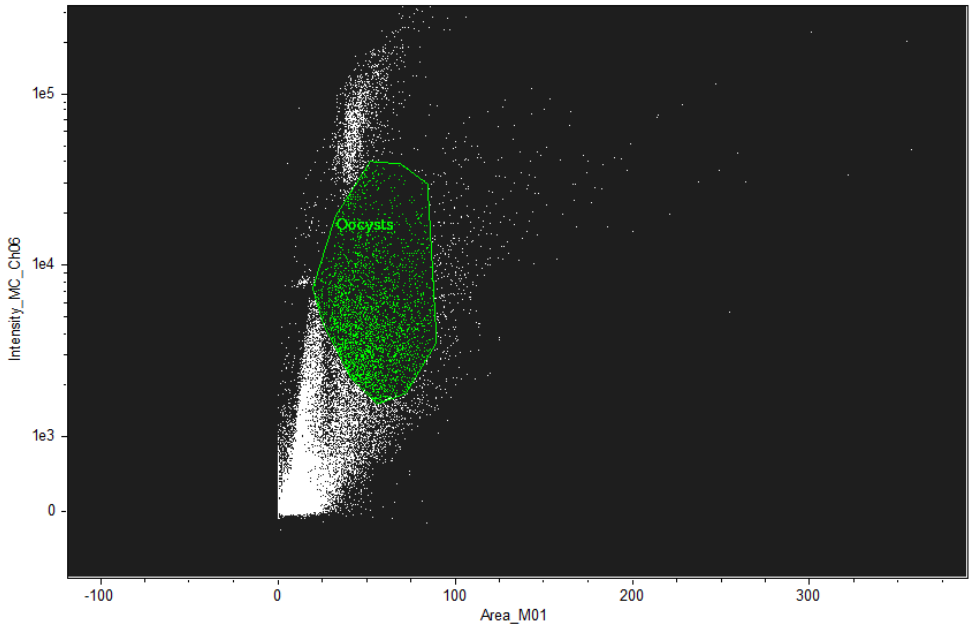

Figure 40. Pseudo FSC -vs- SSC plot for heat-treated Cryptosporidium in which consistent oocysts gates are represented

This could be explained because Heat-treated oocysts are more likely to be suffering from some shape changes and even lysis. Kennedy et al. (2019) determined that for *S. aureus,* heat-treatment had a significant impact on membrane damage and

produced some cell debris; however, formalin treatment tends to maintain cell morphology (Matsuda et al., 2011).

4.4. Conclusions

There was no unequivocal proof from imaging flow cytometry that the different aptamer sequences could bind better to inactivated *Cryptosporidium*. While for the formalin-inactivated *Cryptosporidium* there seemed to be two subpopulations, one of which that displayed high fluorescence intensity, representing only a small number of oocysts (between 1.22 to 19.1 % of the total oocyst population), and one that displayed a fluorescence closer to the control.

For the heat-treated *Cryptosporidium*, the data showed more consistency between the mean and median of fluorescence intensity, indicating more homogeneous populations, except for the sample containing aptamer R4-6. However, because of the potential side-effects of the heat-inactivation process, such as structural changes and possible lysis, it could be that the gates corresponding to *Cryptosporidium* engulf quite a few events that are not *Cryptosporidium* such as lysis debris or reference beads. Moreover, it is likely that because the heat-treated *Cryptosporidium* were in much lower concentration, a substantially larger number of similar magnetic beads were in the gate, and it could be that the shift in fluorescence intensity is due to non-specific interactions with said beads. Nevertheless, this effect on heat-treated oocysts was also shown in Chapter 3 and it is further explored in Chapter 5.

5. Aptamer binding properties under different conditions

5.1. Introduction

Different conditions to improve aptamer binding were tried. In this chapter, three sets of experiments that were performed towards this goal are presented.

5.1.1. Exploration of the effect of pH on aptamer binding affinity.

Due to the negative nature of backbone linkages of ssDNA, aptamers have more affinity towards positively charged surfaces. However, some aptamers work well on neutral surfaces due to shape complementarity and hydrogen bonds, making the aptamer technology also applicable for relatively neutral molecules (Adachi & Nakamura, 2019). However, Lendner & Daugschies (2014) characterized the oocyst's wall and noted that the oocyst's wall is rich in electrons. This could mean that the electrostatic interactions between negatively charged oocysts and the also negatively charged aptamers are detrimental to aptamer binding.

Zhang & Landgraf (2012) noted that this is more of a problem during the SELEX procedure and proposed a series of modifications for selecting aptamers against negatively charged targets. One of the approaches was to eliminate the negative part of the target and leave only the epitope. Once the aptamer was selected, it was able to bind even in highly negative charged environment. However, if repeating the SELEX procedure is not feasible (as with this work), a simpler approach to overcome these repulsive forces is to modify the buffer's pH as proposed by Ahmad et al. (2011).

The objective of this work was to determine whether aptamer performance was linked to the pH and to determine if an improved binding ability could be achieved by overcoming these repulsive forces. It could be that electrostatic repulsion between the oocyst's membrane (which is negatively charged) and the aptamers (also negatively charged) was preventing the aptamers from binding to the target.

5.1.2. E.coli cross-reactivity assays

The objective of this work was to evaluate the selectivity of this aptamer at low pH using other microorganisms like *E. coli* as negative controls to assure that the binding was not due to non-specific electrostatic interactions.

5.1.3. pH effects on aptamer fluorophores

Le Guern et al. (2020) acknowledged that fluorescein is one of the most notorious pH sensitive molecules. They also noted that below pH values of 6.4 fluorescence intensity of fluorescein drastically decreases. Fluorescein under lower pH values shifts from its di-anionic form (at neutral pH) to mono-anionic and cationic species that show a significantly lower fluorescence intensity.

The objective of these experiments was to determine if there was an effect due to pH on the specific aptamer fluorophore, 6-FAM. This was to test the idea that at lower pH, the fluorescence intensity shown in previous sections was due to an intensifying effect of pH on the aptamer fluorophore (6-FAM) instead of due to an increase in binding affinity.

5.1.4. Effect on inactivation contact time for heat-treated oocysts

In Chapter 3, an aptamer binding phenomenon was observed for heat-inactivated *Cryptosporidium*. Although most of the oocyst population showed a fluorescence intensity close to the unstained sample, there was a subpopulation that showed a higher increase in fluorescence intensity. It was hypothesized that it could be that heat-treatment causes some sort of lysis that might enable better binding. To test this hypothesis, heat-treatment was again applied to the oocysts, varying the time the oocysts spend at 80ºC. It was hypothesized that a higher contact time would provoke more oocyst to undergo these changes that enabled better binding and therefore, a higher amount of the oocyst population would show an increase in fluorescence intensity.

5.2. Materials and Methods

Both live and formalin-inactivated *Cryptosporidium* were acquired from Waterborne Inc. The R4-6 aptamer labelled with fluorescein (6-FAM) at the 5’ end was

obtained from Integrated DNA Technologies (IDT). All other reagents were of analytical grade.

5.2.1. Buffer preparation and washing step

Different buffers, using the same stock solution, but adjusted to a different pH were prepared. The stock or main buffer composition was similar to what was described by Hianik et al. (2007). Briefly, an aqueous solution having 140 mM NaCl, 5 mM KCl and 1 mM $MgCl_2$ was prepared. pH was adjusted using 0.1 M HCl or 0.1 M NaOH as needed. Formalin-treated oocysts (10^7 oocysts/mL) were washed in buffers already equilibrated to the desired pH. Two wash steps were performed by centrifuging at 14,000 x g for 10 minutes.

5.2.2. Preparation of aptamer or antibody samples

Aptamers were diluted from the stock solution (1 mM) in folding buffer (DPBS with $CaCl_2$ and $MgCl_2$) to a concentration of 50 µM and heated at 92ºC for 5 minutes, followed by cooling at room temperature for 15 minutes. 20 µL of the above aptamer solution was incubated with each type of inactivated *Cryptosporidium* at each type of buffer for a final aptamer concentration of 10 µM, for 1h. Antibodies with a final concentration of 10 µg/mL were incubated with 100 µL of formalin-treated oocysts for each pH condition. After 1 h of incubation, the samples were washed by centrifuging at 9,000 x g for 15 minutes. The samples were then run through an imaging flow cytometer (ImageStream ® X Mk II Imaging Flow Cytometer, with an excitation laser of 488nm).

5.2.3. *E. coli* cross-reactivity assays

E. coli strain ATCC 10798 was grown on laurel sulphate broth for 24 hours at 37 degrees C before being resuspended in PBS 1X + Formalin 5%. *E. coli* (10^7 CFU/mL) was then washed in each of the buffers twice by centrifugation at 5,000 x g for 10 minutes and resuspension of the pellet on the appropriate buffer at each pH. Aptamers were diluted from the stock solution (1 mM) in folding buffer (DPBS with $CaCl_2$ and $MgCl_2$) to a concentration of 50 µM and heated at 92 ºC for 5 minutes, followed by cooling at room temperature for 15 minutes. 20 µL of the above aptamer solution was incubated with *E. coli* in each pH buffer for a final aptamer concentration of 10 µM, for 1h. After 1 h of incubation these samples were washed by centrifuging at 8,000 x g for 10 minutes. The samples were then run through an imaging flow cytometer.

5.2.4. Study of the effect of pH on the aptamer fluorophores

In a UV-black 96-well plate, 10 µL of 50 µM fluorescein-labelled R4-6 aptamer was diluted in 200 µL of the pH-adjusted buffer used in the previous experiments (pH: 2, 3, 4, 5, 7.2, 10.1). Fluorescence was read in a microplate reader using an excitation of 480 nm. 6Length of heat-treatment inactivation

Samples containing 100 µL of live *Cryptosporidium* at a concentration of 10^6 oocysts/mL were prepared in DPBS. Each vial was place in a hot water bath at 80ºC for either 15, 20, 25, 30, 45 or 60 minutes. To each vial, aptamer R4-6 labelled with fluorescein at the 5' end was added to a final concentration of 600 nM. Samples were incubated for 30 min in a shaker and after the incubation period, unbound aptamers were removed by centrifuging the samples at 6,000 x g for 10 minutes. The supernatant was discarded and the pellet resuspended in 200 µL of DPBS. This process was repeated twice. The samples were then run through a flow cytometer (BD Accuri™ C6 Plus, excitation at 488 nm). Emission was recorded in the green fluorescence range.

5.3. Results and Discussion

5.3.1. Effect of pH on binding affinity.

5.3.1.1. Broad range pH experiment

In Table 11 the mean and median of green fluorescence intensity determined by imaging flow cytometry is shown for each pH. Standard deviations were obtained following the procedures mentioned in Appendix I.

Table 11. Mean and median of fluorescence intensity for each pH

Sample		pH			
		2.4	5.2	7.2	10.2
Unstained	Mean	7612	5137	5088	5211
	Median	7371	5299	5308	5278
	Standard deviation	2415	1648	1630	2350
Aptamer Stained	Mean	150008	8998	10822	6716
	Median	153630	5571	5493	4936
	Standard deviation	108936	3814	9369	9140
Antibody Stained	Mean	8155	108560	104084	148757
	Median	7614	80022	62437	153761
	Standard deviation	4084	85365	107148	113930

The mean and median of fluorescence intensity being fairly close to one another, and the values of standard deviation given, suggests that a single population of oocyst were found (and that the binding was uniform throughout the sample).

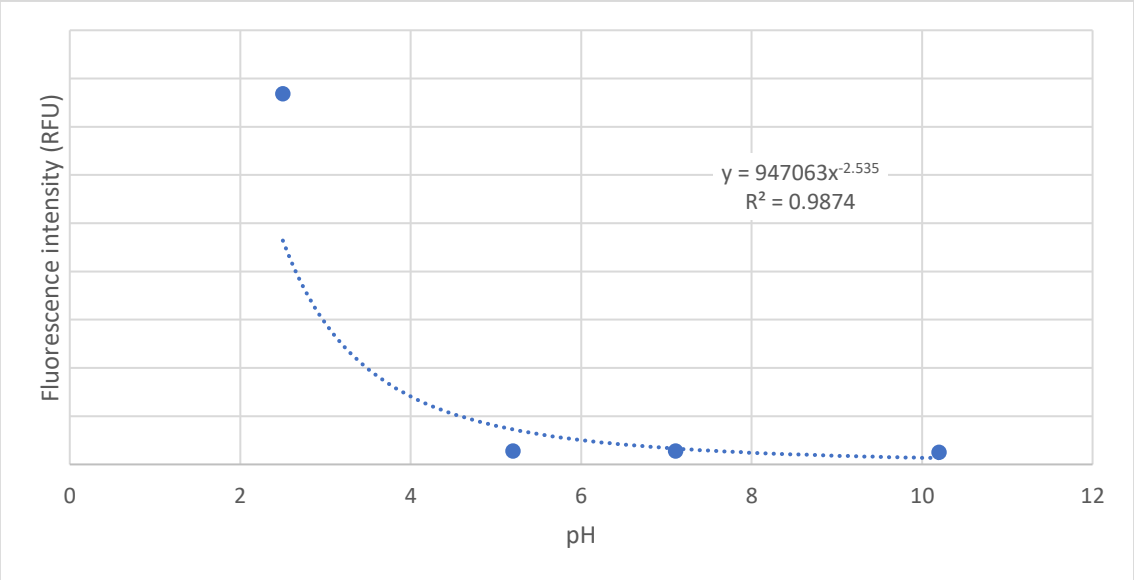

Figure 41.Median of fluorescence intensity as a function of pH

Only for very low values of pH (pH=2.5) was there an increase in fluorescence intensity for aptamer bound oocysts (Figure 41). This binding was also confirmed through imaging, as shown in Figure 42. However, this condition is quite different from those reported in the literature for *Cryptosporidium* aptamers. Iqbal et al. (2015) performed aptamer-oocysts binding electrochemical measurements in PBS with a pH value of 7.4, while Hassan et al. (2021) performed binding assessment experiments in DPBS with a pH of 7.3. Values obtained here are therefore quite far from the pH these aptamers were designed to work in and what other authors used in the literature.

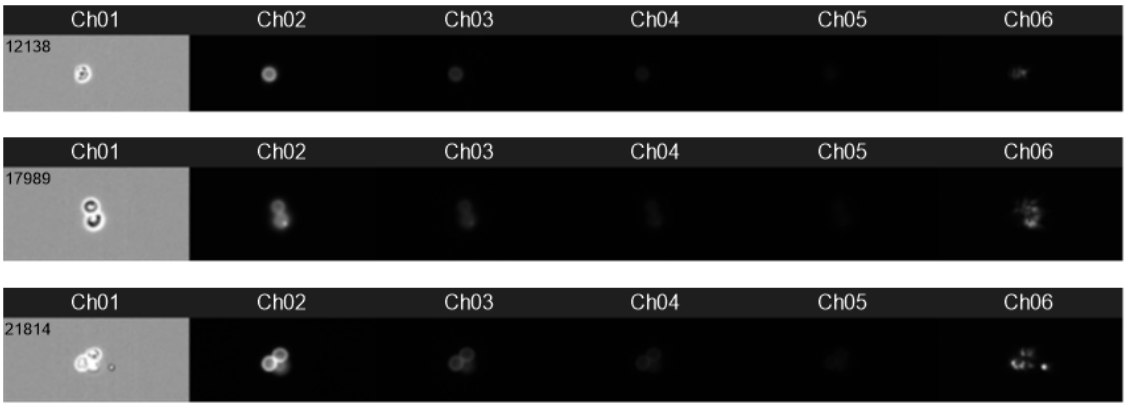

Figure 42. Imaging of C. parvum stained with aptamers at a pH of 2.4. Where Channel 1 is the brightfield, Channel 2 is FITC fluorescence and Channel 6 shows the side scatter.

Since the isoelectric point of oocysts is around 2.5 (Drozd & Schwartzbrod, 1996), this could mean that the aptamer was not binding to the oocyst surface because of electrostatic repulsion between two negative elements. However, it could also mean that the binding is due to non-specific electrostatic interactions due to the low pH of the buffer.

For the antibody-stained oocysts, as shown in Table 11, the effect is the opposite, the lower the pH, the lower the fluorescence intensity. This could be because the antibody binding affinity could be decreased at acidic pH values.

5.3.1.2. Low range pH

The previous experiment was repeated using buffers at lower pH for aptamer-stained, formalin-treated oocysts. The results are shown in Table 12 and Figure 43.

Table 12.Mean of fluorescence intensity as a function of pH – Low pH range

pH	Unstained oocysts		Aptamer-stained oocysts	
	Mean of fluorescence intensity	Standard deviation	Mean of fluorescence intensity	Standard deviation
2	6408	2156	256756	209336
3	6694	1546	175458	82427
4	5528	5228	25419	51168
5.2	4750	2867	9062	3381

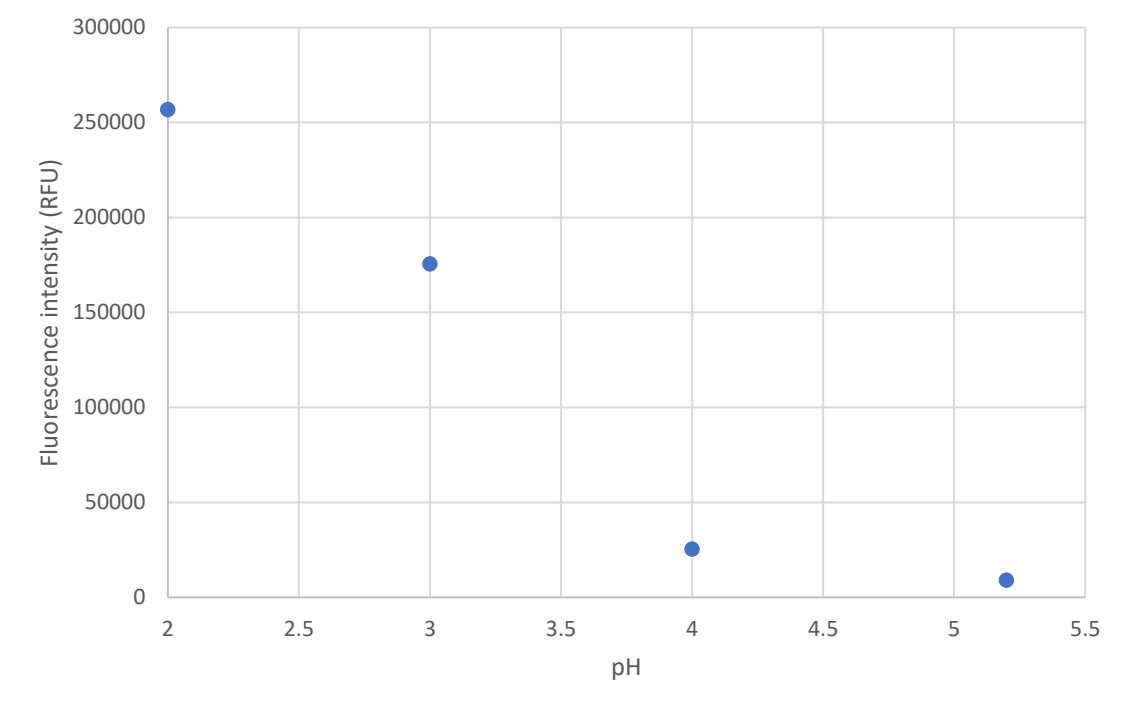

Figure 43. Mean of fluorescence intensity as a function of pH – Low pH range

For pH between 2-4 there was an improvement in binding due to pH. For pH 4 and up, there was no noticeable change in the binding affinity of the aptamers.

It seems that lowering the pH effectively reduced the repulsive electrostatic interactions between aptamers and oocysts and improved binding. However, this effect

was only noticeable up to a pH of 4. These conditions are not commonly used in biological applications and further assays are needed to confirm the specificity of this binding under these pH conditions.

5.3.2. *E. coli* cross-reactivity assay

To gate the *E. coli* population, the sample that contained aptamers at a pH of 2.5 was used. It was assumed that some aptamers were attached to the *E. coli* but not the beads, since the beads are running within the machine and the kinetics of the binding would be slower than the contact time between the machine-run beads and the aptamers, while *E. coli* was incubated with the aptamers for an hour.

The fluorescence intensity was represented in a histogram and the second highest peak was assumed to be the *E. coli* population.

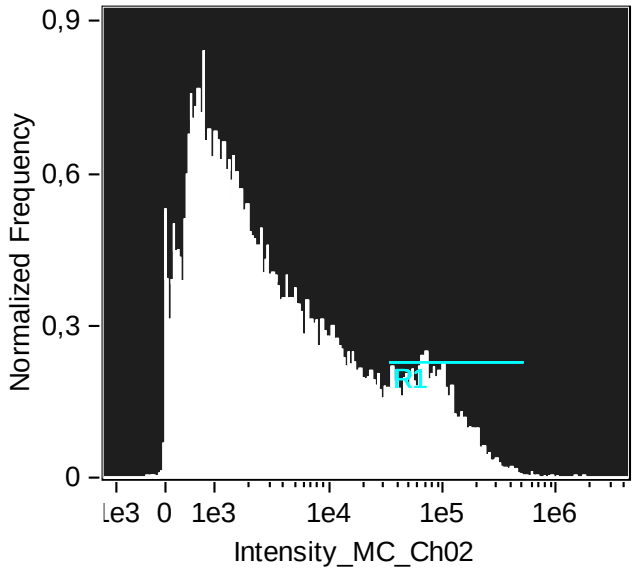

Figure 44. Histogram of fluorescence intensity for all the recorded events. Subpopulation marked as R1 was considered to be E. coli.

The population with higher fluorescence intensity, named R1 was then represented in the pseudo FSC -vs- SSC and a gate according to size and granularity was created around these points.

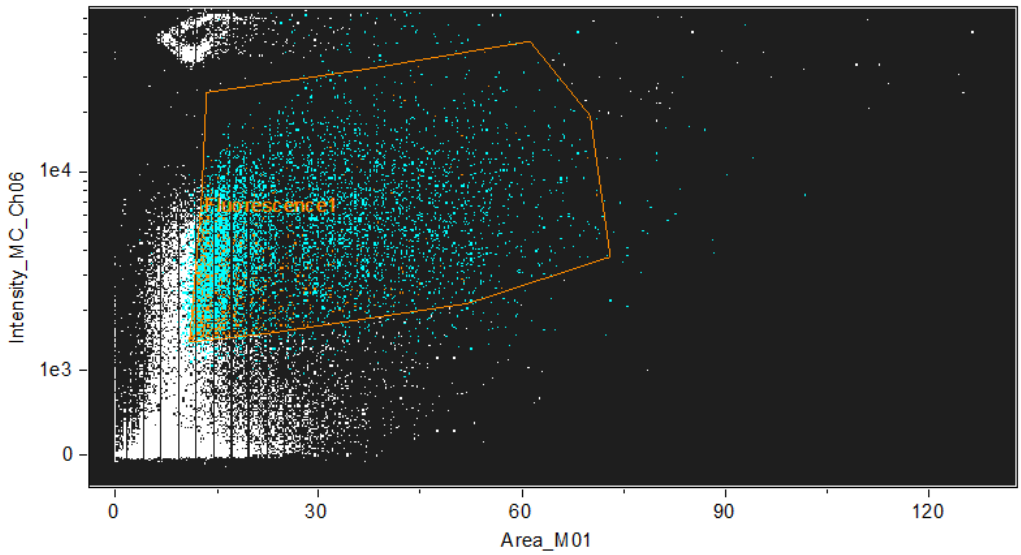

Figure 45. Pseudo FSC -vs- SSC for E. coli and the gate created for this population according to size.

This gate was applied to all samples, and the mean and median of fluorescence intensity was taken within the gate and shown in Table 13.

Table 13.Mean and median of fluorescence intensity dependence on the pH for a negative control using E. coli

Sample	Mean	Median	Standard deviation
Unstained	567	284	353
pH 2	115914	96912	78133
pH 2.5	79736	65901	69966
pH 3	39667	34434	40422
pH 4	35918	31229	41088
pH 5.2	37435	28905	45732
pH 7.2	37940	26809	45197
pH 10.5	32545	20823	38720

There seemed to be a mean fluorescence intensity difference between unstained samples and aptamer-stained samples that varied with pH.

Plotting the median of fluorescence intensity vs pH, there seemed to be a correlation between binding affinity and pH up to a pH of 3, as shown in Figure 46.

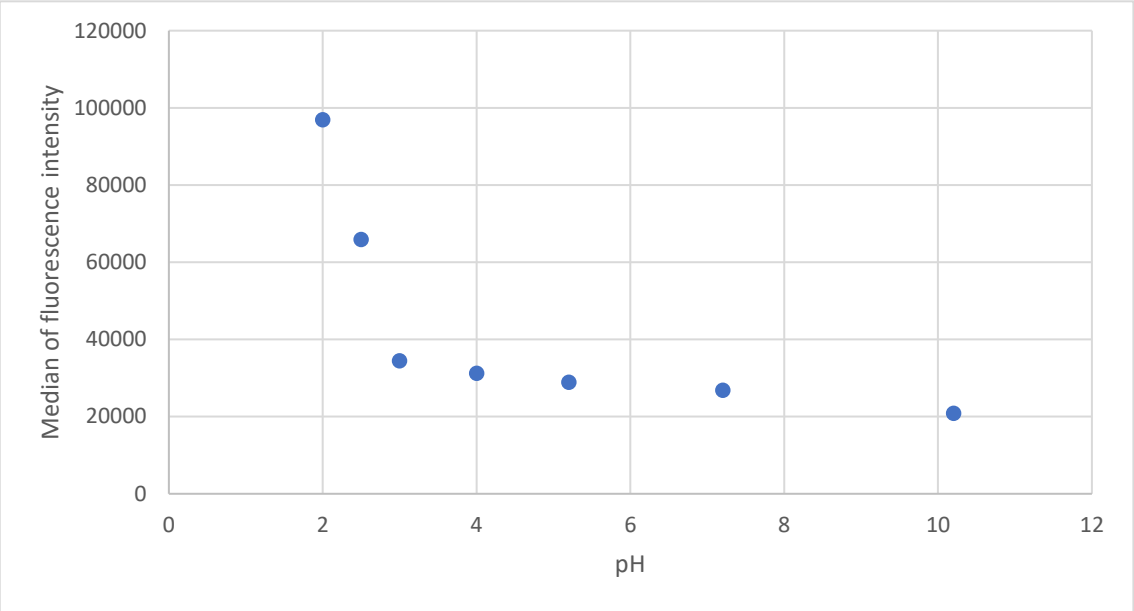

Figure 46. Mean of fluorescence intensity as a function of pH for E. coli cross-reactivity assay.

Binding of the aptamers to *E. coli* was enhanced by lowering the pH. This seems to indicate that the previous binding observed with the oocysts was, in fact, due to non-specific electrostatic interactions, since the aptamer used, aptamer R4-6 was selectively chosen to be specific against *Cryptosporidium*. It is likely that the aptamers non-specifically bind to any negatively charged surface in a non-specific way. However, although less likely it could be that at lower pH, fluorophores like 6-FAM show an increase in fluorescence intensity and that the signal observed in these experiments at low pH is due to some background noise. The next section of this Chapter explores the effect of pH on this fluorophore.

5.3.3. pH effect on aptamer fluorophores

5’ fluorescein-labelled aptamer R4-6 was diluted in buffers with different pH to observe the effect of pH on the fluorophores. These samples were then analyzed using fluorescence plate reader with an excitation of 488 nm. The emission spectrum for each pH is shown in Figure 47.

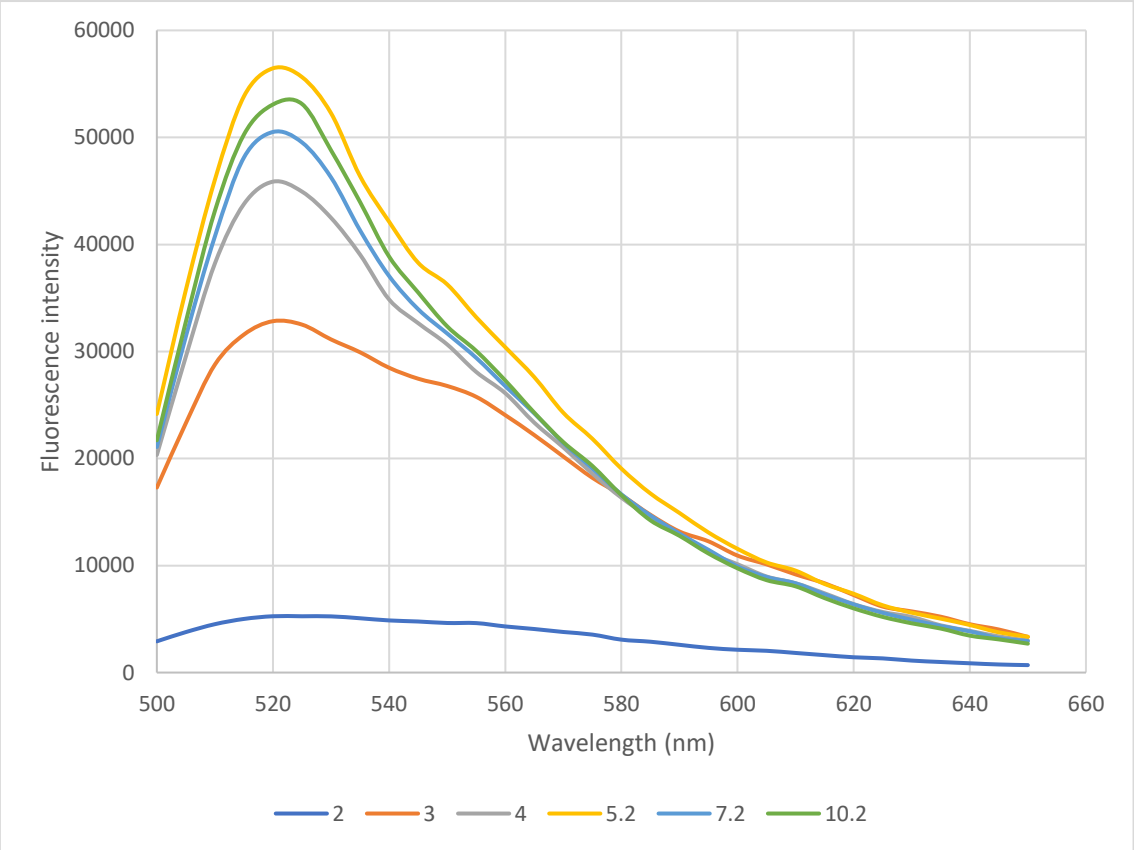

Figure 47.Fluorescence spectrum that shows the effect of pH on fluorescence intensity for the aptamer fluorophore (6-FAM)

The maximum peak at 520 nm was plotted as a function of pH since this peak is the most relevant point of the spectrum. 520 nm also corresponds with green fluorescence. Results are shown in Figure 48 and Table 14.

Table 14. Effect of pH to fluorescence intensity for the aptamer fluorophore (6-FAM)

pH	**2**	**3**	**4**	**5.2**	**7.2**	**10.2**
A_{520}	5263	32832	45868	56458	50509	53078

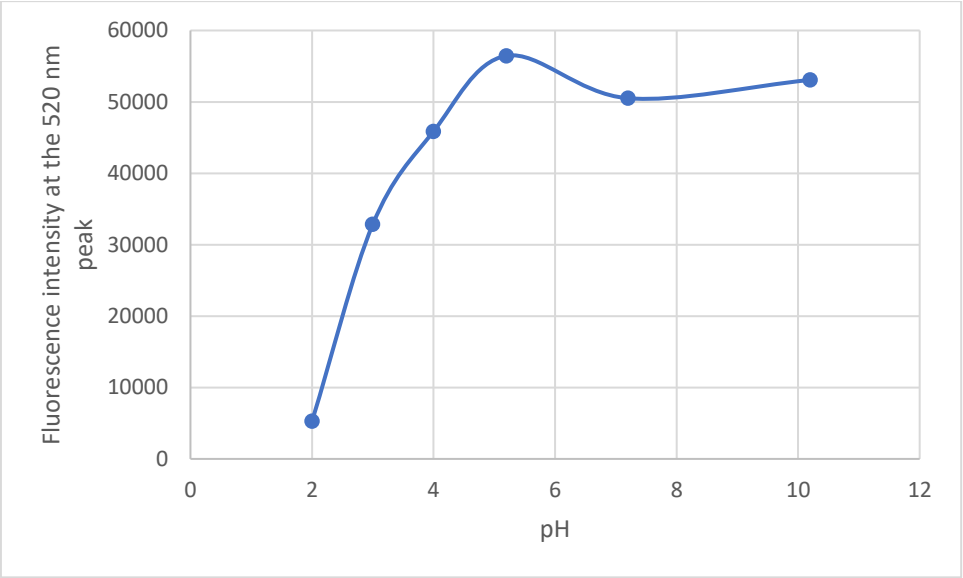

Figure 48.Effect of pH to fluorescence intensity for the aptamer fluorophore (6-FAM)

At low pH the fluorophore activity is significantly lower. The fluorescence intensity is higher as we move to higher pH until it reaches a plateau around a pH of 5. This effect in which at lower pH the fluorescence intensity decreases is also reported by Le Guern et al. (2020). Since the effect of low pH on the fluorophore seems to lower the fluorescence intensity of the aptamers, instead of raising it, it can be concluded that the higher peak in fluorescence intensity on previous oocysts and *E. coli* samples at low pH was not due to the effect of the pH on the aptamer fluorophores but because of a significant increase in non-specific binding.

5.4. Effect of inactivation time for heat-treated Cryptosporidium.

Gating was done following the same strategy as previously described. Briefly, a gate was selected around the most distinct population, as shown in Figure 49.

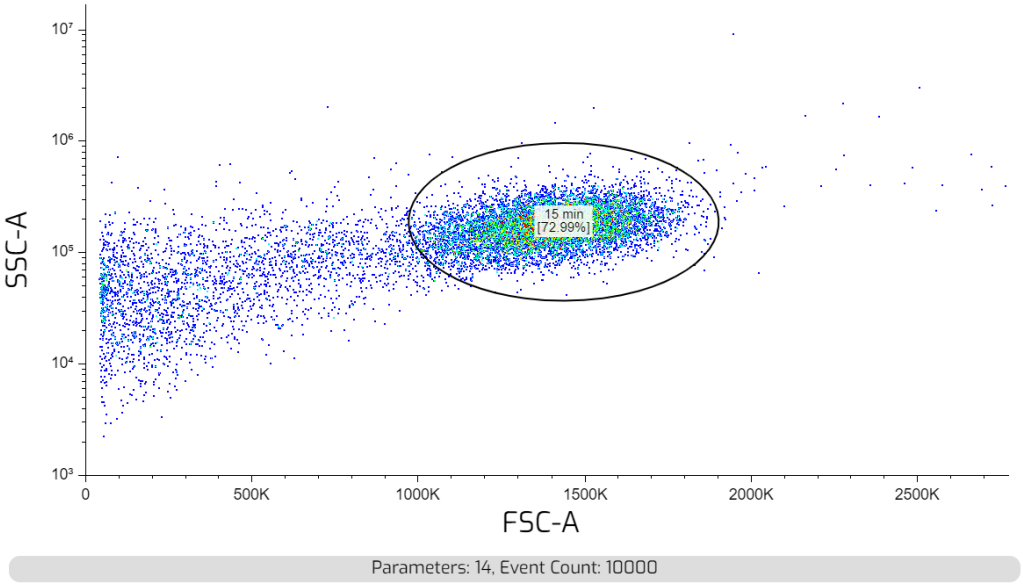

Figure 49. FSC vs SSC plot for an unstained heat-treated oocyst sample and gate created around the oocyst population

As in previous Chapters, the histogram of fluorescence intensity within the gate was taken and the subpopulation containing a higher fluorescence intensity was singled out in each histogram. As an example, the histogram and the subpopulation range chosen is shown in Figure 50 and corresponds to the sample inactivated for 45 min.

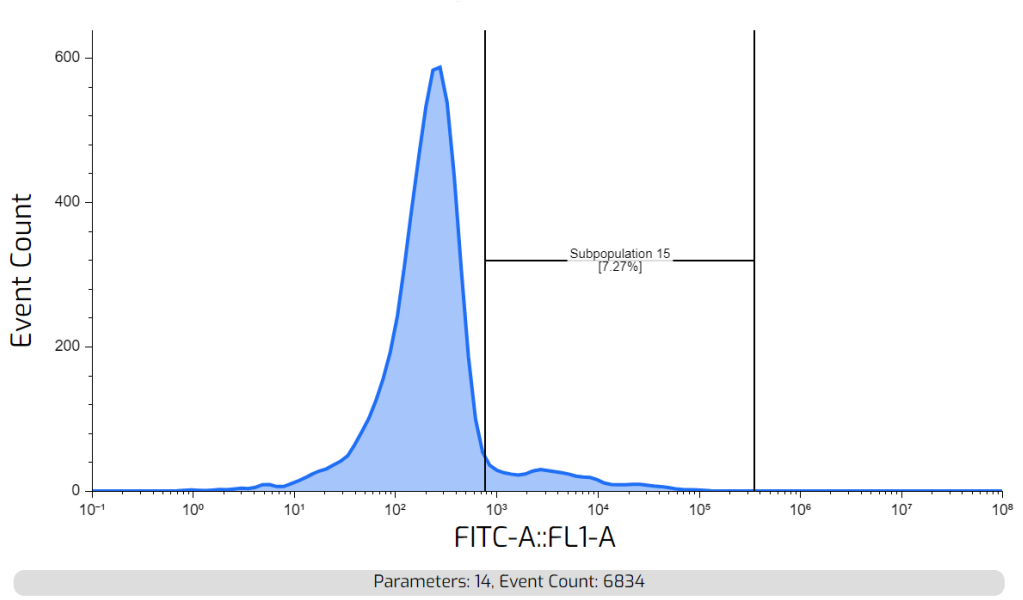

Figure 50. Histogram of fluorescence intensity for an aptamer-stained sample of oocysts heat-inactivated for 45 minutes that shows the chosen high-fluorescence subpopulation

To compare each sample, this gating was applied consistently to all histograms. The percentage of events within this range with respect to the total of the gated population was chosen as the crucial parameter needed to compare each sample. A

higher percentage means that a higher number of oocysts underwent changes necessary for increasing aptamer binding. It was also expected that a higher contact time in an 80ºC water bath would render a higher percentage of high-binding *Cryptosporidium*.

This percentage was represented as a function of the inactivation time as shown in Table 15 and Figure 51.

Table 15.Percentage of events within the range as a function of the inactivation time

Inactivation time (minutes)	Percentage of events within the range (%)
15	2.44
20	7.01
25	5.5
30	2.98
45	7.27
60	2.77

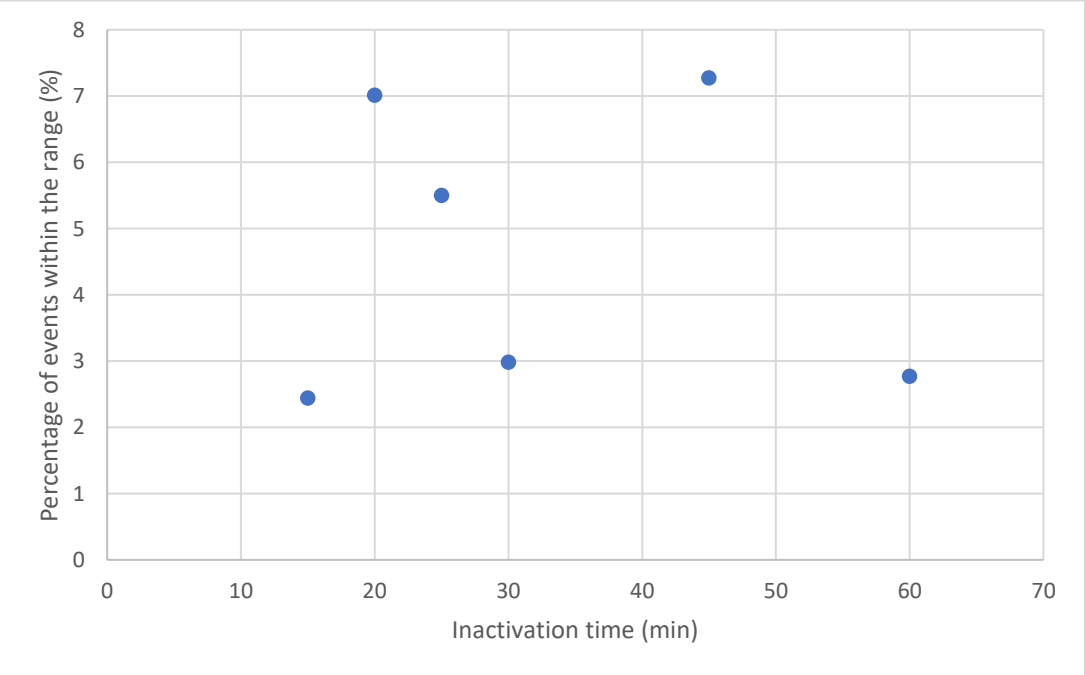

Figure 51. Percentage of events within the range as a function of the inactivation time

No correlation between the percentage of events within the range and the inactivation time was observed. This seems to disprove the original hypothesis around

a better binding for heat-inactivated *Cryptosporidium* due to lysis or other structural changes caused by the heating process. It could be that our initial observation noted in Chapter 3 in which a clear subpopulation with higher fluorescence intensity was shown was because of uneven inactivation or because some other events not corresponding to *Cryptosporidium* were included in the gate.

5.5. Conclusions

While varying some conditions such as pH showed some increase in binding affinity, these improvements showed to be non-specific. For heat-treated *Cryptosporidium,* no correlation between the heat-treatment process and an increase in the number of oocysts detected could be established.

As for the conditions tested, no condition improved the binding affinity of inactivated oocysts to levels shown in the literature for flow cytometry performed on live oocysts. It could be that changes on the oocyst structure that occurred during inactivation could not be overcome or that some other critical property not reported in the literature is crucial for aptamer binding.

6. In-filter testing of *C. parvum*

6.1. Introduction

Cryptosporidium occurrence in natural waters happens in low concentrations. Montemayor et al. (2005) found that while all examined samples contained oocysts, the concentration in river water samples, in a river in north-eastern Spain was 0.43 to 1.36 oocysts/L. Similarly, Bodley-Tickell et al. (2002) studied the occurrence of *Cryptosporidium* in surface waters draining from a livestock farm and determined a median concentration of 0.48 oocysts/L.

Since *Cryptosporidium* causes disease even at low concentrations, sampling large volumes of water is necessary. This in turn means that filtration of large quantities of water is necessary to concentrate *Cryptosporidium* and to be able to safely detect it. EPA Method 1623 requires ten liters of water to be filtered for the detection of *Cryptosporidium*. One of the barriers to better *Cryptosporidium* detection in water monitoring is the low recovery rates, particularly the low efficiency in its elution from the filters used during large volume of water filtration. Some studies report an average recovery rate from elution of 22% and according to EPA standards, a 38% recovery rate is considered acceptable (Pavli et al., 2016). Some research has been done around improving this recovery rate by modifying the filter membrane materials for better elution (Pavli et al., 2016) or improving the elution buffer for improved recovery rates from the filter (Inoue et al., 2003).

Cryptosporidium high resistance to chlorination methods and the nature of recreational water settings (close contact with possible infected individuals, small volume of water and therefore less dilution, etc.) make recreational waters such as pools or spas an important source of transmission. Having access to on-site detection methods, available for use by the general public and possibly recreational facilities staff could make *Cryptosporidium* early detection an important asset to avoid outbreaks.

In this Chapter, the possibility of developing an in-filter, easy to use detection method for *Cryptosporidium* is explored. There were two goals around this sensing strategy. The first one was to eliminate the elution step since this is one of the biggest barriers around detection. The second one was to make this detection method simple

to use for the general public, so *Cryptosporidium* detection could be available and be used at recreational facilities.

This in filter detection involved a short number of steps and its basic mechanism is depicted in Figure 52. Briefly, HRP-labelled antibodies were incubated with *Cryptosporidium* for an hour. After the incubation period the oocyst-antibody complex was passed through a syringe filter followed by a washing step consisting of passing a washing solution through the filter to remove unbound antibodies. 3,3',5,5'-Tetramethylbenzidine (TMB) is then added to observe a blue color change within the filter membrane. When HRP is present, the otherwise colorless TMB working solution turns blue.

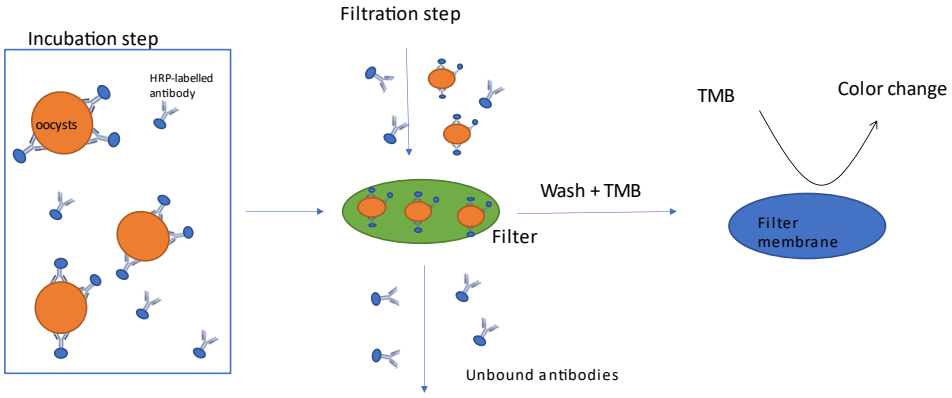

Figure 52. Graphical representation of the working principle behind the in-filter detection of Cryptosporidium

In this chapter, several factors for the determination of the optimal operation conditions of the biosensing technique were studied.

6.1.1. Effect of surfactant and blocking agents on reducing the background noise and false positive results

The syringe PES filters used showed some degree of protein binding, and this translates into the appearance of false positives. To reduce the background noise and therefore the non-specific protein binding of HRP-labelled antibodies when no oocysts were present, different surfactants and blocking agents were tested as pre-coating solutions for the filters. By pre-coating the filters, a reduction of background noise and non-specific binding was expected.

6.1.2. Effect of pore size on reduction of background noise

The objective of this work was to determine whether the pore size of the syringe filter membranes had a noticeable effect on background noise. It was hypothesized that a bigger pore size would allow the unbound antibodies to pass more freely through the filter membrane and therefore there would be less background noise. To examine this effect, a series of antibody dilutions were passed through filters of different pore sizes. Both visual proof of binding and the liquid retained within the filter were collected to this end.

6.1.3. Effect on pore size on the limit of detection for *C. parvum*

The objective of this set of experiments was to determine whether pore size had a significant effect on the LOD of *Cryptosporidium*. In previous sections of this Chapter, antibody concentration and preconditioning agents of the filter were already optimized. Using those conditions, this experiment followed the detection procedure illustrated in Figure 52. Antibodies and oocysts were first incubated together, and the solutions were passed through different kinds of filters followed by washing and the addition of TMB to observe a color change. Oocysts vary in size from 4.2 to 5.4 µm (Global Health, Division of Parasitic Diseases and Malaria, 2019). It could be that bigger pore sizes such as 5 µm let some of the oocysts pass through and therefore some sensitivity would be lost.

6.1.4. Negative control using *E. coli*

The main reason to use pore sizes from 1 µm and above is to promote a better separation of the oocysts from smaller bacteria and debris present in the water to improve *Cryptosporidium* detection and reduce background noise. However, it could be that a high concentration of bacteria still causes an agglomeration of antibodies that can render a false positive. Moreover, it could be that the LOD using high concentrations of *Cryptosporidium* was due to non-specific entrapment of HRP-labelled antibodies instead of specific binding. To determine whether the HRP-labelled antibodies + oocysts interaction was specific and to determine if there was non-specific entrapment due to high concentrations of bacteria, experiments were repeated with *E. coli*.

6.1.5. Effect of incubation time on antibody binding

Providing enough antibody-oocyst contact time could be crucial to improve binding and therefore to increase the detection sensitivity of this approach. To determine if there was an optimal binding time, the LOD number of oocysts was incubated for different periods of time and passed through a 3 µm filter.

6.2. Materials and Methods

1 µm, 3 µm and 5 µm PES syringe filters of 25, 20 and 25 mm of diameter were purchased from Tisch Scientific (Cat. No: SPEC18102; SPEC18112 and SPEC18104). Live *Cryptosporidium* were acquired from Waterborne Inc. Polyclonal IgG Anti-*Cryptosporidium* HRP-labelled antibodies were purchased from GeneTex Inc. (Catalog number: GTX36458). Phosphate-buffered saline (PBS, 10 X), pH= 7.4 was bought from Alfa Aesar and further diluted to 1X in deionized water (DI water). 3,3',5,5'-Tetramethylbenzidine (TMB) was purchased from Sigma-Aldrich (Cat. No :860336). All other reagents were of analytical grade.

6.2.1. Experimental procedure for determining the effect of surfactant and blocking agents on reducing the background noise

Five 1 µm PES filters were precoated with 10 mL of either: 2% Casein in DI; 2% BSA in DI; 2% Tween 20 in PBS (1X, pH=7.4); 2% Tween 80 in PBS (1X, pH=7.4); or just PBS. After passing the precoating solution, the membrane was left for 5 min.

Five 10mL solutions of HRP-labelled antibodies (0.075; 0.15; 0.5; 1 and a control 0 µg/mL) were made in PBS + Tween 80 (0.1%). Solutions were passed through the filter, followed by 40 mL of PBS + Tween80 (0.1%). Finally, 300 µL of TMB was added to the filters and after 10 minutes, results were recorded, both by taking a picture of the filters, and by collecting the liquid retained within the filter in a 96-well plate to measure the absorbance.

6.2.2. Experimental procedure to determine the effect of pore size on non-specific background noise

Five filters of each type (1 µm, 3 µm and 5 µm) were pretreated by passing 10 mL of PBS 1X + Tween80 (2%) and letting it interact with the filter for 5 minutes.

Four 10 mL solutions of HRP-labelled antibodies (0.05; 0.15; 0.5; 1 and a control 0 µg/mL) were made in PBS + Tween80 (0.1%). Each solution was passed through each filter followed by 40 mL of PBS + Tween80 (0.1%) through the filters. 300 µL of TMB was then added into the filters and results were recorded after 5 minutes, both by taking a picture of the filters and by collecting the liquid retained within the filter in a 96-well plate to measure the absorbance.

6.2.3. LOD procedures

For each kind of filter (1 µm, 3 µm and 5 µm), different concentration of oocysts (10^6, 10^5, 10^4 and 0 in 10 mL) were incubated with HRP-labelled antibodies that were at a final concentration of 0.05 µg/mL for 30 minutes.

Simultaneously, each filter was preconditioned by passing 5 mL of PBS 1X + Tween80 (2%) and letting it interact with the filter for 5 minutes

After the incubation period with the antibodies, each oocyst solution was passed through the different size filters followed by 40 mL of PBS + Tween80 (0.1%) through each filter. Then, 300 µL of TMB was added into the filters and results were recorded after 5 minutes, both by taking a picture of the filters and by collecting the liquid retained within the filter in a 96-well plate to measure the absorbance.

6.2.4. Cross-reactivity assays

Different concentrations of *E. coli* (10^6, 10^5, 10^4 and 0 in 10 mL) were incubated with HRP-labelled antibodies that were at a final concentration of 0.05 µg/mL for 30 minutes. 3 µm syringe filters were preconditioned with 5 mL of PBS 1X + Tween80 (2%) and letting it interact with the filter for 5 minutes.

After the incubation period with the antibodies, each *E. coli* solution was passed through the 3 µm filter followed by 40 mL of PBS + Tween80 (0.1%). Then, 300 µL of TMB was added into the filters and results were recorded after 5 minutes, both by taking a picture of the filters and by collecting the liquid retained within the filter into a 96-well plate and analysis by spectrophotometer to record absorbance.

6.2.5. Time dependence assays

Five different solutions of 10^6 oocysts were prepared in 10 mL PBS 1X + Tween80 (0.01%) and incubated with 0.05 µg/mL of anti-*Cryptosporidium* HRP-labelled antibodies for 3, 10, 15, 30 and 60 minutes respectively.

After each incubation period, each solution was passed through a preconditioned 3 µm filter followed by 40 mL of PBS + Tween80 (0.1%). Then, 300 µL of TMB was added into the filter and results were recorded after 5 minutes, both by taking a picture of the filters and in a 96-well plate to measure the absorbance.

6.3. Results and Discussion

6.3.1. Effect of surfactant and blocking agents on reducing the background noise and false positive results

Figure 53 shows the absorbance of the collected liquid for each pre-treatment and antibody concentration sample.

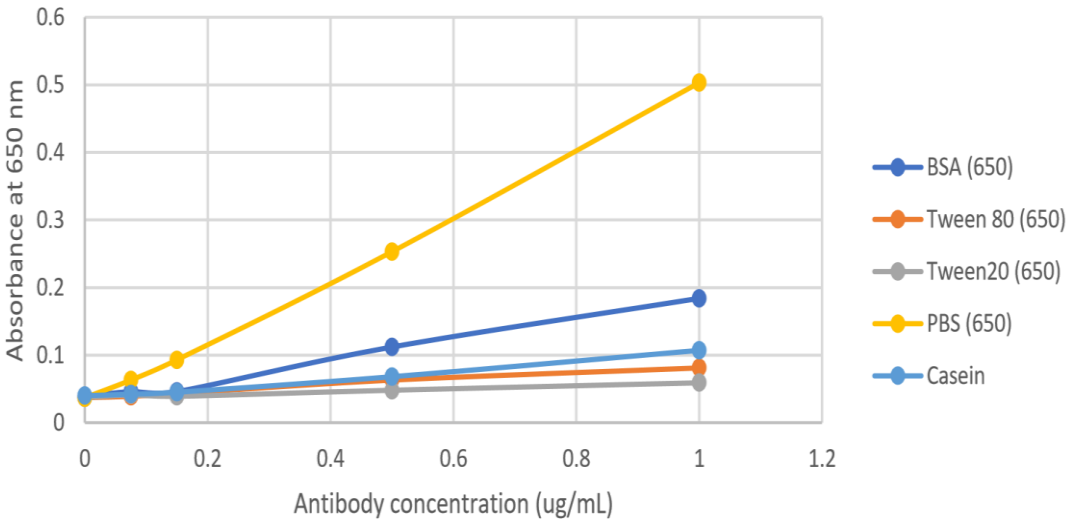

Figure 53. Comparison of the absorbance at 650 nm for different blocking agents

Figure 54 shows a picture of the different preconditioning solutions and the antibody concentrations passed through each filter as a visual proof of non-specific binding and false positive presented at high antibody concentrations.

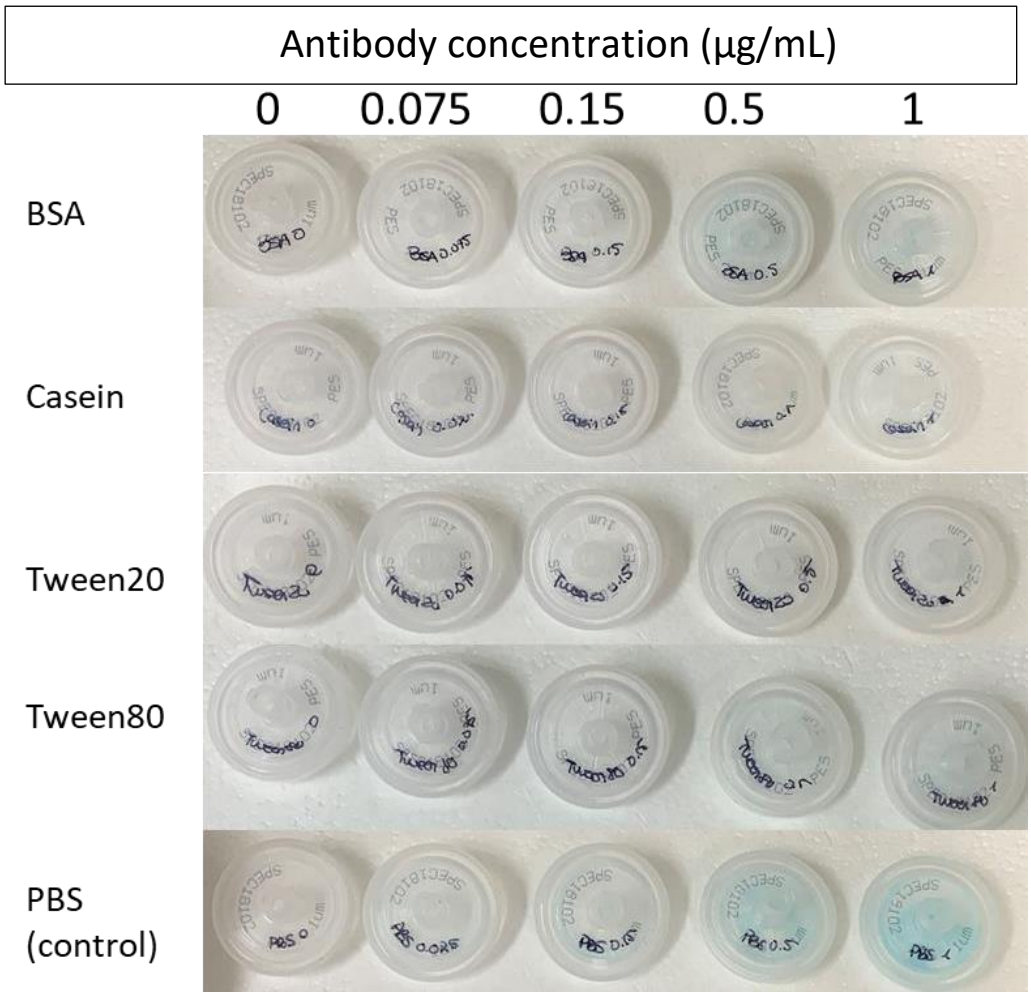

Figure 54. Visual representation of the non-specific binding of antibodies for each kind of pre-treatment agent for a 1 µm pore size, 25 mm diameter filter

Surfactants prevent protein adsorption to solid interfaces by competing for binding sites (Mahler et al., 2010). Moreover, Mahler et al. (2010) advised to do a preflush of a protein-free solution (in their case, they used Tween80 and Tween20) to saturate the filter adsorption sites.

Baldo et al. (1986) compared several nitrocellulose filters and blocking agents and both Tween20, skim milk powder and BSA showed a significant reduction of non-specific binding compared to untreated filters. The comparison between blocking agents depends on the antibody they used and the type of filter. There is no universal best blocking agent but Tween20, skim milk and BSA show a significant reduction of non-specific binding in all the cases, compared to the untreated filters.

Pre-treatment of the filter had a significant effect on non-specific binding of antibodies. The filters without pre-treatment (PBS sample) showed a significantly higher

background signal than those pretreated with surfactants or blocking agents. Pre-treatment with casein, Tween80 and Tween20 showed a higher reduction in background signal compared with BSA.

Since casein, PBS + Tween20 and PBS + Tween80 have a similar effect on background noise, Tween80 was used in subsequent experiments.

6.3.2. Effect of pore size on reduction of background noise

The visual characterization of the non-specific binding was done by taking a picture of the filters 5 minutes after the addition of TMB. These results are shown in Figure 55

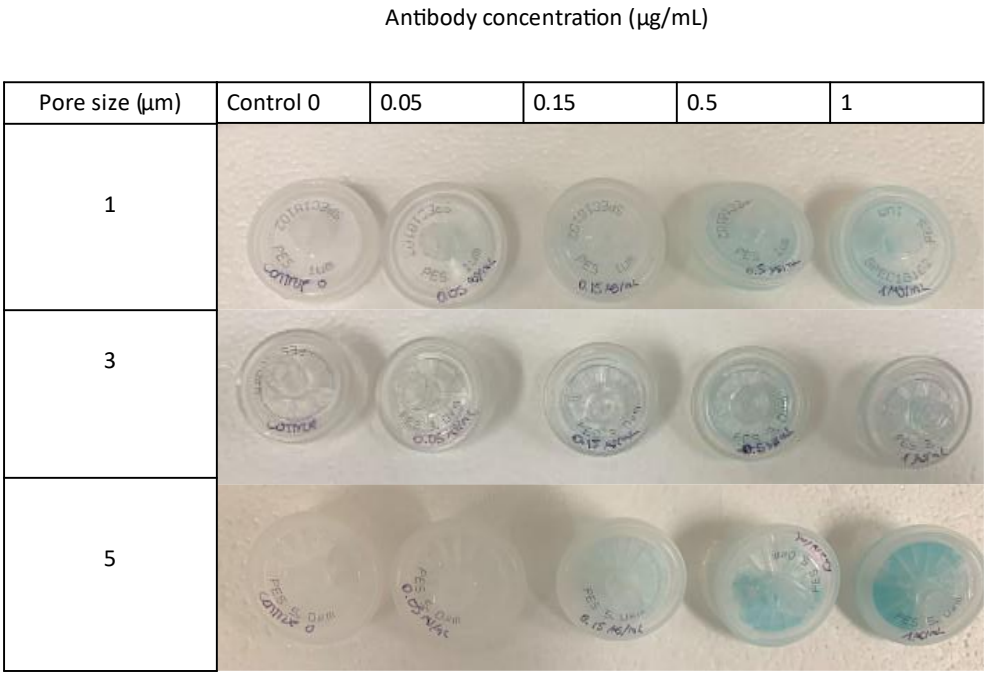

Figure 55. Visual representation of the influence of pore size on non-specific antibody binding. All filters were pretreated equally by using Tween80 (2%).

For almost all pore sizes, concentrations of HRP-labelled antibodies equal or above 0.15 µg/mL render a high signal and therefore high non-specific binding and false positive.

All the retained liquid within the filters was collected in a 96-well plate and the absorbance spectrum of all the samples were measured with a microplate reader. In Figure 56, the absorbance peak at 650 nm for each filter is compared.

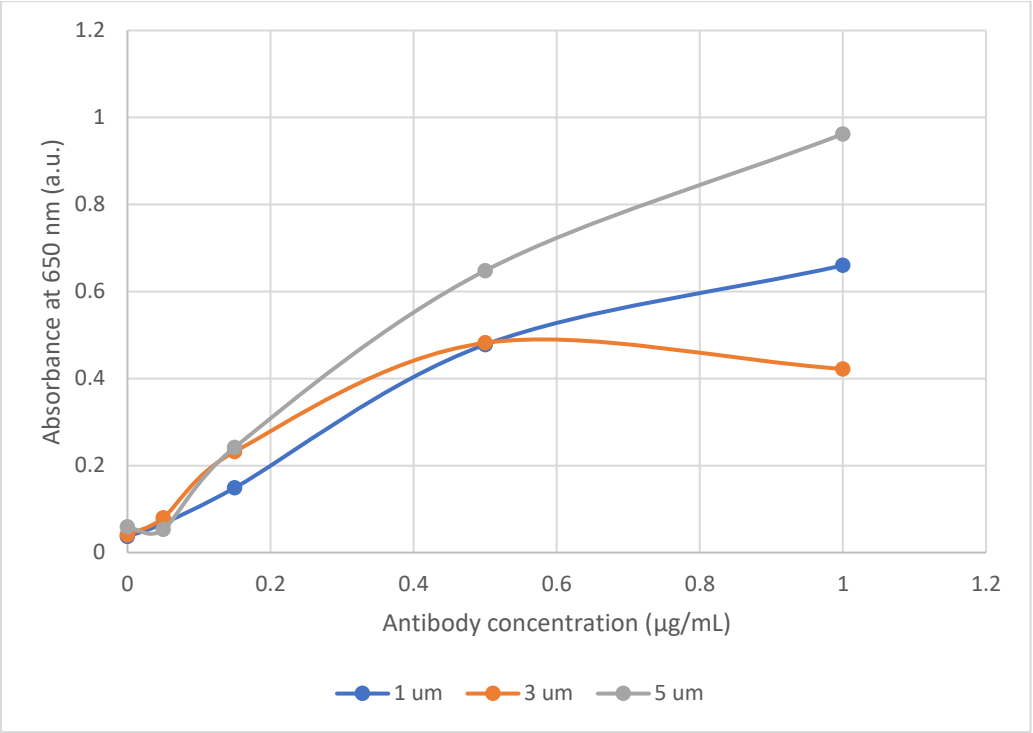

Figure 56. Absorbance peak as a representation of the influence of pore size on non-specific antibody binding

For all filters, concentrations above 0.15 µg/mL had an increase in absorbance and therefore would provoke a false positive. Therefore, 0.05 µg/mL was elected as the optimal antibody concentration for subsequent experiments. No correlation between pore size and non-specific binding was found. While it was hypothesized that a bigger pore size would mean less background signal because the antibodies could pass more freely, these results show that the biggest background signal was found in the biggest pore size filters. Background signal for 3 and 1 µm filters were quite similar. While 3 µm filters had a higher signal than 1 µm filters at lower concentration, 3 µm filters showed less increase as the antibody concentration increased. There does not seem to be a noticeable effect of pore size in the reduction of background noise. Antibody concentration, filter pre-treatment and use of a surfactant had a greater impact on the reduction of background noise. Non-specific binding of the antibodies is likely influenced more by the filter material than the physical attributes of the filter.

6.3.3. Effect on pore size on the limit of detection for *C. parvum*

Figure 57 shows the visual representation for the LOD of each filter. Only higher concentrations of oocysts (10^6 oocysts/ 10 mL) resulted in a signal in every filter. Visually, the signal is higher for pore sizes of 1 and 3 µm.

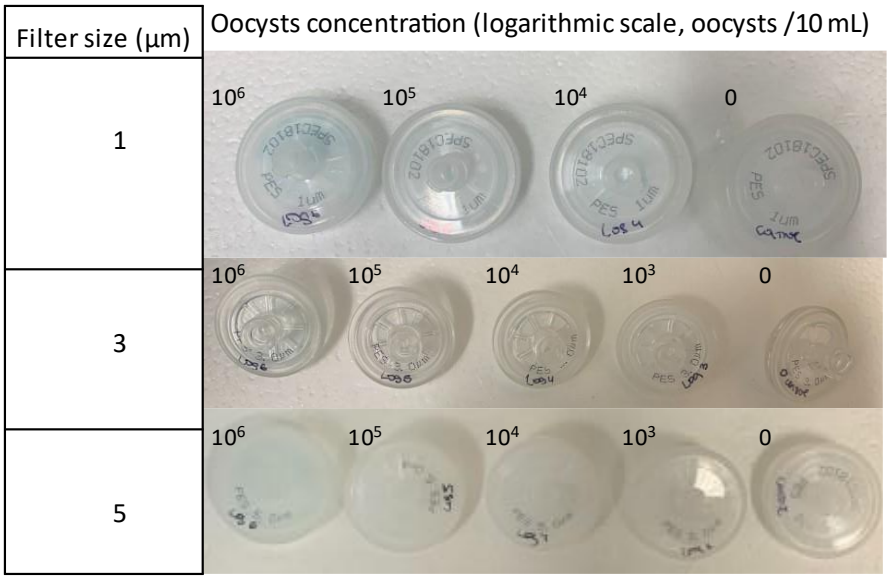

Figure 57. Visual representation of the influence of pore size on Cryptosporidium limit of detection

However, visual representation and comparison by taking a picture has some drawbacks such as lighting and viewing angle. Therefore, the liquid retained in the membrane of each filter was collected and the absorbance was recorded to perform a better comparison between different filters. The absorbance peak at 650 nm was taken for each sample and this comparison is shown in Figure 58.

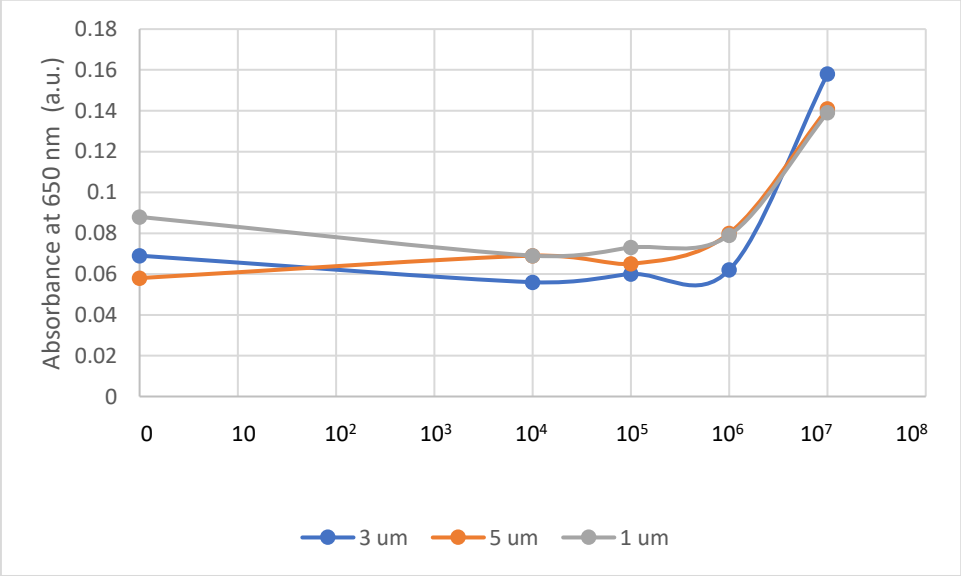

Figure 58.Absorbance peak as a representation of the influence of pore size on Cryptosporidium limit of detection

No significant difference in the LOD as a function of filter pore size was observed. For all filter types, the LOD was 10^6 oocysts/ 10 mL or 10^5 oocysts/mL. In Chapter 3, the LOD obtained with using antibodies in excess, and therefore, the maximum LOD we could achieve with this approach is 10^5 oocysts/mL or 10^4 oocysts in total. Some approaches could be taken to improve this limit of detection such as decreasing the filter surface area. However, finding smaller commercially available syringe filters that are made with similar materials and similar pore size is challenging and the housing often prevents good visual readings.

6.3.4. Negative control using *E. coli*

Figure 59 shows the visual representation for the limit of detection of each filter.

E.coli concentration (CFU/ 10 mL)

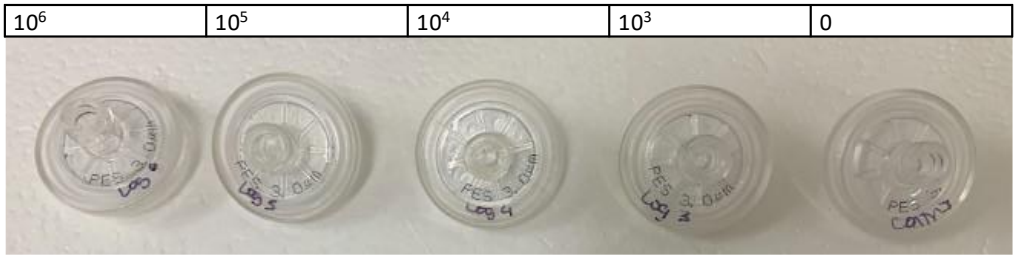

Figure 59. Visual representation of E. coli negative control

No false positives were detected by the naked eye for any *E. coli* concentration. All samples appeared to be colorless, indicating that the use of HRP-labelled specific anti-*Cryptosporidium* antibodies are not likely attaching to *E. coli*. Nevertheless, as with previous *Cryptosporidium* samples, the liquid was collected and analysed by spectrophotometry. Figure 60 shows the spectra for all these samples.

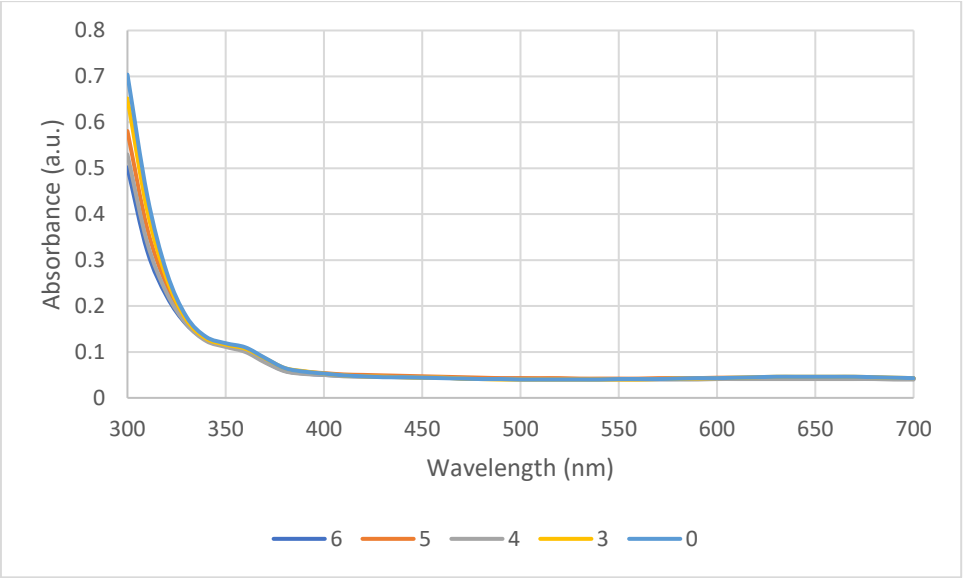

Figure 60. Absorbance spectrum for E. coli samples used as a negative control

As shown in Figure 60, there is no peak of absorbance at 650 nm, which is the characteristic peak for the TMB blue color. This agrees with the visual results where no non-specific binding or false negatives were observed. HRP-labelled anti-*Cryptosporidium* antibodies did not bind *E. coli* and the *E. coli* solution likely competed with the antibodies to reduce non-specific binding of the antibodies to the filter.

6.3.5. Effect of incubation time on antibody binding

In Figure 61 there is a visual representation of the effect of the incubation time on signal acquired.

Figure 61. Visual representation of the effect of incubation time on detection signal. From left to right, the filters were incubated for 3, 10,15,30 and 60 minutes

No signal for incubation periods of 10 minutes or less was detected. For 15 to 30 min, the signal increased while for the one hour incubation time, the signal slightly decreased. The liquid retained by the filter was collected and absorbance was taken, in a similar way than previous experiments in this Chapter. Figure 62 shows the dependence of signal, by taking the peak of absorbance at 650 nm, with time

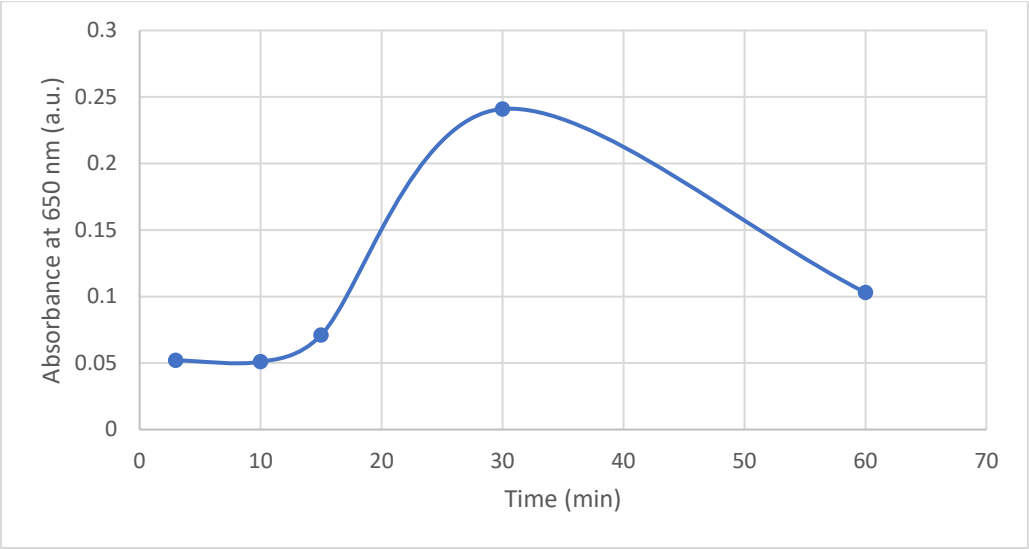

Figure 62. Absorbance peak as a function of time as a representation of the effect of incubation time on detection signal.

Figure 62 shows the phenomena observed visually. An incubation time of 30 minutes was deemed optimal for this assay. Longer antibody-oocyst exposure time may be detrimental for antibody binding. Factors such as light exposure or exposure to room temperature conditions could have been detrimental for antibody stability and binding.

6.4. Conclusions

The possibility of creating an easy to use, in-filter detection method for *Cryptosporidium* was explored in this Chapter. The goal was to avoid low oocyst recovery from elution by eliminating this step.

One of the most problematic points of this sensor was the non-specific binding of the antibodies onto the membrane surfaces. This effect was mitigated by preconditioning the membranes by passing solutions with blocking agents or surfactants like Tween20, Tween80, casein or BSA. It was also found that the pore size of the membrane did not have a significant effect on the reduction of non-specific binding. The two factors that influenced the most on non-specific binding were the use of surfactants on both the preconditioning solution, the solution in which antibodies and oocysts were incubated and the concentration of antibodies used. For all samples it was found that antibody concentrations higher than 0.05 µg/mL generated background noise and false positives.

No correlation between the limit of detection and filter pore size was observed. The best LOD that was achieved with this scheme was 10^6 oocyst/10 mL or 10^5 oocysts/mL, which is a rather high limit of detection compared to other biosensors that use antibodies and that are described in Chapter 2. Previously reported LODs ranged from single oocyst detection in 100 µL achieved by Li et al. (2021) , which would equal to 50 oocysts/ mL, to 500 oocysts/mL by Laczka et al. (2013).

Results showed in Chapter 3, in which an excess of the same antibody concentration was used in a smaller, more concentrated volume of oocysts (and therefore, higher chances of oocyst/antibody encounter) showed a limit of detection of 10^5 oocysts/mL or 10^4 oocysts total (because only 100 µL was used). Considering that by filtering the solutions and therefore concentrating the oocysts, the total number of oocysts is a better way of describing the limit of detection. This in-filter approach could likely be improved ten-fold, given the results from Chapter 3. Some improvement methods like modifying the antibody-oocyst incubation time were explored and 30 minutes incubation time proved to be optimal.

Other improvement methods remained challenging. For example, reducing the surface area of the filters was limited by the availability of commercial filters with small diameter, the right material of fabrication and the right pore size. PES membranes are preferred as they are very low protein binding. There is some availability for other commercially available filters of these characteristics. However, they tend to be made of glass fiber, which has a significant higher affinity for protein binding. Since reducing the non-specific binding of antibodies is crucial to this approach and to avoid false positives, these membranes cannot be used for this purpose.

Another improvement could have been to increase the antibody concentration but as it was shown in this Chapter, this involved a higher risk of false positives.

7. Conclusions and future work

This work explored the complexities of aptamer and antibody binding under different conditions with the aim of building a cost-effective cheap and easy to use sensor that could be implemented for the use of the general public.

First, the gaps for “easy-to-use by the general public” and “easy to carry” biosensors were identified. Laboratory conditions were then explored to understand how the inactivation of *Cryptosporidium* affected its ability to be “stained” using fluorescein labelled aptamers and antibodies. Both understanding the best binding mechanism and protocol, as well as using a low-risk form of *Cryptosporidium* was sought. It was found that inactivation procedures did not play a significant role on the LOD when using HRP-labelled antibodies. However, inactivation procedures did play a bigger role when using more sensitive techniques such as flow cytometry and using FITC-labelled antibodies. Formalin-treated *Cryptosporidium* showed the highest binding using this approach.

For FITC-labelled antibodies, various staining protocols were tested. There was no advantage in binding the antibodies to the live oocyst before proceeding with the inactivation protocol. Binding affinity was higher when the oocysts were inactivated first and then stained with FITC-labelled antibodies. Fluorescein conjugated aptamers did not provide the same increase in detection as with FITC-labelled antibodies. It is possible that this is because the aptamers had a lower affinity for the oocyst and overall there was less binding to the oocyst, or the signal given off by the fluorescein was just not as strong as the signal given off by FITC. A direct comparison using the same fluorescent probe was not possible because of the availability of the materials at the time of undertaking this work. Still, other reasons were considered for the differences including possible changes in the structure of the oocysts after inactivation. SELEX procedures are highly sensitive to the conditions in which the aptamers were selected. Since Iqbal et al. (2015) used commercially available oocysts that were provided by a supplier that preserves recently shed oocysts, it could be that other samples, such as environmental samples, or our inactivated samples, had other membrane characteristics that led to a lower affinity.

Different aptamer sequences were then tested on formalin-treated oocysts with the aim of finding an aptamer sequence that could bind to some structure that it was conserved during the inactivation process. This was done by staining the oocysts with 6-FAM labelled aptamers and using a flow cytometer to determine the fluorescence intensity. Unfortunately, the results obtained did not point to a better performing other aptamer sequence.

Effects on aptamer binding as a function of pH and heat-treatment contact time were also explored. It was discovered that a very low pH values (less than pH=3) aptamers show a high binding affinity. However, cross-reactivity assays using *E. coli* as a negative control showed that this higher binding affinity was due to non-specific interactions rather than *Cryptosporidium*-specific binding. It was also found that there was no correlation between heat-treatment processes and aptamer binding.

Finally, a proof-of-concept detection scheme for *Cryptosporidium* was developed. This biosensing technique was developed to overcome two drawbacks of current *Cryptosporidium* detection. Current *Cryptosporidium* detection methods require the filtration of large quantities of water, which increases the likelihood of capturing oocysts; however, once the oocyst is captured, current practice requires the oocyst to be dislodged and recovered. The latter is the step where losses have been observed, and a major bottleneck of the entire process. The second drawback is that current methods are not easy to transport, easy to use technologies that can be used by the general public.

For this approach several parameters were optimized. First, the effect that preconditioning the filter with several blocking agents was explored with the goal of achieving a lower rate of non-specific antibody-membrane binding. It was found that this non-specific interaction was greatly mitigated using blocking agents such as Tween20, Tween80 and casein. The concentration of antibodies was also optimized. A maximum concentration of 0.05 µg/mL was selected because it was the highest one that did not render any non-specific binding.

The effect of pore size on non-specific binding and *Cryptosporidium* LOD was also explored. It was found that these parameters were not as dependent on the pore size; however, membrane material did play a role on non-specific binding.

The in-filter detection approach was only able to detect 10^6 oocyst/10 mL or 10^5 oocysts/mL, which is a rather high LOD compared to other biosensors that use antibodies and that are described in Chapter 2 of this thesis. However, according to colorimetric results in which the LOD was explored in Chapter 3 as a function of the inactivation methods in which we used a much more sensitive approach for the colorimetric detection of the oocysts via the same HRP-labelled polyclonal antibodies, it may be possible to decrease the LOD ten-fold. These results showed a limit of detection of 10^5 oocysts/mL, but the volumes used were 100 µL, implying the ability to detect 10^4 oocysts in total. Since this in-filter sensors is sensitive not to the concentration of the oocysts, but the total number of oocysts retained within the filter, the lowest number of oocysts that these antibodies will be able to detect is 10^4 oocysts in total, which is ten time less than our current limit of detection.

The next steps that should be taken to improve *Cryptosporidium* detection include:

- conjugating FITC to the aptamers and verify binding of aptamers to the oocysts;
- exploring better aptamer-binding conditions that would make these aptamers bind to a similar or higher level than that observed for antibodies and that correspond to those observed in the literature;
- finding new aptamer sequences that could bind to a wider arrange of inactivated *Cryptosporidium* and *Cryptosporidium* in conditions found in natural waters.
- finding other source of HRP-labelled anti-*Cryptosporidium* antibodies or aptamers that could render a lower limit of detection to be used in this in-filter approach;
- finding, or creating membrane filters with a lower diameter and big pore size (1-3 µm) that are also made of a low protein binding material, so the oocysts can be confined into a smaller area and therefore, a higher colorimetric signal would appear.

References

Adachi, T., & Nakamura, Y. (2019). Aptamers: A review of their chemical properties and modifications for therapeutic application. Molecules, 24(23), 4229.

Adeyemo, F. E., Singh, G., Reddy, P., Bux, F., & Stenström, T. A. (2019). Efficiency of chlorine and UV in the inactivation of Cryptosporidium and Giardia in wastewater. PLoS ONE, 14(5). 10.1371/journal.pone.0216040

Ahmad, K. M., Oh, S. S., Kim, S., McClellen, F. M., Xiao, Y., & Soh, H. T. (2011). Probing the limits of aptamer affinity with a microfluidic SELEX platform. PloS One, 6(11), e27051.

Andrew Filby. (2019). Imaging Flow Cytometry : A brief overview

Arshavsky-Graham, S., Heuer, C., Jiang, X., & Segal, E. (2022). Aptasensors versus immunosensors—Which will prevail? Engineering in Life Sciences, 22(3-4), 319-333. 10.1002/elsc.202100148

Baldo, B. A., Tovey, E. R., & Ford, S. A. (1986). Comparison of different blocking agents and nitrocellulose in the solid phase detection of proteins by labelled antisera and protein A. Journal of Biochemical and Biophysical Methods, 12(5-6), 271-279.

Barteneva, N. S., Fasler-Kan, E., & Vorobjev, I. A. (2012). Imaging Flow Cytometry. Journal of Histochemistry and Cytochemistry, 60(10), 723-733. 10.1369/0022155412453052

Bodley-Tickell, A. T., Kitchen, S. E., & Sturdee, A. P. (2002). Occurrence of Cryptosporidium in agricultural surface waters during an annual farming cycle in lowland UK. Water Research, 36(7), 1880-1886. 10.1016/S0043-1354(01)00398-0

Boi, G., Scalia, C. R., Gendusa, R., Ronchi, S., & Cattoretti, G. (2016). Disaccharides Protect Antigens from Drying-Induced Damage in Routinely Processed Tissue Sections. Journal of Histochemistry and Cytochemistry, 64(1), 18-31. 10.1369/0022155415616162

Chalmers, R. M., Davies, A. P., & Tyler, K. (2019). Cryptosporidium. Microbiology, 165(5), 500-502.

Cowperthwaite, M. C., & Ellington, A. D. (2008). Bioinformatic analysis of the contribution of primer sequences to aptamer structures. Journal of Molecular Evolution, 67(1), 95-102.

Cram, L. S. (2002). Flow cytometry, an overview. Methods in Cell Science, 24(1), 1-9. 10.1023/A:1024198904819

Crowther, J. R. (2009). The ELISA guidebook. Springer.

Drozd, C., & Schwartzbrod, J. (1996). Hydrophobic and electrostatic cell surface properties of Cryptosporidium parvum. Applied and Environmental Microbiology, 62(4), 1227-1232.

DuPont, H. L., Chappell, C. L., Sterling, C. R., Okhuysen, P. C., Rose, J. B., & Jakubowski, W. (1995). The infectivity of Cryptosporidium parvum in healthy volunteers. New England Journal of Medicine, 332(13), 855-859.

EPA. (2001). Cryptosporidium: Drinking Water Health Advisory. (Report No. EPA-822-R-01-009). United States Environmental Protection Agency Office of Science and Technology. https://www.epa.gov/sites/default/files/2015-10/documents/cryptosporidium-report.pdf Last accessed on: August 31, 2022.

EPA. (2005). Method 1623: Cryptosporidium and Giardia in Water by Filtration/IMS/FA. (Report No. EPA 815-R-05-002). United States Environmental Protection Agency Office of Water. https://www.epa.gov/sites/default/files/2015-07/documents/epa-1623.pdf Last accessed on: August 31, 2022.

Francy, D. S., SimmonsIII, O. D., Ware, M. W., Granger, E. J., Sobsey, M. D., & SchaeferIII, F. W. (2004). Effects of Seeding Procedures and Water Quality on Recovery of Cryptosporidium Oocysts from Stream Water by Using U.S. Environmental Protection Agency Method 1623. Applied and Environmental Microbiology, 10.1128/AEM.70.7.4118-4128.2004

General Information for the Public | Cryptosporidium | Parasites | CDC. (2021). https://www.cdc.gov/parasites/crypto/general-info.html. Last accessed on: August 31, 2022.

Gharpure, R., Perez, A., Miller, A. D., Wikswo, M. E., Silver, R., & Hlavsa, M. C. (2019). Cryptosporidiosis outbreaks—United states, 2009–2017. Morbidity and Mortality Weekly Report, 68(25), 568.

Gibson, A. R., & Striepen, B. (2018). Cryptosporidium. Current Biology, 28(5), R193-R194.

Global Health, Division of Parasitic Diseases and Malaria. (2019). CDC - DPDx - Cryptosporidiosis. Centers for Disease Control and Prevention. https://www.cdc.gov/dpdx/cryptosporidiosis/index.html. Last accessed on: August 31, 2022.

Hassan, E. M., Dixon, B. R., Sattar, S. A., Stalker, A., Örmeci, B., & DeRosa, M. C. (2021). Highly sensitive magnetic-microparticle-based aptasensor for Cryptosporidium parvum oocyst detection in river water and wastewater: Effect of truncation on aptamer affinity. Talanta, 222, 121618.

Hassan, E. M., Dixon, B. R., Sattar, S. A., Stalker, A., Örmeci, B., & DeRosa, M. C. (2021). Highly sensitive magnetic-microparticle-based aptasensor for Cryptosporidium parvum oocyst detection in river water and wastewater: Effect of truncation on aptamer affinity. Talanta, 222, 121618.

Hassan, E. M., Örmeci, B., DeRosa, M. C., Dixon, B. R., Sattar, S. A., & Iqbal, A. (2021). A review of Cryptosporidium spp. and their detection in water. Water Science and Technology, 83(1), 1-25.

Health Canada. (2019). Enteric Protozoa: Giardia and Cryptosporidium. https://www.canada.ca/en/health-canada/services/environmental-workplace-health/reports-publications/water-quality/enteric-protozoa-giardia-cryptosporidium.html. Last accessed on: August 31, 2022.

Henri, J., Bayat, N., Macdonald, J., & Shigdar, S. (2019). A Guide to Using Nucleic Acid Aptamers in Cell Based Assays. International Society on Aptamers, 23

Hianik, T., Ostatná, V., Sonlajtnerova, M., & Grman, I. (2007). Influence of ionic strength, pH and aptamer configuration for binding affinity to thrombin. Bioelectrochemistry, 70(1), 127-133.

Hlavsa, M. C., Aluko, S. K., Miller, A. D., Person, J., Gerdes, M. E., Lee, S., Laco, J. P., Hannapel, E. J., & Hill, V. R. (2021). Outbreaks associated with treated recreational water—United States, 2015–2019. American Journal of Transplantation, 21(7), 2605-2609.

Ho, D., Schierts, J., Zimmerman, Z., Gadsden, I., & Bruttig, S. (2009). Comparison of frozen versus desiccated reference human red blood cells for hemagglutination assays. Transfusion, 49(10), 2173-2180. 10.1111/j.1537-2995.2009.02270.x

Inoue, M., Rai, S. K., Oda, T., Kimura, K., Nakanishi, M., Hotta, H., & Uga, S. (2003). A new filter-eluting solution that facilitates improved recovery of Cryptosporidium oocysts from water. Journal of Microbiological Methods, 55(3), 679-686.

Iqbal, A., Labib, M., Muharemagic, D., Sattar, S., Dixon, B. R., & Berezovski, M. V. (2015). Detection of Cryptosporidium parvum Oocysts on Fresh Produce Using DNA Aptamers. PloS One, 10(9), e0137455. 10.1371/journal.pone.0137455

Iqbal, A., Liu, J., Dixon, B., Zargar, B., & Sattar, S. A. (2019). Development and application of DNA-aptamer-coupled magnetic beads and aptasensors for the detection of Cryptosporidium parvum oocysts in drinking and recreational water resources. Canadian Journal of Microbiology, 65(11), 851-857.

Jenkins, M. C., O'Brien, C. N., & Trout, J. M. (2008). Detection of Cryptosporidium parvum oocysts by dot-blotting using monoclonal antibodies to Cryptosporidium parvum virus 40-kDa capsid protein. Journal of Parasitology, 94(1), 94-98.

Jennens, M. G. (1954). The effect of desiccation on antigenic structure. Microbiology, 10(1), 127-129.

Kajimura, J., Ito, R., Manley, N. R., & Hale, L. P. (2016). Optimization of Single- and Dual-Color Immunofluorescence Protocols for Formalin-Fixed, Paraffin-Embedded Archival Tissues. Journal of Histochemistry and Cytochemistry, 64(2), 112-124. 10.1369/0022155415610792

Kang, C. D., Cao, C., Lee, J., Choi, I. S., Kim, B. W., & Sim, S. J. (2008). Surface plasmon resonance-based inhibition assay for real-time detection of Cryptosporidium parvum oocyst. Water Research, 42(6-7), 1693-1699.

Kang, C. D., Lee, S. W., Park, T. H., & Sim, S. J. (2006). Performance enhancement of real-time detection of protozoan parasite, Cryptosporidium oocyst by a modified surface plasmon resonance (SPR) biosensor. Enzyme and Microbial Technology, 39(3), 387-390.

Kennedy, D., Cronin, U. P., Piterina, A., & Wilkinson, M. G. (2019). Heat and Chemical Treatments Affect the Viability, Morphology, and Physiology of Staphylococcus aureus and Its Subsequent Antibody Labeling for Flow Cytometric Analysis. Applied and Environmental Microbiology, 85(17)10.1128/AEM.01006-19

Kniel, K. E., & Jenkins, M. C. (2005). Detection of Cryptosporidium parvum oocysts on fresh vegetables and herbs using antibodies specific for a Cryptosporidium parvum viral antigen. Journal of Food Protection, 68(5), 1093-1096.

Kramer, M. F., Vesey, G., Look, N. L., Herbert, B. R., Simpson-Stroot, J. M., & Lim, D. V. (2007). Development of a Cryptosporidium oocyst assay using an automated fiber optic-based biosensor. Journal of Biological Engineering, 1(1), 1-11.

Laczka, O., Skillman, L., Ditcham, W. G., Hamdorf, B., Wong, D. K., Bergquist, P., & Sunna, A. (2013). Application of an ELISA-type screen printed electrode-based potentiometric assay to the detection of Cryptosporidium parvum oocysts. Journal of Microbiological Methods, 95(2), 182-185.

Le Guern, F., Mussard, V., Gaucher, A., Rottman, M., & Prim, D. (2020). Fluorescein derivatives as fluorescent probes for ph monitoring along recent biological applications. International Journal of Molecular Sciences, 21(23), 9217.

Lendner, M., & Daugschies, A. (2014). Cryptosporidium infections: molecular advances. Parasitology, 141(11), 1511-1532.

Li, T., Bu, G., & Xi, G. (2021). Effects of heat treatment on the antigenicity, antigen epitopes, and structural properties of β-conglycinin. Food Chemistry, 346, 128962.

Li, Y., Deng, F., Hall, T., Vesey, G., & Goldys, E. M. (2021). CRISPR/Cas12a-powered immunosensor suitable for ultra-sensitive whole Cryptosporidium oocyst detection from water samples using a plate reader. Water Research, 203, 117553.

Luka, G. S., Najjaran, H., & Hoorfar, M. (2022). On-chip-based electrochemical biosensor for the sensitive and label-free detection of Cryptosporidium. Scientific Reports, 12(1), 1-11.

Luka, G., Samiei, E., Dehghani, S., Johnson, T., Najjaran, H., & Hoorfar, M. (2019). Label-free capacitive biosensor for detection of Cryptosporidium. Sensors, 19(2), 258.

Luka, G., Samiei, E., Tasnim, N., Dalili, A., Najjaran, H., & Hoorfar, M. (2022). Comprehensive review of conventional and state-of-the-art detection methods of Cryptosporidium. Journal of Hazardous Materials, 421, 126714.

Luo, S., Nguyen, K. T., Nguyen, B. T. T., Feng, S., Shi, Y., Elsayed, A., Zhang, Y., Zhou, X., Wen, B., Chierchia, G., Talbot, H., Bourouina, T., Jiang, X., & Liu, A. Q. (2021). Deep learning-enabled imaging flow cytometry for high-speed Cryptosporidium and Giardia detection. Cytometry. Part A: The Journal of the International Society for Analytical Cytology, 99(11), 1123-1133. 10.1002/cyto.a.24321

Matsuda, Y., Fujii, T., Suzuki, T., Yamahatsu, K., Kawahara, K., Teduka, K., Kawamoto, Y., Yamamoto, T., Ishiwata, T., & Naito, Z. (2011). Comparison of Fixation Methods for Preservation of Morphology, RNAs, and Proteins From Paraffin-Embedded Human Cancer Cell-Implanted Mouse Models. Journal of Histochemistry and Cytochemistry, 59(1), 68-75. 10.1369/jhc.2010.957217

Mahler, H., Huber, F., Kishore, R. S., Reindl, J., Rückert, P., & Müller, R. (2010). Adsorption behavior of a surfactant and a monoclonal antibody to sterilizing-grade filters. Journal of Pharmaceutical Sciences, 99(6), 2620-2627.

McKeague, M., & DeRosa, M. C. (2012). Challenges and Opportunities for Small Molecule Aptamer Development. Journal of Nucleic Acids, 2012, e748913. 10.1155/2012/748913

McKinnon, K. M. (2018). Flow Cytometry: An Overview. Current Protocols in Immunology, 120, 5.1.1-5.1.11. 10.1002/cpim.40

Messner, M. J., Chappell, C. L., & Okhuysen, P. C. (2001). Risk assessment for Cryptosporidium: a hierarchical Bayesian analysis of human dose response data. Water Research, 35(16), 3934-3940.

Montemayor, M., Valero, F., Jofre, J., & Lucena, F. (2005). Occurrence of Cryptosporidium spp. oocysts in raw and treated sewage and river water in north-eastern Spain. Journal of Applied Microbiology, 99(6), 1455-1462. 10.1111/j.1365-2672.2005.02737.x

Nakamura, Y. (2011). Aptamer: Biology to applications. Nucleic Acid Drugs, 135-152.

Nguyen, H. H., Park, J., Kang, S., & Kim, M. (2015). Surface Plasmon Resonance: A Versatile Technique for Biosensor Applications. Sensors (Basel, Switzerland), 15(5), 10481-10510. 10.3390/s150510481

Otali, D., Stockard, C. R., Oelschlager, D. K., Wan, W., Manne, U., Watts, S. A., & Grizzle, W. E. (2009). The combined effects of formalin fixation and individual steps in tissue processing on immuno-recognition. Biotechnic & Histochemistry : Official Publication of the Biological Stain Commission, 84(5), 223-247. 10.3109/10520290903039094

Pavli, P., Venkateswaran, S., Bradley, M., & Bridle, H. (2016). Enhancing Cryptosporidium parvum recovery rates for improved water monitoring. Chemosphere, 143, 57-63.

Phillip, M., Kleinman, D., Potashnik, G., & Insler, V. (1984). Antigenicity of sperm cells after freezing and thawing. Fertility and Sterility, 41(4), 615-619.

Phillips, K. S., & Jirí Homola. (2008). Surface Plasmon Resonance Based Sensors. Springer.

Poitras, C., Fatisson, J., & Tufenkji, N. (2009). Real-time microgravimetric quantification of Cryptosporidium parvum in the presence of potential interferents. Water Research, 43(10), 2631-2638.

Public Health Agency of Canada. (2011). Pathogen Safety Data Sheets: Infectious Substances – Cryptosporidium parvum. https://www.canada.ca/en/public-health/services/laboratory-biosafety-biosecurity/pathogen-safety-data-sheets-risk-assessment/cryptosporidium-parvum-pathogen-safety-data-sheet.html. Last accessed on: August 31, 2022.

Robertson, L. J., Campbell, A. T., & Smith, H. V. (1992). Survival of Cryptosporidium parvum oocysts under various environmental pressures. Applied and Environmental Microbiology, 58(11), 3494-3500.

Schüling, T., Eilers, A., Scheper, T., Walter, J., Schüling, T., Eilers, A., Scheper, T., & Walter, J. (2018). Aptamer-based lateral flow assays. AIMS Bioengineering, 5(2), 78-102. 10.3934/bioeng.2018.2.78

Shah, N. J. (2019). Southern, Western and Northern Blotting. Introduction to Basics of Pharmacology and Toxicology (pp. 399-406). Springer.

Stott, D. I. (1989). Immunoblotting and dot blotting. Journal of Immunological Methods, 119(2), 153-187.

Tanner, J. A., Kinghorn, A. B., & Cheung, Y. (2018). Preface to Aptamers. *Aptamers* (pp ix-x). MDPI.

Thiruppathiraja, C., Saroja, V., Kamatchiammal, S., Adaikkappan, P., & Alagar, M. (2011). Development of electrochemical based sandwich enzyme linked immunosensor for Cryptosporidium parvum detection in drinking water. Journal of Environmental Monitoring, 13(10), 2782-2787.

Usukura, J. (1993). Rapid freezing and subsequent preparation methods in retinal cell biology. Methods in Neurosciences (pp. 37-53). Elsevier.

Zhang, Q., & Landgraf, R. (2012). Selecting molecular recognition. What can existing aptamers tell us about their inherent recognition capabilities and modes of interaction Pharmaceuticals, 5(5), 493-513.

Zheng, J., Tang, X., Wu, R., Yan, Q., Tang, H., Luo, J., Niu, S., Qu, Y., & Sun, L. (2015). Identification and characteristics of aptamers against inactivated Vibrio alginolyticus. LWT-Food Science and Technology, 64(2), 1138-1142.

Appendix. Approximations made to obtain standard deviations.

Standard deviations for flow cytometric results were calculated either via the software floreada.io for conventional flow cytometry or Amnis IDEAS for Imaging flow cytometry. However, just by taking the standard deviation from the gated population, for some experiments, we get very high standard deviations (see Table 16 as an example). But when represented in a histogram (see Figure 63), most of these curves follow a gaussian distribution that do not match with the values of standard deviation represented. It was hypothesized that there are a small number of events that have a high fluorescence intensity that could be causing this differences (represented with an arrow in Figure 63). Since these events are spread out through the X axis, to determine the corrected standard deviation, a smaller range engulfing most of the events in the histogram (see Figure 63) will be made, and the standard deviation inside this gate will be taken. For samples with two peaks, both peaks will be engulfed in the range (see figure 64).

Table 16. Statistical values for flow cytometry performed with 6-FAM labelled aptamers in which no corrections to the Standard deviation has been done

Sample		Mean of fluorescence intensity	Median of fluorescence intensity	Standard deviation
Desiccation	Control	129	136	65
	Protocol 1	496	212	5,410
	Protocol 2	1,028	428	3,364
Formalin	Control	137	125	83
	Protocol 1	534	333	8,999
	Protocol 2	556	344	8,194
Heat-treatment	Control	191	179	88
	Protocol 1	4,562	460	17,862
	Protocol 2	1,409	316	7,756
Freeze-treatment	Control	136	126	85
	Protocol 1	1,272	563	7,414
	Protocol 2	872	502	3,850
E.coli	*Control*	49	46	29
	Protocol 1 - stained	262	39	3,608

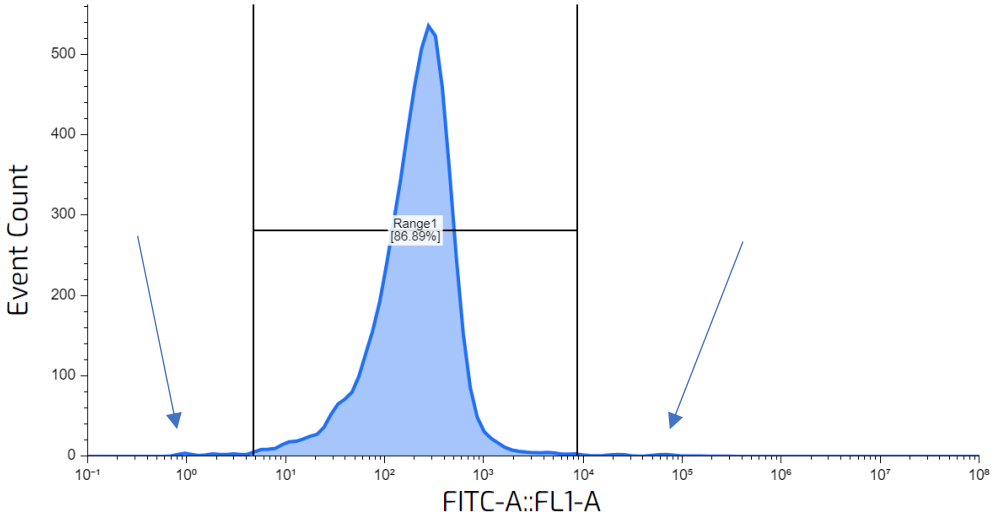

Figure 63. Representation of a histogram in which a smaller range containing the most significant values has been draw

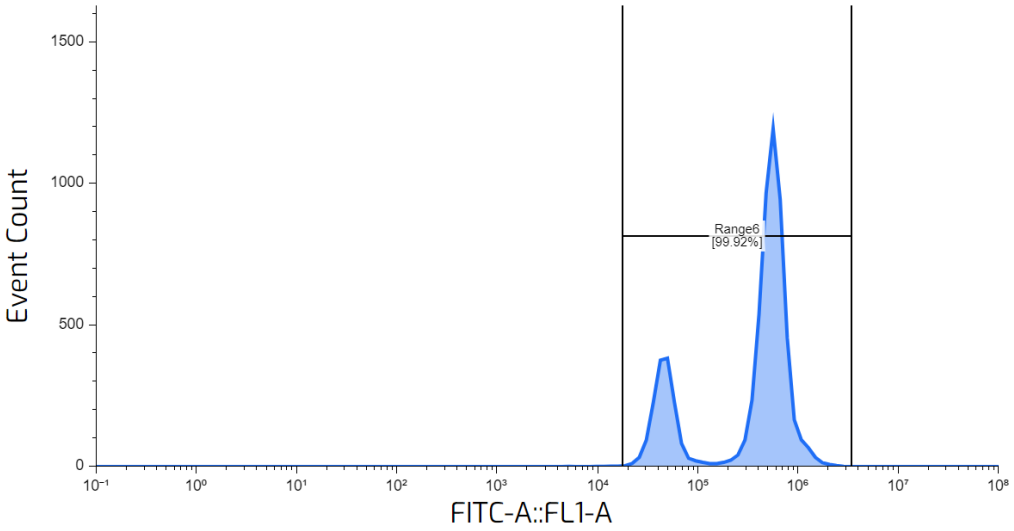

Figure 64. Range selected for a sample with two fluorescence peaks